CHEMICAL AND MORPHOLOGICAL VARIATION OF POLY(ESTER AMIDE) SYNTHESIS AND FABRICATION AND THEIR USE IN MAST CELL STABILIZATION AND WOUND HEALING

A Thesis
Presented to the Faculty of the Graduate School
Of Cornell University
in Partial Fulfillment of the Requirements for the Degree of
Doctorate of Philosophy

By:

Alicia Nicole Potuck

May 2015

© Alicia Nicole Potuck 2015

ALL RIGHTS RESERVED

CHEMICAL AND MORPHOLOGICAL VARIATION OF POLY(ESTER AMIDE) SYNTHESIS AND FABRICATION AND THEIR USE IN MAST CELL STABILIZATION AND WOUND HEALING

Alicia Nicole Potuck, Ph.D.

Cornell University 2015

Based on their unqiue chemical and mechanical properties, amino acid-based poly(ester amide) polymers (AA-PEAs) have demonstrated excellent performance for utility in biomedical devices. Owning to their chemical composition, AA-PEAs underwent hydrolytic and enzymatic degradation to facilitate both *in vitro* and *in vivo* biodegradation. Variations in the amino acid incorporated in monomer synthesis altered polymer characterisitics such as hydrophobicity (L-Phenylalanine) and Hydrophilicity/surface charge (L-Arginine). Attibuted to the bioanalogous pseudo-protein compostion of AA-PEAs, these polymers have shown low cytotoxicity, low proinflammatory cytokine production, and excellent cell adhesion. Therefore, these polymers are an excellent platform to which biomedical device and drug delivery systems can be built.

Variable techniques in polymer fabrication offered an expanded field of AA-PEA function. Hydrophobic AA-PEAs were fabricated into 2D films and nano-scale 3D fibers with biomimetic function and hydrophilic AA-PEAs were incorporated into self-assembled microparticles and hydrogels. Hydrophobic films and fibers allowed for longer *in vitro* polymer retention, while hydrophilic AA-PEAs were utilized to integrate cationic charge into hybrid systems to improve cell/biomaterial interactions. In all cases, AA-PEAs alone or combined into a hybrid system offered equivalent mechanical performance with equal or better cell compatibility.

By examining which parameters of polymer composition (hydrophobicity, T_g, morphology, surface charge) stimulate cellular response, a new generation of more funcational and biocompatibile devices can be fabricated. Both microparticles with reduced surface charge and hydrogels with cationic surface charge by addition of arginine-based AA-PEAs showed improved performance over their commercial counterpart. Similarly, incorporation of small molecules into hydrophobic AA-PEA polymer systems did not detrimentally affect cell compatibility, indicating these materials as excellent candidates for drug delivery. This work shows that although hydrophobicity and morphology may play a supporting role in cell response, surface charge dominates inflammatory response and cell adhesion.

BIOGRAPHICAL SKETCH

Alicia Potuck received a B.S. in Chemistry from Rensselaer Polytechnic Institute in 2010. Following this, she entered the Ph.D program in Chemistry and Chemical Biology and Cornell University. She received her M.S. degree in July 2012 under the guidance of Dr. C.C. Chu with a focus on Polymer Science for biomaterial engineering. Following completion of her M.S., she continued on to complete this thesis examining the effects of polymer composition on macrophage response and drug release.

During her time at Cornell University, Alicia served as a graduate teaching assistant in the department of Chemistry and Chemical biology. As a result of her time teaching, she was awarded the Bayer Teaching Excellence Award (2010-2011, 2011-2012). After completion of her thesis, Alicia accepted an industrial position to continue direct lab-to-consumer research.

To my family (especially my twin sister Kristen) for their unwavering support

ACKNOWLEDGEMENT

I have been fortunate during my thesis studies to work with and be mentored by many exceptional researchers. I would like to take the next few paragraphs to highlight those which made my research and growth as a scientist possible.

Firstly, I would like to begin by acknowledging and sincerely thanking Dr. Chih-Chang Chu for his invaluable and steadfast support during my thesis research. Dr. Chu helped me to grow immeasurably as a researcher, offering guidance in project conception, trouble-shooting, manuscript preparation, and freedom to learn new techniques and fields. I offer enormous thanks to the members of my committee for their expertise and commitment to my progression through graduate school.

I would also like to highlight the invaluable support of the Rebecca Q. Morgan Foundation for their generous financial support, without which I would not have been able to pursue research I am truly passionate about. The financial research support provided by Jim and Becky Morgan allowed me to expand beyond the Chemistry department to the lab of Dr. C.C. Chu and focus on research combining polymers and biomedical applications. Furthermore, face-to-face meetings with the Morgans delivered excellent research discourse and perspective on the value of biomedical research.

I would like to thank Dr. Cynthia Leifer for her instrumental expertise and mentoring on macrophage behavior and function. I cannot express enough thanks to Dr. Leifer for her hours of

project discussion and planning, as well as her knowledge of assays and cell preparation. Her knowledge and patience helped me to better understand the intricacies of cell-biomaterial interactions. Furthermore, I would also like to thank Jody Lopez (technician in the lab of Dr. Cynthia Leifer) for her patient guidance in teaching me the correct protocols for handling cells and running assays. Her assistance was paramount in the completion of cytokine assays and cell survival.

In addition, I would like to recognize the positive influence that the undergraduate researchers I have had the opportunity to work with has had on my growth as a researcher. I have had the pleasure of working with Sarah Meyers, Stephanie Cheng, Kevin Hua, Kelly Guerin, Beth Weed, Connie Li, Justin Kim, and Ashley Weiner. I am indebted to these undergraduate collaborators, as they have taught me how to look at projects from different perspectives and how to approach projects using a multidisciplinary tactic. I also would like to thank Elaine Higashi (MEng 2013) for her diligent work and bright personality.

I would like to thank Drs. Baird and Holowka and Marcus Wilkes for their support, advice, and assay work on the mast cell projects. I could not have successfully completed these projects without their valuable contribution. I would like to thank Drs. Dequn Wu, Mingyu He, Hong Xiao, and graduate student Ying Ji for sharing their valuable expertise. I would also like to thank Dr. Jason Spector and Ope Asanbe for their contributions in completion of the polymer coated *in vivo* retrieved suture project. I would like to thank my fellow graduate students in the Chemistry department for their

constant support and kind words along the way. Lastly, I would like to thank my family from the bottom of my heart for their resolute backing and encouragement through the tough times.

TABLE OF CONTENTS

LIST OF FIGURES

LIST OF TABLES

Chapter 1. Review on Mast Cells and mast cell stabilization drug delivery systems

1.1 Introduction

In all drug delivery systems, choice of model drug is crucial to facilitate effective drug release and targeted delivery to the site of action pursuing specific cell types. A gamut of both drug and material parameters must be considered when developing an effective drug delivery system including; 1) polymer degradation rate and products, 2) drug mechanism of action *in vitro* and *in vivo*, and 3) drug functionality, solubility, and interactions with polymer carriers. Drug delivery modality is also a key parameter as development of intravenous drug delivery varies significantly from site of action devices due largely to concerns stemming from ADME (absorption, distribution, metabolism, and excretion) mechanisms including (but not limited to) hepatic first pass metabolism.

1.2 Mast Cells and wound healing

Appropriate choice of drug for the targeted biological response is also paramount to producing an effectual drug delivery system. Drug delivery devices can be utilized in many applications including, related to this work, wound healing. The wound healing process is comprised of three main phases; 1) inflammation, 2) tissue formation, and 3) tissue remodeling.[1]A key component of the wound healing process is recruitment of mast cells to the wound site to begin and promote the phases of wound healing. Mast cells are commonly found in connective tissues (dermis) and situated in close proximity to blood vessels.[2] In pioneering thesis dissertation work, Paul Ehrlich was the first researcher to describe the now hallmark metachromatic granules present within mast cells[3], followed by Selye who characterized the functionality of these cytoplasmic granules.[4] Metachromism stems from biological granule components

present within mast cell cytoplasm, leading to interactions between basic aniline dyes (i.e. toluidine blue) with polyanion proteoglycan mediators (heparin for example), resulting in staining of mast cells.[5]

The granules present within mast cells and released upon degranulation are of utmost concern to researchers as these mediators influence all stages of wound healing. These granules are membrane bound vessicles that fuse with the plasma membrane and discharge their water soluble contents which include a wide range of functionalities including cytokines, proteases, growth factors, etc. For example, in the first stage of wound healing of inflammation, mast cells release proinflammatory mediators upon degranulation such as chymases, tryptases, and carboxypeptidase A which stimulate inflammatory responses.[6] In particular, many biogenic amines are released, including histamine, which has been widely studied in mast cell allergic responses for its stimulation of vasodilation and capillary permeability, common markers of inflammatory allergic response.[7-9] In this inflammatory phase, mast cells work hand in hand with macrophage cells to undergo phagocytosis and work to promote wound site debridement, along with releasing chemotactic factors such as leukotrienes, cytokines, and proteases that serve to draw other immune cells such as neutrophils and basophils to the site.[2]

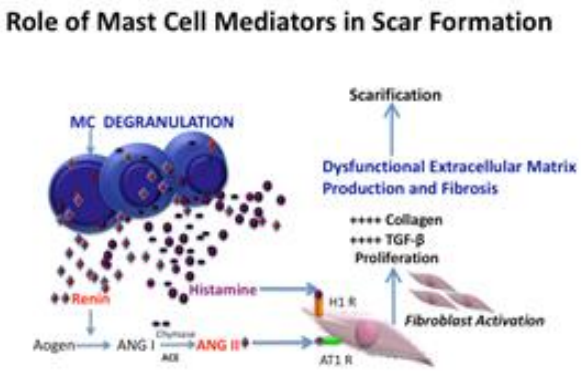

Figure 1. Role of mast cell degranulation in TGF-β release and fibroblast activation, leading to increased fibrosis and scar formation. *Image courtesy of Dr. Randi Silver*.

Growth of new tissue depends on generation of a scaffold, namely production of the extracellular matrix. In the second phase of wound healing, mast cells promote matrix deposition and remodeling via the release of many complex mediators that serve as a chemotaxis agent for fibroblasts, eliciting migration to the wound site to promote collagen synthesis. Collagen production is a main component of the extracellular matrix, offering a scaffold for building cell growth and adhesion. These mediators act upon fibroblast cells to support fibrogenic activity including (but not limited to) cytokines(IL-4, IL-6, heparin, TNF)[2,10] and growth factors (TGF).[11]

In the final stage of wound healing (tissue remodeling), mast cells continue to release mediators that stimulate healing functionalities which in this phase include lytic compounds (serine proteases and metalloproteinases), along with growth factors and cytokines.[2] Unlike in the second phase of wound healing, in the final phase, mast cells attract myofibroblasts, which facilitate wound contraction and finalize overall wound healing.[2]

Although mast cells are essential in promoting wound healing through chemotaxis of other cell types and matrix deposition, controversy mars these cells as they are implicated in the development of numerous diseases including autoimmune disorders. For example, mast cells are pinpointed as a contributor to the progression of multiple sclerosis in the brain through degranulation of proteolytic enzymes leading to inflammation and breaching of the blood brain barrier for mononuclear cell infiltration.[12]Moreover, mast cells are linked to upregulation of mediators which stimulation fibroblast cells, resulting in an overall increase in collagen deposition, leading to an undesirably more pronounced scar formation (Fig. 1). Due to the action of degranulation of many mediators (including those

upregulating proinflammatory response), mast cells have been linked to chronic allergic inflammation as a result of the binding of IgE antibodies with high affinity FcεRI receptors.[13] Researchers have now classified an entire subset of diseases linked to mast cells which consist of disorders such as mast cell leukemia, lymphoma, peptic ulcer disease, cutaneous disease, and many more.[14]

1.3 Mast Cell Stabilizers

To mitigate mast cell degranulation and limit the potential for the development ofmast cell-mediated diseases, researchers have developed a family of drugs referred to as mast cell stabilizers. Seeking alternatives to topical antihistamines and corticosteroids (low efficacy and unwanted side effects), researchers focused on finding low toxicity drugs that could effectively mute or prevent mast cell degranulation. Filling this niche, researchers developed the small molecule drug Cromoyln sulfate. When given before antigen challenge, cromolyn sulfate inhibits mast cell degranulation with very low toxicity, therefore limiting proinflammatory mediator availability to stimulate inflammation.[15] Ketotifen also functions in a similar manner to prevent proinflammatory responses linked to degranulation, often found in ocular conjunctivitis or chronic inflammatory disorders such as irritable bowel syndrome.[16] Although not completely elucidated in literature, researchers believe mast cell stabilizers work ~~through~~ in~~and~~ IgE-dependent fashion, some functioning as a calcium ion antagonist to prevent Ca^{2+} influx after allergen stimulation of IgE.[15]

Due to its small size (< 500g/mol), aqueous solubility, and potent effect on mast cells, ketotifen fumarate (KF) is an attractive drug to combine with polymer-based drug delivery systems. Ketotifen fumarate is the furamic salt of the base drug ketotifen, but is much more favorable as the salt imparts

higher aqueous solubility. Ketotifen fumarate, a benzocyclohepatathiopene compound, acts as an H_1 histamine receptor anti-histamine agent to treat common conditions such as allergic conjunctivitis, allergic dermatitis, rhinorrhea – all associated with histamine release and stimulation.[17] A common shortfall of both ketotifen and it's fumarate salt is the unfavorable first pass metabolism effect upon oral and systemic ingestion, thus requiring effective delivery to use a site-of-action approach.[18] Therefore, use in polymer carriers in a site-of-action device such as contact lens or patches would significantly increase the potential amount of drug deliverable and desired response.

1.4 Ketotifen Drug Delivery Systems

To address the needed site-of-action approach, many researchers have developed novel drug delivery devices spanning the range from microspheres to gels to patches to deliver the required KF for the biological application. Using a transdermal patch approach, Patel *et al* fabricated ethyl cellulose/hydroxypropyl methyl cellulose scaffolds with KF impregnation and quantified between 67-95% drug release for varying formulation conditions after 24 hours at 37℃.[18] Choosing a vastly different fabrication approach, Guerrero *et al* fabricated micron scale poly (lactic acid) and copolymer poly (lactic glycolic acid) spheres encapsulating KF to create a biodegradable drug delivery for site-of-action delivery to the intraperitoneal cavity.[19]They found a burst release of KF from the microspheres of around 10% after 9 hours, and a maximal release of between 57-67% after 350 hours *in vitro* incubation.[19] Therefore, material choice (polymer characteristics) and polymer fabrication methodology clearly aid in dictating release rate of KF from the carrier.

Although mast cells are distributed throughout the body in the dermis and near blood vessels, a large number of mast cells are found in the eye[20-22] and function to influence ocular response. Therefore, researchers have greatly expanded the arsenal of drug delivery devices to specifically target mast cell degranulation using mast cell stabilizers in ocular applications. One such application is incorporation of mast cell stabilizers (specifically KF) into polymer based contact lens for sustained drug delivery in treatment of allergic reactions and conjunctivitis. Venkatesh *et al* fabricated copolymer (poly(AX-co-HEMA-co-PEG200DMA where X varied based on starting polymer) molecularly imprinted hybrid hydrogels networks with ketotifen fumarate for sustained drug release.[23] They proposed that since imprinted hydrogels exhibited lower KF diffusion rates than non-imprinted hydrogels, KF may exhibit random walk diffusion along the polymer network thus extending its release profile.[23] Similarly, Karlgard *et al* doped (doping can be defined as drug suspended or trapped in a vehicle) commercially available contact lenses (silicon-based and p-HEMA) with KF and found that during a 24 hour *in vitro* release study KF did not have a burst release from polymer materials and was more effectively taken up by ionic polymer lens and released more slowly by non-ionic polymer lens.[24] Although two brief examples are given above, a multitude of studies have employed KF as a model drug to treat ocular disorders using polymer carriers.[25-28]

Regardless of the application, a few reoccurring trends are found in literature when examining polymer carriers for KF. Firstly, when comparing polymer characteristics, KF is released more slowly from hydrophobic polymers.[18,19] Secondly, many *in vitro* release studies include very short timelines (i.e. between 24 and 350 hours).[18,19,24,29] Contrastingly, the wound healing process can begin as early as a few hours, leading up to complete healing on the order of weeks or more. Therefore, to address currently

obvious need for long term novel and improved performance polymer based drug carriers for mast cell stabilization, methodologies can be conceptualized to include more hydrophobic polymers and longer release times to improve patient compliance and reduce cost for repeated application using hydrophobic fibers (Chap. 4) or from slow release entrapment in gels (Chap. 5). Chapters four and five address these two pillars for device improvement and present improved performance systems for KF delivery.

Chapter 2. Review on Macrophages and their role in wound healing

2.1 Introduction

The macrophage first described by Metchnikoff in 1893 was so called as a result of its behavior as a "large eater", referring to its characteristic behavior of phagocytosis, or engulfing foreign materials or cell debris.[30]Macrophage cells, or mononuclear phagocytes (commonly denoted Mϕ), are unspecified progenitor cells present in bone marrow that migrate to a wound or area of damaged tissue, stimulated through chemotaxis, with the main function of removal of extraneous cellular material or debris through phagocytosis. Macrophages remove apoptotic cells (termed efferocytosis) in damaged tissue.[31]Beyond its debridement behavior, macrophages display plasticity in their phenotype, often shifting between multiple roles in the wound healing process from stimulating inflammation to matrix deposition and tissue regeneration. This review chapter will touch briefly on the multiple tasks macrophages play in wound healing and their interplay with polymeric biomaterials.

2.2 Macrophages in wound healing

The main function of macrophages in the overall wound healing process is defense against pathogens and foreign materials. In the span of wound healing (≥ 10 days) including the phases of inflammation, proliferation, and remodeling, macrophages have the highest resident population between 3-5 days.[32] Tissue and circulating monocytes remain in a dormant un-activated state until recruited to the wound site and stimulated to become activated macrophage cells.[3] In the early stages of wound healing, monocytes differentiate into macrophages, which in turn recruit additional macrophage cells to the wound site through release of chemoattractant agents, specifically monocyte chemoattractant protein-1.[32]

Early on, activated macrophages release the cytokines interleukin-1 (IL-1), IL-6, and tumor necrosis factor alpha (TNF-α) in early and mid-inflammatory wound healing responses responses.[32] Activation can be stimulated through many routes including physical and chemical prompts. TNF-α, in particular, is a notable pro-inflammatory cytokine whose release increases wound site vasodilation and potential cell apoptosis. Furthermore, presence of bacterial factors such as lipopolysaccharide can further activate macrophage cells, increasing the extent of proinflammatory response. In the next phase of wound healing, macrophages secrete anti-inflammatory cytokines (such as IL-10) and upregulate receptors (mannose) necessary for foreign body giant cell formation and deposition of new extracellular matrix.[33] The further downstream remodeling steps are characterized by macrophage proactive repair characteristics such as promotion of angiogenesis, enhanced fibrinogenic action, and upregulation of proteins associated with the extracellular matrix.[33] In essence, macrophages play a key role in wound healing from the initial inflammatory response to downstream matrix remodeling. Therefore, macrophage behavior upon incubation with foreign materials is invaluable in understanding the complex cascade of the wound healing response.

As mentioned above, one of the most important duties of macrophage cells is phagocytosis of apoptotic cells and pathogens in the wound site. Macrophage phagocytosis begins by cell surface receptor adherence to the particle, followed by internalization through a phagosome vesicle.[34] Macrophage phagocytosis has been hypothesized to be directed by three main factors; number of particles, size of particles, and shape of particles.[34] Lam *et al* discovered using J774 mouse macrophage cells that macrophage cells have enormous "reserves" of surface area which materialize as membrane wrinkles which gradually smooth during the process of phagocytosis to vastly increase the available cell

surface area.[35] They found that during phagocytosis, macrophages can effortlessly increase their surface area greater than 5x more than a resting macrophage cell, observing efficient uptake of opsonized polystyrene beads of 30μm in diameter.[35] Although macrophage cells can take up large particles with ease, studies indicate that during the process of large particle (≥ 5μm diameter) uptake, frustrated phagocytosis may occur, leading to extracellular release of reactive oxygen species intended for degradation of the particle.[33] Therefore, macrophages display unique immune cell phagocytic behavior capable of wound debridement to facilitate improved wound healing.

2.3 Macrophage Plasticity

Macrophages exhibit what researchers refer to as "plasticity", or the ability of the cells to adapt to their environment and stimulate production of necessary wound debridement/healing components. Macrophages are generally characterized into two main categories based on phenotype; M1 (classically activated) and M2 (wound healing). M1 macrophages, typically found in the early stages of wound healing, are described by proinflammatory responses; secretion of elevated levels of proinflammatory cytokines, oxygen and reactive nitrogen species, and excellent tumoricidal and microbial responses.[36] Because M1 macrophages release potent proinflammatory cytokines such as IL-1, Il-6, and TNF-α, they are key constituents in early onset and chronic inflammation.[36] M1 macrophages become differentiated to a proinflammatory phenotype through stimulation by proinflammatory cytokines such as IFN-γ, TNF-α, IL-1β and many more released by T_H1 (thyroid hormone receptor), natural killer cells, and antigen presenting cells.[33] As a result of differentiating into an activated M1 phenotype, macrophage cells in this state undergo a high rate of phagocytosis to remove pathogenic debris. Of concern to researchers,

prolonged activation of M1 macrophages can lead to tissue damage through destruction of matrix components.[33] Van Loon *et al* have found that upon implantation of a foreign biomaterial, macrophage response is typically M1, including the elevated release of IL-8, MCP-1 (macrophage chemoattractant protein), and MIP-1β (macrophage inflammatory protein) chemokines.[33] Therefore, in planning drug delivery and wound healing devices, understanding the behavior and extent of macrophage activation will influence the overall efficiency and longevity of the device.

Once the initial proinflammatory macrophage response in normal wound healing has subsided, M2 macrophages can then infiltrate the wound, stimulating a wound healing and tissue repair response. M2 macrophages are often termed "alternatively activated" with their main function being the release of anti-inflammatory cytokines (which serve to mute proinflammatory cytokine response), tissue repair, and tissue remodeling. Much like M1 macrophage activation, alternative macrophage activation can be stimulated by release of cytokines, primarily IL-4 (to lesser extent; IL-10, TGF-β).[33] M2 macrophages are unique from M1 macrophages, as the M2 phenotype can further be divided into subcategories; M2a (wound healing), M2b (regulatory), and M2c (anti-inflammatory). While all M2 macrophages release high levels of IL-10 (known anti-inflammatory agent), low levels of IL-12 (enhances cytoxicity), and upregulation of arginase-1, each subcategory of M2 macrophages play an important role in reparative wound healing. M2a macrophages are considered profibrogenic and are characterized by the elevated release of IL-4 which leads to activation of fibroblasts and increased collagen formation. M2b macrophages serve to lessen inflammation and "dampen" immune response through release of IL-10.[33] M2c, a lesser studied M2 macrophage sub-phenotype, targets later stage immune suppression and matrix deposition through matrix components.[37] In general, M2 macrophages promote wound repair through

upregulation of angiogenic factors, production of extracellular matrix proteins, and production of tissue inhibitors of metalloproteinases.[33]

2.4 Macrophage Response to Biomaterials

Van Loon *et al* postulate that when examining the complex interactions between macrophage cells and implanted biomaterials, polymer surface chemistry and surface roughness can direct macrophage response; the interaction at the cell-biomaterial interface can direct the identity and amount of macrophage stimulation including cytokines, chemokines, and gene expression.[33] In the same vein, Brodbeck *et al* probed deeper to suggest that selective macrophage cytokine release is in fact directed by polymer surface chemistry through adherence of macrophages to adsorbed proteins on the biomaterial surface via cell surface integrins.[38] They suggest that carefully designing the biomaterial surface to direct the type and duration of macrophage response will greatly improve overall biocompatibility of the material.[38]

Looking more closely at the specifics of macrophage activation at the cell/biomaterial adhesion interface, surface chemistry at this junction plays a significant role in macrophage activation and cytokine release. To evaluate the influence of surface chemistry on macrophage activation, leading researchers fabricated films of varying surface characteristics (hydrophobic, hydrophilic, hydrophilic/neutral, hydrophilic/anionic, hydrophilic/cationic).[39] To achieve the varied surface chemistries, Jones *et al* utilized polyethylene terephthalate (PET, hydrophobic) , PET coated with poly(styrene-co-benzyl N,N-dimethyldithiocarbamate) (BDEDTC, hydrophobic), BDEDTC grafted with either acrylamide (PAAm, hydrophilic/neutral), the sodium salt of acrylic acid (PAANa, hydrophilic/anionic), or methyl iodide salt of N-[3-(dimethylamino)propyl] acrylamide

(DMAPAAmMeI, hydrophilic/cationic).[39] Jones *et al* found that at early time points adherent macrophages on varying surface chemistry films produced some cytokines (IL-6 and IL-1β) and chemokines (IL-8 and MCP-1) characteristic of classical M1 macrophage activation, yet also produced M2-type cytokines and chemokines (IL-10, eotaxin-2), indicating biomaterial stimulation of adherent macrophages is not solely a single phenotype.[39] More specifically, at early time points (3 days), hydrophilic/neutral PAAm polymers stimulated the highest proinflammatory IL-1β (2090 pg protein) while hydrophobic BDEDTC polymers stimulated the least (204 pg protein).[39] At later time points (10 days), PAAm stimulated the highest anti-inflammatory cytokine IL-10 production (1220 pg protein) while hydrophilic/anionic PAANa polymers stimulated the least IL-10 production (25 pg protein).[39] While PAAm exhibited a notable reduction in the number of adherent macrophage cells, Jones *et al* discovered that the small population of adhered macrophage cells over -stimulated cytokine response, leading to the highest release at both 3 and 10 days.[39] The authors suggest that their observation of decreased proinflammatory cytokine production (IL-1β) for all surface chemistries of film tested after three days is likely due to the natural resolution of inflammation with time.[39] Similarly, Brodbeck *et al*used the same base materials as Jones *et al* and found decreased macrophage adhesion and fusion to PAAm and PAANa materials with increased cell apoptosis (57% and 46%, respectively), leading to reduced cell/biomaterial interface interactions.[40] Lastly, Chen et al utilized lithography techniques to fabricate devices with micron and nanometer scale gratings along passive commercial materials (polycaprolactone, poly lactic acid, poly dimethylsiloxane) and found mouse macrophage (RAW264.7) adhesion greatest on nanoscale patterned surfaces at 48 hours compared to 2D control with increased proinflammatory cytokine (TNF-α) production with increased pattern size (300nm to 1μm) through 24

hours.[41]They concluded that material surface topography can significantly affect macrophage adhesion, cytokine secretion, and morphology, especially when patterned sizes are on the micron scale.[41]

Therefore, a complex milieu of surface chemistries, topography, and wound environment signals direct macrophage activation, leading the macrophage phenotype to become either classically or alternatively activated. Much research[39-41] has been done to assess polymer characteristics that stimulate macrophage activation to aid in design of future biomaterials to reduce inflammation, fibrosis, and improve wound healing. In conclusion, examining macrophage behavior in wound healing is essential to understand mechanisms of response to foreign body materials and offers an opportunity to direct macrophage phenotype to promote wound healing. Using the principles and behavior trends dicussed in this review chapter, macrophage behavior is analyzed from a cell/biomaterial perspective using self-assembled microparticles (Chap. 3) and fibrous membranes (Chap. 4), to better understand how to predict biocompatibility and wound healing models.

References for review chapters

1) Epstein, F. H., A. J. Singer, and R. A.f. Clark. Cutaneous Wound Healing. *N. Engl. J. Med.* 1999; 341.10: 738-46.
2) Noli, C., and A. Miolo. The Mast Cell in Wound Healing. *Veterinary Dermatology* 2001;12.6: 303-13.
3) Ehrlich, P.Beitrage zur Kenntnis der granulierten Bindegewebszellen und der eosinophilen leukocyten. *Archiv für Anatomie und Physiologie*1879*;* 3*:* 166–9.
4) Selye, H.The Mast Cells. *Washington, DC: Butterworths,* 1965.
5) Ronnberg, E., F. R. Melo, and G. Pejler. Mast Cell Proteoglycans. *J. Histochem. Cytochem.* 2012; 60.12: 950-62.
6) De Silva, E. Z., M. C. Jamur, and C. Oliver. Mast Cell Function: A New Vision of an Old Cell. *J. Histochem. Cytochem.* 2014; 62.10: 698-738.
7) Plaut, M., J. H. Pierce, C. J. Watson, J. Hanley-Hyde, R. P. Nordan, and W. E. Paul. Mast Cell Lines Produce Lymphokines in Response to Cross-linkage of FcεRI or to Calcium Ionophores. *Nature* 1989; 339.6219: 64-67.
8) Proud, D., G. Bailey, R. Naclerio, C. Reynolds, A. Cruz, P. Eggleston, L. Lichtenstein, and A. Togias. Tryptase and Histamine as Markers to Evaluate Mast Cell Activation during the Responses to Nasal Challenge with Allergen, Cold, Dry Air, and Hyperosmolar Solutions. *J. Allergy Clin. Immunol.* 1992; 89.6: 1098-110.
9) Bienenstock, J., M. Tomioka, H. Matsuda, R. H. Stead, G. Quinonez, G. T. Simon, M. D. Coughlin, and J. A. Denburg. The Role of Mast Cells in Inflammatory Processes: Evidence for Nerve/Mast Cell Interactions. *Int.Arch. Allergy Immunol.* 1987; 82.3-4: 238-43.
10) Kovacs, E.J.Fibrogenic cytokines: the role of immune mediators in the development of scar tissue. *Immunol. Today*1991*;* 12*:* 17–23.
11) Bressler, R.B., Lesko, J., Jones, M.L.*et al.*Production of IL-5 and granulocyte-macrophage colony-stimulating factor by naive human mast cells activated by high-affinity IgE receptor ligation. *J. Allergy Clin. Immunol.* 1997*;* 99*:* 508–514.
12) Benoist, C., and D. Mathis. Mast Cells in Autoimmune Disease. *Nature* 2002; 420.6917: 875-78.
13) Williams, C. M.m., and S. J. Galli. The Diverse Potential Effector and Immunoregulatory Roles of Mast Cells in Allergic Disease. *J. Allergy Clin. Immunol.* 2000; 105.5: 847-59.
14) Longley, J., T. P. Duffy, and S. Kohn. The Mast Cell and Mast Cell Disease. *J. Am. Acad. Dermatol.* 1995; 32.4: 545-61.
15) Allansmith, M. R., and R. N. Ross. Ocular Allergy and Mast Cell Stabilizers. *Surv. Ophthalmol.* 1986; 30.4: 229-44.
16) Serna, H., M. Porras, and P. Vergara. Mast Cell Stabilizer Ketotifen [4-(1-Methyl-4-piperidylidene)-4H-benzo[4,5]cyclohepta[1,2-b]thiophen-10(9H)-one Fumarate] Prevents Mucosal Mast Cell Hyperplasia and Intestinal Dysmotility in Experimental Trichinella Spiralis Inflammation in the Rat. *J. Pharmacol. Exp. Ther.* 319.3 (2006): 1104-111.
17) Rossi, S. *AMH 2004: Australian Medicines Handbook 2004*. Adelaide, S.A.: Australian Medicines Handbook Pty, 2004.

18) Patel HJ, Patel JS, Patel KD. Transdermal patch for ketotifen as asthmatic drug. *Int. J. PharmTech Res.* 2009;1.4: 1297-1304.
19) Guerrero, S., E. Muñíz, C. Teijón, R. Olmo, J. M. Teijón, and M. D. Blanco. Ketotifen-loaded Microspheres Prepared by Spray-drying Poly(D,L-lactide) and Poly(D,L-lactide--glycolide) Polymers: Characterization And evaluation. *J. Pharm. Sci.* 2008; 97.8: 3153-169.
20) Mcmenamin, P. G. The Distribution of Immune Cells in the Uveal Tract of the Normal Eye. *Eye* 1997; 11.2: 183-93.
21) Vannas, S. Mast Cells In Glaucomatous Eyes.*Acta Ophthalmol.* 37.4 (1959): 330-39.
22) Macleod, J. D. A., D. F. Anderson, S. M. Baddeley, S. T. Holgate, J. I. Mcgill, and W. R. Roche. Immunolocalization of Cytokines to Mast Cells in Normal and Allergic Conjunctiva. *Clin. Exp. Allergy* 1997; 27.11: 1328-334.
23) Venkatesh, S., J. Saha, S. Pass, and M. Byrne. Transport and Structural Analysis of Molecular Imprinted Hydrogels for Controlled Drug Delivery. *Eur. J. Pharm. Biopharm.* 2008; 69.3: 852-60.
24) Karlgard, C.c.s., N.s. Wong, L.w. Jones, and C. Moresoli. In Vitro Uptake and Release Studies of Ocular Pharmaceutical Agents by Silicon-containing and P-HEMA Hydrogel Contact Lens Materials. *Int. J. Pharm.* 2003; 257.1-2: 141-51.
25) Xu, J., X. Li, and F. Sun. In Vitro And In vivo evaluation of Ketotifen Fumarate-loaded Silicone Hydrogel Contact Lenses for Ocular Drug Delivery. *Drug Delivery* 2011; 18.2: 150-58.
26) Ali, M., S. Horikawa, S. Venkatesh, J. Saha, J. W. Hong, and M. E. Byrne. Zero-order Therapeutic Release from Imprinted Hydrogel Contact Lenses within in Vitro Physiological Ocular Tear Flow. *J. Controlled Release* 2007; 124.3: 154-62.
27) Ciolino, J. B., C. H. Dohlman, and D. S. Kohane. Contact Lenses for Drug Delivery. *Semin. Ophthalmol.* 2009; 24.3: 156-60.
28) Tieppo, A., C.j. White, A.c. Paine, M.l. Voyles, M.k. Mcbride, and M.e. Byrne. Sustained in Vivo Release from Imprinted Therapeutic Contact Lenses. *J. Controlled Release* 2012; 157.3: 391-97.
29) Guerrero, S., C. Teijón, E. Muñiz, J. M. Teijón, and M. D. Blanco. Characterization and in Vivo Evaluation of Ketotifen-loaded Chitosan Microspheres. *Carbohydr. Polym.* 2010; 79.4: 1006-013.
30) Ovchinnikov, D.A. Macrophages in the Embryo and Beyond: Much More than Just Giant Phagocytes. *Genesis*2008;46.9: 447-62.
31) Mosser, D.M., and J.P. Edwards. Exploring the Full Spectrum of Macrophage Activation. *Nat. Rev. Immunol.*2008;8.12: 958-69.
32) DiPietro, L. Wound Healing: The Role of Macrophages and Other Immune Cells. *Shock*1995;4.4: 233-40.
33) van Loon, S.L.M., A. I. P. M. Smits, A. Driessen-Mol, F. P. T. Baaijens and C. V. C. Bouten. The Immune Response in In Situ Tissue Engineering of Aortic Heart Valves, Calcific Aortic Valve Disease, Dr. Elena Aikawa (Ed.). 2013.
34) Griffin, F., Griffin, J., Leider,J., and S. Silverstein. Studies on the Mechanism of Phagocytosis.*J. Exp. Med.*1975;142: 1263-282.

35) Lam, J., M. Herant, M. Dembo, and V. Heinrich. Baseline Mechanical Characterization of J774 Macrophages. *Biophys. J.* 2009;96.1: 248-54.
36) Sica, A., and A. Mantovani. Macrophage Plasticity and Polarization: In Vivo Veritas.*J. Clin. Invest.*2012;122.3: 787-95.
37) Mantovani, A., A. Sica, S. Sozzani, P. Allavena, A. Vecchi, and M. Locati. The Chemokine System in Diverse Forms of Macrophage Activation and Polarization.*Trends Immunol.* 2004;25.12: 677-86.
38) Brodbeck, W.G., Y. Nakayama, T. Matsuda, E. Colton, N.P. Ziats, and J.M. Anderson. Biomaterial Surface Chemistry Dictates Adherent Monocyte/macrophage Cytokine Expression In Vitro. *Cytokine*2002;18.6: 311-19.
39) Jones, J.A., D.T. Chang, H. Meyerson, E. Colton, I.K. Kwon, T. Matsuda, and J.M. Anderson. Proteomic Analysis and Quantification of Cytokines and Chemokines from Biomaterial Surface-adherent Macrophages and Foreign Body Giant Cells.*J. Biomed. Mater. Res., Part A*2007;83A.3: 585-96.
40) Brodbeck, W. G. Biomaterial Adherent Macrophage Apoptosis Is Increased by Hydrophilic and Anionic Substrates In vivo.*Proc. Natl. Acad. Sci. U.S.A.*2002;99.16: 10287-0292.
41) Chen, S., J.A. Jones, Y. Xu, H.Y. Low, J.M. Anderson, and K.W. Leong. Characterization of Topographical Effects on Macrophage Behavior in a Foreign Body Response Model.*Biomaterials*2010;31.13: 3479-491.

Chapter 3. Electrostatically Self-assembled Biodegradable Microparticles From Pseudo-Proteins and Polysaccharide: Fabrication, Characterization and Biological Properties

Published: Potuck, Alicia N., Beth L. Weed, Cynthia A. Leifer, and C. C. Chu. "Electrostatically Self-Assembled Biodegradable Microparticles from Pseudoproteins and Polysaccharide: Fabrication, Characterization, and Biological Properties." Biomacromolecules 16.2 (2015): 564-77.

Abstract

Electrostatically self-assembling hybrid microparticles derived from novel cationic unsaturated arginine-based poly (ester amide) polymers (UArg-PEA) and anionic hyaluronic acid (HA) were fabricated into submicron sized particles in an aqueous medium with subsequent UV crosslinking treatment to stabilize the structure. These hybrid microparticles were characterized for size, charge, viscosity, chemical structure, morphology, and biological properties. Depending on the feed ratio of cationic UArg-PEA to anionic HA, the crosslinked microparticles formed spherical structures of 0.772 - 22.08 μm diameter, while the uncrosslinked microparticles formed a core with an outer petal-like structure of 2.49 - 15 μm diameter. It was discovered that the morphological structure of the self-assembled microparticles had a profound influence on their biological property. At a 1:1 feed ratio of UArg-PEA to HA, the uncrosslinked microparticles showed no cytotoxicity toward NIH 3T3 fibroblasts at concentrations up to 20 μg/mL, and the crosslinked particles exhibited no cytotoxicity at concentrations up to 10 μg/mL. The UArg-PEA/HA hybrid microparticles exhibited significantly lower macrophage-induced pro-inflammatory response (via TNF-alpha) than a pure hyaluronic acid control, while retaining the beneficial anti-inflammatory IL-10 production by HA. The UArg-PEA/HA microparticles also stimulated size-dependent induction of arginase activity. Therefore, self-assembling of these two types of biomaterials in a favorable non-toxic aqueous environment, having complementary biological properties like the currently reported UArg-PEA/HA hybrid microparticles, may provide a new class of biomaterials for improving overall tissue microenvironment promoting wound healing.

3.1 Introduction

Recent innovations in biomedical sciences and engineering are quickly catapulting nano and micron sized particles to the forefront of scientific advancements in the treatment of disease and improvement of wound healing. This is due in part to the unique characteristics of the particles: 1) small size (<10nm - > 50 μm in diameter), 2) high surface area, and 3) ability to locally or systemically deliver cargo. Much work has been done on fabricating and characterizing biodegradable nanoparticles from commercially available sources, such as polylactic acid, polyglycolic acid, and their copolymers[1], as well as delivery options, for example, topically [2] or via injection. [3] Although synthetic polymers have excellent *in vitro* and *in vivo* compatibility, fabrication often requires use of harsh organic solvents such as chloroform or benzene, potentially increasing *in vivo* toxicity. On the other hand, naturally-derived polymers like chitosan and dextran can be readily dissolved in aqueous solutions, eliminating the need for organic solvents and thus offering improved *in vivo* compatibility.

Hyaluronic acid (HA), a negatively-charged glycosaminoglycan polymer found in the extracellular matrix of living organisms, consists of two basic units: 1) D-glucuronic acid, and 2) D-N-acetylglucosamine.[4] HA is a strong candidate for use in biomimetic extracellular matrix wound healing models because of its excellent biorecognition as a naturally occurring polymer[5], collagen reduction capabilities, and ability to serve as an innate lubricant for tissue.[6] Attributed to its native occurrence in humans, and highly dependent on molecular weight of polymer fragments, HA exhibits excellent biocompatibility and anti-inflammatory properties.[7] In addition to its favourable interaction within the body, hyaluronidase enzymes will naturally degrade HA over time. Moreover, research has shown that

chemical conjugation[8] and photocrosslinking[9] methods have created successful HA particles for potential drug delivery applications.

A new family of polymers, amino-acid based poly(ester amide) (AA-PEA), have been developed using non-toxic starting materials (amino acids, fatty diols, and dicarboxylic acids)[10-14], which have been shown to have muted inflammatory characteristics.[15] Using fabrication techniques of emulsion, electrospinning, and photo-induced reaction, different physical forms of AA-PEA materials can be engineered for a variety of medical applications such as microspheres[16], fibrous membranes[17], and 3D microporous hybrid hydrogels with naturally-based polysaccharides[18-20], or commercially available polymers.[21-23] By varying the characteristics of the starting materials, both pendant[19,22,23] and backbone [18,21,26] double bonds can also be incorporated into the polymer to facilitate a photo-crosslinking approach to fabrication of AA-PEA based hybrid hydrogels. Native enzymes present in the body such as α-chymotrypsin and arginase aid in AA-PEA biodegradation, in conjunction with hydrolysis of esters present within the AA-PEA backbone.

Among the reported amino acids used to synthesize AA-PEAs, Arginine (Arg) is unique because it contains cationic charge and retains charge over a wide range of pH due to the pendant guanidine group with the highest pI value (10.76). Hence, Arg-based PEAs are cationic in physiological pH and are also water soluble.[24-26] Research has shown that using unsaturated arginine AA-PEA material and modified HA creates excellent hydrogels for drug delivery [19] with improved HeLa attachment and viability on hydrogel scaffolds, but no work has been reported about a facile and beneficial microparticle fabrication system from the hybrids of AA-PEA and HA.

Arginine-based AA-PEAs (Arg-PEAs) were chosen as a model of cationic unsaturated polymer due to their surface charge and inherent biological activity. Arg-PEAs have shown high biosafety (low cytotoxicity) at many concentrations, excellent cell adhesion, and high binding capacity toward plasmid DNA. [24,25] Owning to their cationic surface charge, Arg-PEAs had equivalent transfection efficiency as commercially available Superfect®, with notably reduced cytotoxicity.[26] Therefore, Arg-PEA characteristics of high solubility in polar solvents (such as water) and little/no cytotoxicity offers potential to facilitate biocompatibility via hybridization with commercial materials.

Upon interaction with biomaterials, many cell types including neutrophils, monocytes, and macrophages respond to initiate the acute phase of inflammation. Macrophages can acquire an M1 phenotype and release pro-inflammatory cytokines such as TNF-α and IL-1β that contribute to the foreign body response.[27] These macrophages are denoted as classically activated or "killer" macrophages. Macrophages can also adopt an M2 phenotype and promote wound healing and tissue repair. M2 macrophages, also called "alternatively activated" macrophages, are associated with reduced inflammation *in vivo*[28], increased arginase activation, and anti-inflammatory mediator production such as IL-10, TGF-β, and prostaglandin E_2.[29] These characteristics promote tissue repair, regeneration, and immune-regulation.[30] The anti-inflammatory cytokine IL-10 can both dampen inflammation caused by proinflammatory cytokines and lessen of matrix deposition, ultimately resulting in visibly reduced scar formation. [31, 32]

In this paper, we report the fabrication using cationic UArg-PEA and anionic HA polymers into micron and submicron size particles with a simple aqueous-based microparticle fabrication method. The resulting microparticles had inherent photo-reactive double bonds that could be photo-crosslinked to

achieve more stable microparticles. These self-assembled microparticles were characterized for their physical, chemical, and *in vitro* biological properties. These new microparticles exhibited muted inflammatory response, physical, and chemical characteristics that support their further testing in wound healing models.

3.2 Experimental

Materials

4-Nitrophenol, p-Toluenesulfonic Acid monohydrate, L-Arginine, and fumaryl chloride were purchased from Alfa Aesar (Hersham, UK). Triethylamine was purchased from Fischer Scientific (Fairlawn, NJ). Ethylene glycol was purchased from Mallinckrodt Chemicals (Phillipsburg, NJ). DMSO was purchased from VWR Scientific (West Chester, PA). Irgacure 2959 was purchased from Ciba Specialty Chemicals (Tarrytown, NY). All other reagents including hyaluronic acid (1000 kDa) were purchased from Sigma Aldrich (Milwaukee, WI, USA). All experiments used sterile filtered distilled water.

Synthesis and characterization of the Arg-based PEA

Unsaturated arginine-based poly(ester amide) polymers were synthesized using the previously reported method. [21, 26] Briefly, two monomers were synthesized; 1) di-p-Nitrophenyl ester of dicarboxylic acid (nucleophilic addition/elimination reaction of p-nitrophenol and fumaryl chloride), and 2) toluenesulfonic acid salt of bis(L-Arginine) ethyl diester (via esterification reaction of L-Arginine and ethylene glycol). These two monomers underwent solution polycondensation in DMSO at 70°C using triethylamine as an acid scavenger to form the final polymer. Unsaturated AA-PEA polymer was precipitated in cold ethyl acetate, allowed to purify for 24 hours, decanted and dried, re-dissolved in

methanol, and precipitated in ethyl acetate (process repeated 2x more). Final polymer was stored at 4°C until use. This polymer is designated as 2-UArg-PEA-2S (two referring to methylene length of fumarate, and two to length of diol used) and will further be referred to as UArg-PEA.

Fabrication of uncrosslinked UArg-PEA/HA microparticles

HA and UArg-PEA precursor solutions of pre-determined concentration were made by dissolving solid UArg-PEA polymer or powder HA to a final stock concentration (10mg/mL). UArg-PEA solution was a free flowing slightly yellowish solution, while HA solution was colorless and largely viscous. The aqueous suspension agent for polymer solutions (which were used for microparticle fabrication) was UV-treated, sterile-filtered distilled water.

Microparticle fabrication was completed by adding the two precursor solutions at predetermined ratios in a scintillation vial with contact stirring. For example, 1:1 UArg-PEA/HA hybrid microparticles were formulated by firstly adding HA (5mL of 10mg/mL stock solution) into a clean, UV sterilized scintillation vial. Stirring was applied at a rate of ~1000rpm. UArg-PEA (5mL of 10mg/mL stock solution) was then added dropwise over a course of approximately30 minutes, followed by stirring for an additional 30 minutes. Samples were lyophilized by freezing microparticle solutions at -20℃, followed by 48 hours lyophilisation at reduced pressure (0.08 torr) and temperature (-50℃) using Labconco Freeze Dry system (Labconco, Kansas City, MO, USA) and stored at a room temperature until use. All microparticle solutions exhibited a cloudy, slightly yellow opacity (prior to any microparticle precipitation).

Fabrication of UV crosslinked UArg-PEA/HA microparticles

Crosslinked hybrid microparticle solutions were prepared with predetermined feed ratios of UArg-PEA/HA, with the addition of Irgacure photo-initiator (15mg). The mixed solutions were then UV photocrosslinked using a long wavelength UV lamp (365 nm, 100 W) for 20 min. Final solutions were then lyophilized and stored for analysis. Crosslinked samples will be referred to using **XL** to denote UV-photocrosslinking.

Fluorescent Tagging UArg-PEA/HA microparticles

Dry, lyophilized UArg-PEA/HA microparticles were placed in a clean scintillation vial with stir bar. Sterile filtered distilled water was added into dry microparticles to reach a predetermined concentration (5mg/mL). After brief stirring to ensure proper suspension of microparticles in solution, fluorescein isothiocyanate (FITC) was added to the solution (covered to shield from light). The resulting solution was stirred four hours to ensure complete chemical modification of FITC to amine groups of UArg-PEA. FITC-labeled UArg-PEA/HA solutions were placed in dialysis tubes (Specta Biotech Cellulose ester dialysis membrane (100-500D) from Spectrum Laboratories, Rancho Dominguez, CA, USA) and dialyzed against distilled water for 48 hours. Dialysis was used to ensure the removal of unreacted FITC from microparticle solutions to facilitate better imaging capabilities and reduced *in vitro* toxicity. Microparticle suspensions were lyophilized at -50°C to acquire a dry powder which was stored in the dark at -20°C until use.

Material Characterization

UArg-PEA/HA microparticle chemical composition (~2-3mg lyophilized power) was analysed using ATIR (Nicolet Magna-IR 560, Nicolet Instrument Corp., Madison, WI, USA) Size and ζ-potential of the microparticles were analysed using Malvern Zetasizer Nano-ZS (Worcestershire, UK).

Morphology of microparticles and qualitative size was visualized with FEI F20 TEM STEM (FEI, Hillsboro, NJ, USA). For TEM imaging, microparticles were suspended in distilled water then deposited onto copper grids for imaging. Viscosity measurements were taken using TA-Instruments AR-2000 Rheometer (TA instruments, New Castle, DE, USA). Samples were prepared by placing approximately 500µl of aqueous hybrid microparticle solution or precursor on rheometer bottom plate with 20mm cone. Viscosity measurements were done at a rate of 0-90 1/s, in triplicate.

Cellular Imaging

RAW 264.7 mouse macrophage cells were cultured in complete DMEM (CDMEM, 10% low endotoxin fetal bovine serum (FBS), 10,000 IU/mL penicillin, 10,000 µg/mL streptomycin, 1mM Hepes, 200mM L-glutamine, and 100mM Sodium pyruvate) at 37°C with 5% CO_2. All media reagents were purchased from Mediatech (Manassas,VA, USA) except FBS, which was purchased from PAA Laboratories (Dartmouth, MA, USA).

For Confocal imaging, RAW264.7 macrophages were plated on UV sterilized 12mm round glass coverslips and 10µg/mL FITC-labelled UArg-PEA/HA microparticles were added. After 24 hours, cells were washed two times with Hanks buffered salt solution (HBSS) (Cellgro, Manassas, VA, USA), fixed with 3% paraformaldehyde, washed with phosphate buffered saline (PBS), stained for 15 minutes using Cell Mask Deep Red plasma membrane dye (10µL dye/10mL sterile 1x PBS) (Life Technologies, Grand Island, NY, USA), rinsed with PBS, and mounted glass slides using Prolong Anti-Fade Gold with DAPI (Life Technologies, Grand Island, NY, USA). Brightfield images were collected using a Leica SP5 confocal microscope with an oil immersion 63x objective. Images taken using Cell Mask plasma

membrane dye were taken using a 20x dry objective. All samples were imaged within 24 hours of slide mounting to prevent fading of fluorescent dyes.

Cellular Toxicity

NIH3T3 mouse embryonic fibroblast cells were cultured in complete DMEM and plated at 10,000 cells/well in a 96-well plate. Solutions of microparticles (1:1 UArg-PEA/HA and 1:1 UArg-PEA/HA XL) were suspended in complete DMEM, sonicated for 3 minutes to ensure reduction of aggregates, and added at predetermined concentrations (20μg/mL, 10μg/mL, 5μg/mL, or 0 ug/ml (control)) for 3 days. To assess toxicity, Cell Counting kit-8 (CCK-8 assay)(Sigma Aldrich, Milwaukee, WI, USA) reagent was added to each well (10μl CCK-8 reagent to 100μl CDMEM). After two hours, the assay plate was read at 450nm. Data were calculated using Prism and displayed as percent viability normalized to untreated control.

Macrophage Cytokine ELISA Assay

Supernatants from RAW 264.7 macrophages were collected 24 hours after incubation with 10μg/mL of the indicated hybrid microparticle or precursor solutions. Tumor necrosis factor alpha (TNF-α) and Interleukin 10 (IL-10) were measured using the corresponding ELISA Maxx mouse kit (Biolegend, San Diego, CA, USA) according to manufacturer's instructions. TMB substrate (KPL, Gaithersburg, MD, USA) was used for developing, and 2N H_2SO_4 solution was used to stop the reaction prior to reading the absorbance at 450nm. Recombinant cytokine was used to generate a standard curve, which was used to calculate cytokine concentrations by linear regression using Prism software.

Macrophage Nitric Oxide Assay

Supernatants from RAW 264.7 macrophages were collected 24 hours after incubation with 10μg/mL of the indicated hybrid microparticle or precursor solutions. The supernatants were assayed for nitrite using the Promega Griess Assay according to manufacturer's instructions (Promega, Madison, WI, USA). Sodium nitrite was used to generate a standard curve. Absorbance was read at 540nm, and the concentration of nitrite was calculated by linear regression using Prism Software.

Arginase Activity Assay

Supernatants from RAW 264.7 macrophages were collected 24 hours after incubation with 10μg/mL of the indicated hybrid microparticle or precursor solutions. Arginase activity was measured using an established protocol.[18]Urea was used to generate a standard curve, which was used to calculate arginase activity using linear regression and plotted using Prism, with absorbance read at 540nm.

Statistical Analysis

All data in tables and figures represent the mean ± standard deviation. All samples were tested for significance using one-way ANOVA and Tukey's honest significant difference post-hoc. The number of replicates tested (n) are given to provide reproducible independent data analysis. Statistically significant samples are denoted (*) when $p < 0.05$, (***) when $p < 0.01$.

3.3 Results and Discussion

Fabrication of UArg-PEA/HA self-assembled microparticles

Using the fabrication technique of aqueous electrostatic self-assembly, arginine-based poly(ester amide)/hyaluronic acid hybrid microparticles were fabricated based on two water soluble ionically-charged polymer precursors (Fig. 2). The feed ratio of these two charged precursor components (Fig. 3a) determines microparticle characteristics of size, surface charge, viscosity, and biological property. Based

on the amounts of cationic polymer (UArg-PEA) to anionic polymer (HA), the two polymeric precursors could self-assemble into uncrosslinked (Fig. 3b,c) or UV-induced photo-crosslinked microparticles (Fig. 3d). The use of a solely aqueous-based formulation of microparticles, and hence the elimination of harsh and toxic organic solvents, makes this fabrication process ideal for biomaterials.

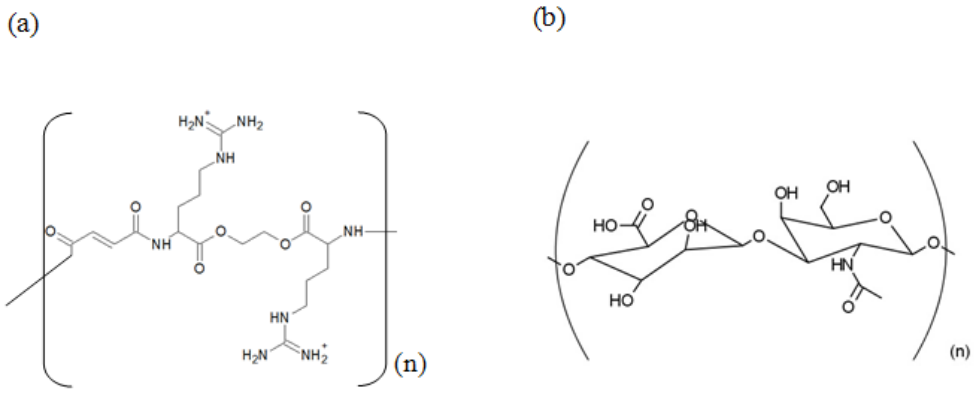

Figure 2. Chemical structures of (a) 2-UArg-PEA-2S poly(ester amide) (UArg-PEA), (b) Hyaluronic Acid (HA)

During the fabrication of UArg-PEA/HA microparticles, the formulations using 1:4, 1:2, and 1:1 of UArg-PEA to HA precursors feed ratios formed opaque solutions (Figure 4) with a light yellow color

with and without UV photocrosslinking (Figure 4c,e). The solutions with a larger feed ratio than 1:1 (i.e. larger content of UArg-PEA compared to HA) led to precipitation upon precursor mixing, with and without UV photocrosslinking (Figure 4d,f). Due to this precipitation problem, the solutions from 2:1 and 4:1 feed ratios were not characterized for viscosity, size, or surface charge, and the remainder of microparticle characterization was focused on the feed ratios of 1:1, 1:2, and 1:4 UArg-PEA to HA formulations.

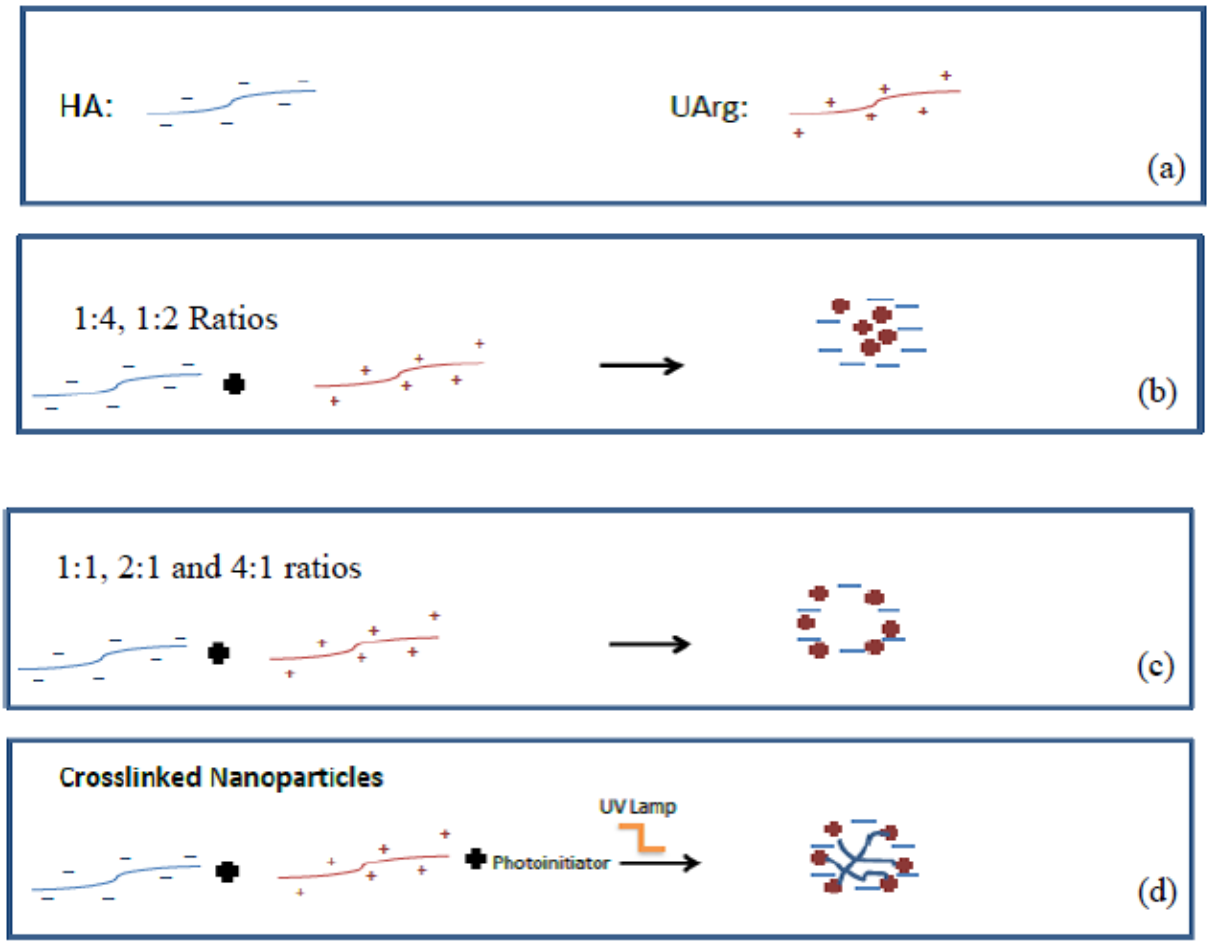

Figure 3. Schematic representations of the microparticles formulated at different feed ratio of UArg-PEA to HA precursors. (a) microparticle precursor components, (b) microparticle morphology from 1:4

and 1:2 feed ratios, (c) microparticle morphology from 1:1, 2:1 and 4:1 feed ratios (d) UV-Photocrosslinked (XL) microparticle morphology

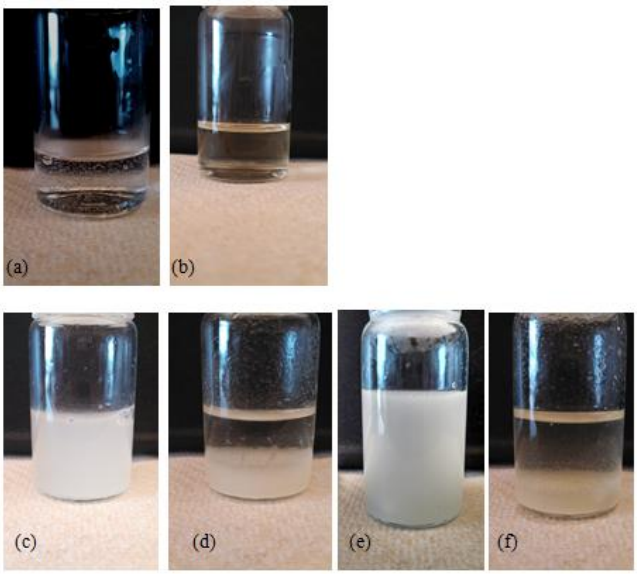

Figure 4. AqueousSolution mixtures of precursor solutions and hybrid microparticles, (a) 10mg/mL hyaluronic acid, (b) 10mg/mL 2-UArg-PEA-2S (denoted UArg-PEA), (c) 1:1 UArg-PEA/HA microparticle solution, (d) 2:1 UArg-PEA/HA microparticle solution, (e) 1:1 UArg-PEA/HA XL microparticle solution, (f) 2:1 UArg-PEA/HA XL microparticle solution

Material Characterization

ATIR Spectra of microparticles

UArg-PEA shows bands at 1648-1650cm^{-1}, 1540-1542cm^{-1}, 1735-1742cm^{-1}, and 3290cm^{-1} for carbonyl, amide II, ester, and NH vibrations, respectively. These data are consistent with previously reported work.[26] Hyaluronic acid spectra shows a peak in the 3500-3000cm^{-1} range representing O-H

stretching, coupled with NH stretching, attributed to N-acetyl. HA chemical structure also contributes amide I and amide II stretching modes, along with peaks at ~1612cm^{-1} and ~1415cm^{-1} for asymmetric and symmetric COO^- vibrations. [8]

Due to similarities in amide I and amide II peaks, as well as broad peaks above 3000cm^{-1}, carbonyl peak of UArg-PEA was used to characterize presence of AA-PEA polymer in the electrostatically formed microparticle. In all samples (both uncrosslinked and crosslinked), peaks for both HA and UArg-PEA were prominent, with the absorbance carbonyl peak of UArg-PEA at ~1735cm^{-1} [1] directly dependent on the feed ratio of the microparticle solutions. For example, while the carbonyl peak in microparticles formed at 1:4 UArg-PEA/HA feed ratio was present, it was almost indistinguishable compared to other characteristic peaks. Overlapping carbonyl peak of UArg-PEA in 1:1 UArg-PEA/HA microparticles was very clearly evident (Figure 5a).

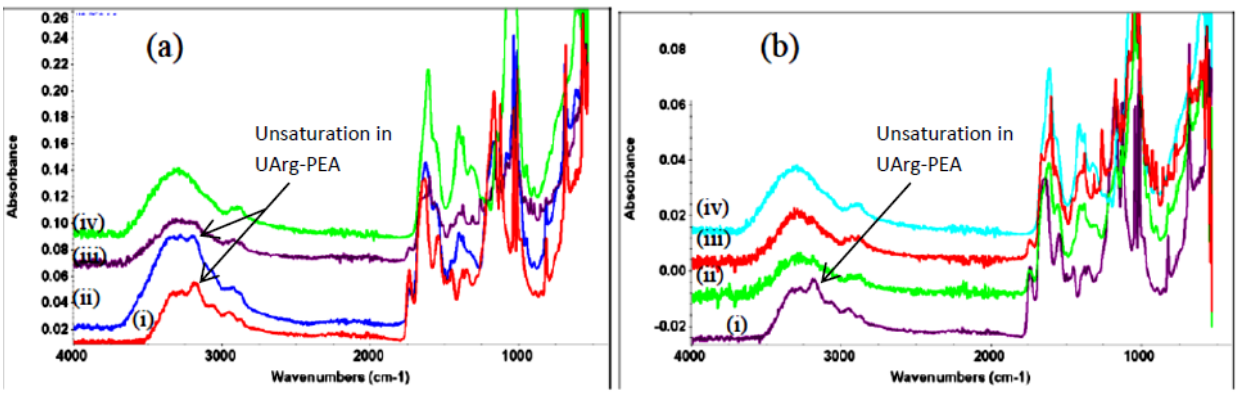

Figure 5. FTIR Spectra of UArg-PEA/HA self-assembled microparticles (a) 1:1 UArg-PEA/HA (ii) uncrosslinked and (iii) crosslinked, (b) 1:4ratio UArg-PEA/HA microparticles (ii) uncrosslinked and (iii) XL. In both spectra precursor polymers are included; (i) UArg-PEA and (iv) HA.

Infrared Spectroscopy was also used to verify crosslinking in hybrid microparticles. Some overlap in the 1680-1640cm^{-1} (C=C) is observed with UArg-PEA carbonyl peaks, therefore (=C-H) stretching mode near 3100cm^{-1} was used to identify the presence of unsaturation in UArg-PEA species (XL microparticles will result in saturation of C=C bond). For hybrid 1:1 UArg-PEA/HA microparticle samples, the presence of unsaturated carbon double bond is evident for non-crosslinked samples (3195cm^{-1}) but is absent in XL microparticles substantiating the hypothesis of successful crosslinking of microparticles (Figure 5B). Microparticles with higher feed ratios of HA to UArg-PEA (1:4 and 1:2 UArg-PEA/HA) did not exhibit loss of unsaturation (peak evident at 3195cm^{-1} in both uncrosslinked and crosslinked microparticles) after UV crosslinking indicating the concentration of UArg-PEA present in solution was too low to effectively create crosslinking sites (Figure 3b). Molecular weight differences in polymer precursors (HA 1000kDa and UArg-PEA 30-60 kg/mol) highly influence crosslinking behaviour, as HA high molecular weight severely hinders UArg-PEA ability to electrostatically interact with neighbouring chains upon mixing in uncrosslinked and XL 1:4 and 1:2 microparticle solutions. [19,26]

Viscosity of UArg-PEA/HA microparticle solutions

Precursors' and hybrid UArg-PEA/HA solutions were tested to determine the effect of feed ratio of UArg-PEA to HA on viscosity of microparticle solutions. The magnitude of viscosity difference between the two precursors (HA and UArg-PEA) at 10mg/mL stock solution is quite large, i.e., 0.6480 ± .015 vs. 0.0119 ± .004 Pa·s, respectively, with the viscosity of the hybrid microparticle solutions falling between these two precursors' viscosity values. Hatakeyama *et al* postulated that, attributing to high molecular weight and intermolecular forces, individual HA macromolecular domains overlap in an aqueous solution, leading to a high level of molecular entanglements and chain-chain interactions, i.e.,

resulting in increased solution viscosity.[4] The differences in precursor viscosity can be accredited to polymer dissolution in aqueous media; HA forms random coils which trap water within polymer chain coils (increasing solution viscosity), while UArg-PEA polymer chains do not form such high intermolecular forces, resulting in UArg-PEA solution viscosity similar to a pure water.

In this study, we determined the limit of UArg-PEA to HA feed ratio that could form microparticles effectively. The uncrosslinked UArg-PEA/HA microparticle solutions showed a direct correlation with HA feed ratio and viscosity (Fig. 6); as the feed ratio of HA to UArg-PEA increased, viscosity became more characteristic of the HA precursor. Similarly, increasing the feed ratio of UArg-PEA in microparticle formulations decreased the overall solution viscosity. This can be attributed to the low solution viscosity of the UArg-PEA precursor, as the viscosity is similar to that of pure water, increasing the feed ratio of UArg-PEA acted to decrease the overall solution viscosity, compared to the HA precursor alone. It is postulated that in uncrosslinked UArg-PEA/HA microparticle solutions, HA polymer chains assembled into hybrid microparticles could still maintain complex molecular entanglements causing the viscosity to remain high. The significant MW difference between UArg-PEA (30-60 kg/mol)[26]and HA (1 000 kDa) precursors may also be responsible for dictating electrostatic and viscosity characteristics of the hybrid microparticles. The uncrosslinked hybrid microparticle solutions maintained a much higher viscosity due to the much higher molecular weight anionic precursor HA that dominated solution property with significantly larger polymer chains and further chain-chain interactions.

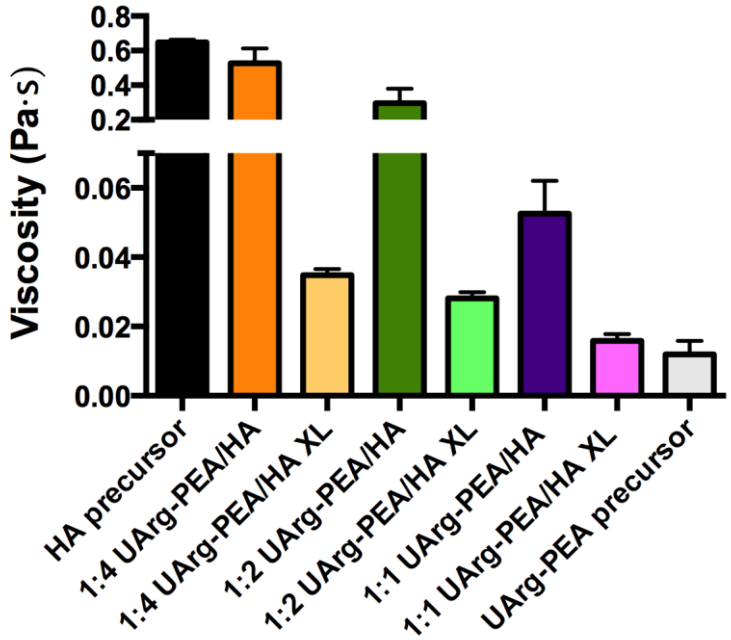

Figure 6. Viscosity measurements of uncrosslinked and crosslinked UArg-PEA/HA self-assembled microparticle solutions (in units of Pa·s) (All values are given as an average of three independent measurements ± std. dev) [2:1 and 4:1 UArg-PEA/HA not tested as precipitate formed].

The crosslinked UArg-PEA/HA-XL microparticles, however, showed lower solution viscosity than the corresponding uncrosslinked ones, and was closer to that of UArg-PEA precursor, even at high HA feed ratios. It is believed that the crosslinking process would bring polymer chains together to form a tighter and more compact network, contributing to a reduction in solution viscosity as shown in the UArg-PEA/HA XL microparticles. Hybrid microparticle solutions with the greatest feed ratio of UArg-PEA to HA (4:1, 2:1) exhibited prominent microparticle precipitation (in both XL and uncrosslinked samples), therefore accurate viscosity readings could not be obtained.

Size and ζ-potential of UArg-PEA/HA microparticles

Uncrosslinked hybrid microparticles had diameters between 2μm - 16μm attributed to anionic HA "petals" surrounding the UArg-PEA core (Table 1). The uncrosslinked hybrid microparticle formulations at lower UArg-PEA contents (i.e., UArg-PEA to HA feed ratios at 1:4 and 1:2) showed a slight decrease in microparticle diameter as the UArg-PEA contents increased (e.g., 7.4% size reduction from 1:4 to 1:2). Increasing UArg-PEA to HA feed ratio to 1:1 UArg-PEA/HA significantly reduced microparticle diameter when compared to 1:4 feed ratio (83% size reduction). This trend is a result of the reduced solution viscosity and a decrease in HA polymer chain-chain entanglements which can lead to a higher level of electrostatic interaction with UArg-PEA in self-assembly. Unlike the 1:1 UArg-PEA/HA feed ratio formulation, microparticles with a low UArg-PEA feed ratio to HA (1:4 and 1:2), did not show a decrease in size after UV photocrosslinking compared to uncrosslinked formulations, substantiating the hypothesis that these feed ratios do not have a high enough UArg-PEA unsaturation concentration to provide adequate level of >C=C< crosslinking sites for discrete microparticle formation. Rather, we postulate that microparticle formulations with a low UArg-PEA/HA feed ratio (1:2 and 1:4) promote microparticle aggregation via UArg-PEA crosslinking into branched or network, thus attributing to increased microparticle diameter after UV treatment.

Table 1. Size and Zeta Potential of uncrosslinked and crosslinked UArg-PEA/HA self-assembled microparticles[†]

Microparticles	Size (μm)		ζ-potential (mV)	
UArg-PEA/HA Feed Ratio	Uncrosslinked	Crosslinked (XL)	Uncrosslinked	Crosslinked (XL)
HA precursor	--	--	-80.80 ± 5.44	--
1:4	15.49 ± 0.28	22.08 ± 0.19	-44.0 ± 2.20	-37.2 ± 0.906
1:2	14.34 ± 0.20	20.08 ± 0.62	-38.50 ± 1.73	-33.20 ± 1.26
1:1	2.492 ± 0.03	0.772 ± 0.01	-41.90 ± 4.83	-29.90 ± 1.05
2:1	**	**	**	**
4:1	**	**	**	**
UArg-PEA precursor	--	--	11.10 ± 0.60	--

**Precipitate Formed

[†]All values are given as an average of three independent measurements ± std. dev

Charge balance or imbalance does have an effect on particle size, but our data indicate that crosslinking had a more profound effect than charge, e.g., 97% reduction by photocrosslinking (double bond density) vs. 86% reduction by charge only. Charge balance (or imbalance) becomes a leading factor upon application to biological systems, as cationic polymer such as UArg-PEA can interact with anionic cell membranes. Besides charge effect on microparticle size, we believe HA inter-chain entanglements and random coil behavior had a greater effect on microparticle size and formation than

charge interaction. For example, examining uncrosslinked versus crosslinked microparticle viscosity, disruption of HA coil structure via UArg-PEA crosslinking decreases overall solution viscosity, compared to their uncrosslinked counterparts.

To understand the morphological mechanism of electrostatic self-assembly of unsaturated arginine-based poly(ester amide)s and hyaluronic acid precursors, the surface charge of microparticles formed (ζ-potential in mV) was measured and the data are given in Table 1. Surface charges of the pure HA and UArg-PEA controls are -80.80 ± 5.44 and +11.10 ± 0.60 mV, respectively, while both XL and uncrosslinked hybrid microparticles have their ζ-potential between these two controls, ranging from -29 to -45 mV. It is interesting to recognize that the hybrid microparticles fabricated from the highest UArg-PEA contents without precipitation (i.e., 1:1 feed ratio) didn't reach positive ζ-potential, supporting the hypothesis that the HA forms an electronegative shell around the UArg-PEA core due to the significantly larger MW of HA precursor than UArg-PEA precursor. With an increase in the cationic UArg-PEA content (from 1:4, 1:2, to 1:1 feed ratios), the ζ-potential decreases in magnitude of negativity; however, the hybrid microparticles at the highest UArg-PEA contents without precipitation (1:1) still did not reach cationic character. Much like the viscosity data, the high molecular weight and vast chain-chain interactions of HA precursor influenced microparticle self-assembly. This trend is predominantly evidenced by hybrid microparticles (even at the highest UArg content) assembling with a net negative surface charge.

Previous literature has shown HA can be successfully incorporated into hybrid particles with excellent biological properties.[4-7] For example, Huang *et al* fabricated hybrid self-assembling poly (lactic glycolic) acid –hyaluronic acid nanoparticles (100-200nm range) with a surface charge of around -30mV

with excellent endocytosis and drug delivery capabilities. [33] Huang *et al* suggested that the excellent endocytic activity of poly(lactic glycolic) acid (PLGA)-hyaluronic acid nanoparticles assembled from PLGA-HA block copolymers could be due to a strong HA-CD44 surface receptor interaction.[33] Similar HA-CD44 receptor interaction in the current UArg-PEA/HA hybrid microparticles may also play a role as our macrophage endocytotsis data (described later) indicated that UArg-PEA/HA hybrid microparticles can be uptaken by macrophage. Native surface receptor interactions mitigate the concern of the anionic surface charge character of the UArg-PEA/HA hybrid microparticles which may lead to a less endocytosis due to an electrostatic repulsion between the negative charged UArg-PEA/HA hybrid microparticles and the negatively-charged cell phospholipid membranes.

Transmission electron Microscopic imaging of UArg-PEA/HA microparticles

TEM (Transmission Electron Microscopy) was used to characterize microparticle morphology using 1:1 UArg-PEA/HA and 1:1 UArg-PEA/HA XL microparticles. Uncrosslinked 1:1 UArg-PEA/HA hybrid microparticles self-assembled into a central core (postulated as UArg-PEA) with an outer petal-like structure (Figure 7a). The ζ- potential of 1:1 UArg-PEA/HA microparticles is negative (-41.9 mV) (Table 1), demonstrating the anionic precursor HA (rather than cationic UArg-PEA) is located near the surface of the microparticle formed, supporting a model where the outer petal-like structure is the HA. The crosslinked 1:1 UArg-PEA/HA XL samples, however, formed nicely rounded spheres (Figure 7b). A general schematic of hypothesized microparticle formation at different feed ratio of the two precursors is given in Figure 2.

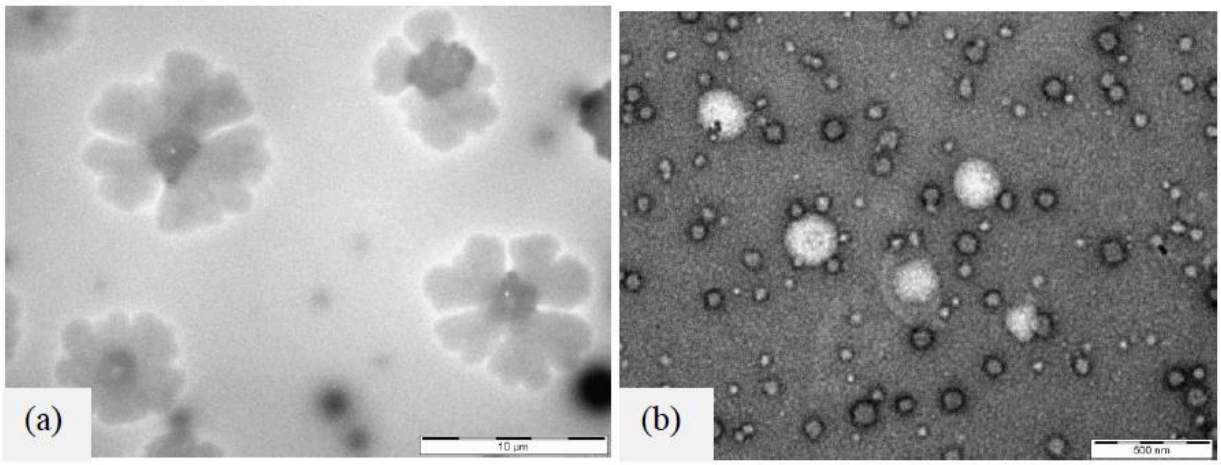

Figure 7. Morphology Imaging UArg-PEA/HA self-assembled microparticles (a) TEM image 1:1 ratio UArg-PEA/HA, (b) TEM image 1:1 ratio UArg-PEA/HA XL

Based on surface charge and morphology of UArg-PEA/HA hybrid microparticle data, we postulate that HA forms an anionic shell around cationic UArg-PEA polymers at the feed ratios studied. Upon dissolution in aqueous media, HA branched polymer chains can form a "random coil occupying molecular domain" which traps large amounts of water increasing the HA solution viscosity.[4] We hypothesize that self-assembly of uncrosslinked UArg-PEA/HA hybrid microparticles lead UArg-PEA to be encapsulated within HA random coils (since UArg-PEA has low viscosity far closer to pure water than HA), positioning HA on the outer shell of the hybrid microparticle. Contrasting uncrosslinked self-assembly of precursor polymers into petal-like structures, XL hybrid microparticles formed spherical structures attributed to UArg-PEA inter-chain crosslinking disruption of HA random coil shell, leading to reduced HA chain-chain interactions, characterized by reduced viscosity, size, and ζ-potential.

1:1 UArg-PEA/HA uncrosslinked and crosslinked microparticles formulation ratio demonstrated moderate viscosity, good solution interaction of the two polymer precursors, and ease in

characterization. Formulations with larger HA contents (1:4 and 1:2 UArg-PEA/HA) are not suitable as they did not show a high enough degree of crosslinking to form XL microparticles. The formulations with larger UArg-PEA content in the feed ratio (i.e., 1:1 and 2:1) were therefore used in macrophage cell culture characterization for the purposes of determining the overall effects of feed ratio of UArg-PEA to HA and crosslinking on macrophage stimulation.

Biological Response to UArg-PEA/HA microparticles

Cellular toxicity

To evaluate cell cytotoxicity, NIH3T3 mouse embryonic fibroblasts were incubated with 1:1 UArg-PEA/HA hybrid microparticles for 3 days. The 1:1 hybrid microparticles exhibited little to no toxicity at each microparticle concentration (20, 10, and 5 μg/mL) while the XL version of the same particles (1:1 UArg-PEA/HA XL) exhibited dose-dependent cytotoxic effects (Fig. 8). The NIH3T3 cells incubated with 1:1 UArg-PEA/HA XL particles at 5μl/mL had 84% viability, whereas increasing the concentration to 10μg/mL and 20μg/mL reduced NIH3T3 viability (65% and 64%, respectively).

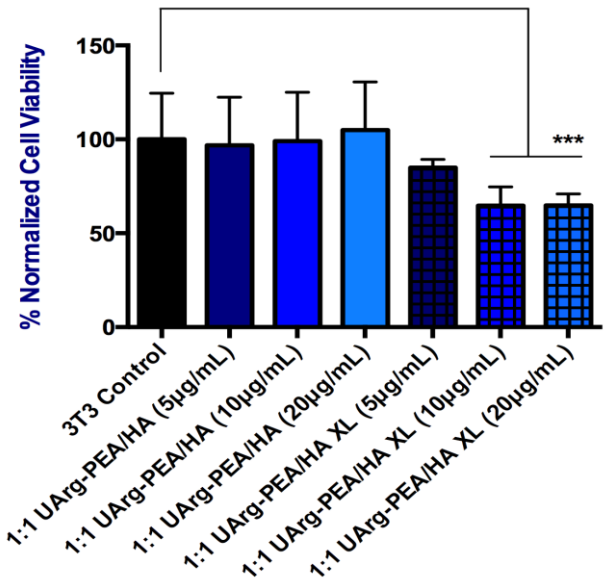

Figure 8. 3T3 Mouse Embroyonic Fibroblast Cell viability assay. All samples (n=3) were incubated for 3 days at 37°C and 5% CO_2 (results normalized to 3T3 control). Statistical significance given when $p < 0.01$, *** and $p < 0.05$, *.

Since a photoinitator was used to induce UV-photocrosslinking of XL microparticles, concern arises as to the influence on cytotoxicity as a result of residual unreacted photoinitiator present in XL microparticle formulations. Results for 3T3 fibroblast cytotoxicity indicate reduced viability of fibroblast cells with XL microparticles versus that of uncrosslinked microparticles. We believe the cytotoxicity at the higher concentration of the precursors (>/= 5 mg/mL of XL samples) might not be related to initiator based on two facts. First, although cytotoxicity data show a marked decrease in 3T3 fibroblast cell viability at 10µg/mL microparticle concentrations, but no additional reduction in cell viability at 20 µg/mL at a constant feed amount of initiator, an indication of theminimal effect of initiator. Secondly, the photoinitiator used, Irgacure 2959, has been proven to have minimal cytotoxicity to mammalian cells in literature[34-36]. Schuster *et al* advocate the use of Irgacure 2959 for its low toxicity (LD_{50}> 1g/kg) for use in photocrosslinking of biocompatible bone replacement materials.[35] Liska *et al* used a photinitiator

concentration as high as 1 wt% (vs. 0.15wt% in the present study) to ensure complete double bond conversion in soluble photopolymer applications, citing photoreactivity and biocompatibility as parameter in choice of photoinitiator.[36] Wu *et al* also used the same UV liable photoinitiator (Irgacure 2959) as utilized in this study at a ratio of 1% total polymer precursor weight to crosslink novel UArg-PEA/pluronic diacrylate hydrogels and found no toxicity from the crosslinked hydrogels to bovine aortic endothelial cells in using a conventional live/dead assay.[21] Therefore, those published studies suggest that the photoinitiator used in this study is indeed biocompatible and may not be the culprit in crosslinked microparticle 3T3 cytotoxicity.

Akin to the biocompatible photoinitiator used, pure and hybrid Arg-PEA polymers have been shown to have excellent *in vitro* compatibility with little/no cytotoxicity in rat aortic A10 smooth muscle cells (SMC). [24-26] A wide range of saturated and unsaturated Arg-PEAs stimulated A10 SMC growth with little/no detectable cytotoxicity at varying polymer concentrations (15-1500μg/mL); these Arg-PEAs also showed improved cell transfection with minimal or no cytotoxicity when compared to commercially available transfection agents (SuperFect®).[25,26] Wu *et al* also demonstrated excellent A10 SMC cell viability using both saturated Arg-PEAs (varying methylene chain length from 2 to 8) and unsaturated Arg-PEAs at both 4 and 48 hours incubation.[25] Similarly, Wu *et al* also found that by incorporating oligoethylene glycol into arginine-based AA-PEA synthesis to create Arg-PEEAs (amino acid based poly(ether ester amide)s, excellent cell viability of the new Arg-PEEAs could be achieved using many different cell types (bovine aortic endothelial cells, rat smooth muscle cells, and rat mesenchymal stem cells) with greater viability and transfection efficiency than commercially available agents.[37] Yamanouchi *et al* found using saturated Arg-PEAs (varying diol component in fabrication 2-

Arg-XS) excellent A10 SMC viability could be achieved at varying polymer-DNA ratios (500-9000x) for unsurpassed (nearly 100%) DNA delivery into A10 SMC cells via endocytosis mechanisms.[24] Overall, the family of arginine-based AA-PEAs shows excellent cell viability and proliferation over many cell types and material concentrations, thus indicating these materials are optimal candidates for use in medical applications.

Incorporation of arginine into a wide variety of AA-PEA polymers also improves cell performance. For instance, Phenylalanine-Arginine copolymer AA-PEAs exhibited excellent bovine aortic endothelial cell (BAEC) adhesion and viability with reduced proinflammatory cytokine production compared to the FDA approved poly(ϵ-caprolactone).[38] Arginine-based PEA's with pendant allyl glycine groups to provide photocrosslinkable function groups in AA-PEAs, also exhibited excellent biocompatibility with BAEC. [23]

Similarly, hyaluronic acid does not elicit a cytotoxic effect on cells. Burdick *et al* discovered, upon encapsulation in hyaluronic acid hydrogels, 3T3 fibroblasts maintained viability at HA concentration (2-5 wt%) and low compression modulus; but cell viability decreased with increasing HA concentration (10-20 wt%) and compression modulus due to increased crosslinking density leading to decreasing nutrient availability to cells.[39] In summary, both the UArg-PEA and HA precursors have been characterized to promote cell viability, with little/no toxicity. Therefore, upon microparticle fabrication, no cytotoxicity was observed at any concentration tested for uncrosslinked UArg-PEA/HA microparticles, while XL microparticles showed a dose-response behaviour.

Cellular uptake of particles

To measure the capability of macrophage uptake of these hybrid microparticles, the 1:1 UArg-PEA/HA hybrid microparticle solutions were labelled with FITC fluorescent dye. Since hyaluronic acid does not have amine sites for the dye conjugation, the resultant labelling of microparticles is on the UArg-PEA precursor. The XL microparticles (green) associated with, and were engulfed by, the RAW 264.7 macrophage cells (Figure 9c,f). Each macrophage phagocytosed multiple (>3-4) microparticles. In contrast, although the uncrosslinked microparticles (Figure 9b,e) associated with macrophages, they were poorly phagocytosed.

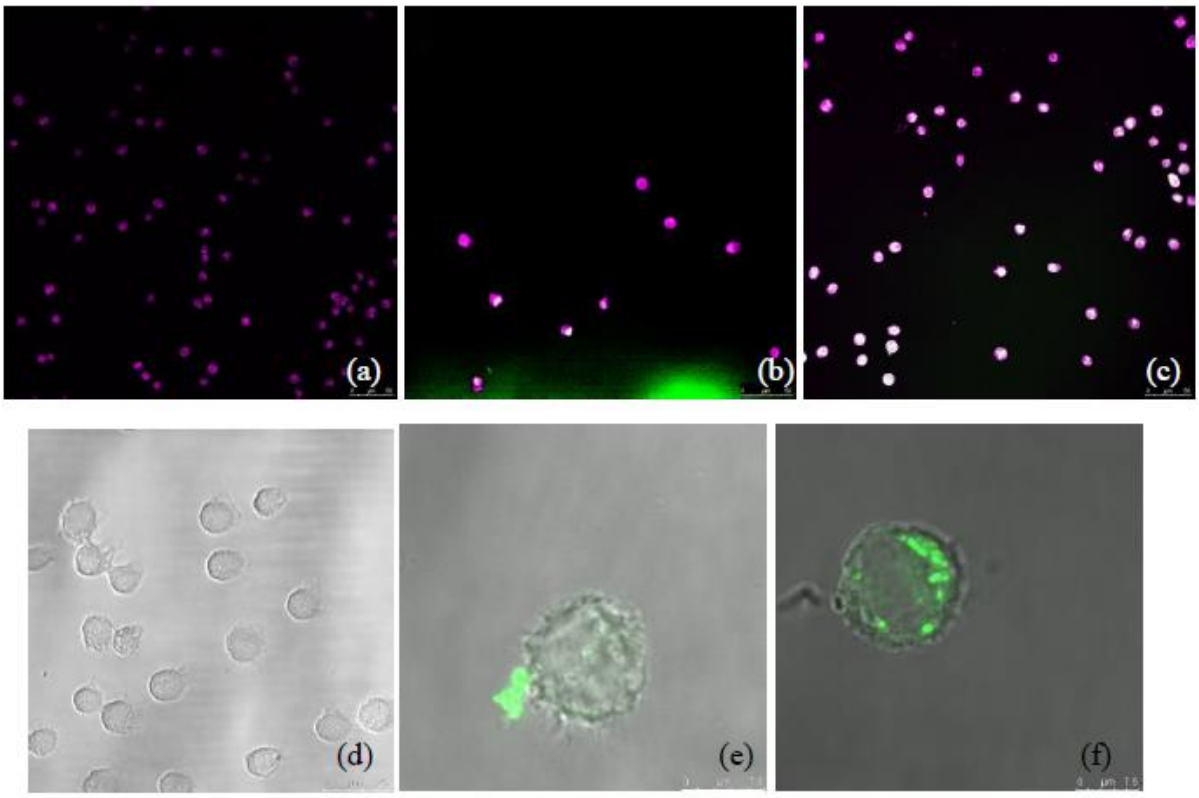

Figure 9. Microparticle uptake. RAW264.7 macrophage interactions with microparticles (Cy5 and FITC channels), (a) Confocal Image RAW macrophages (on glass, no microparticles) (b) Confocal Image RAW macrophages with FITC labeled 1:1 UArg-PEA/HA microparticles, (c) Confocal Image RAW macrophages with FITC labeled 1:1 UArg-PEA/HA XL microparticles, (d) Brightfield RAW cells

(on glass, no microparticles), (e) Brightfield with FITC labeled 1:1 UArg-PEA/HA microparticles (zoom), (f) Brightfield with FITC labeled 1:1 UArg-PEA/HA XL microparticles (zoom).

Limited phagocytosis of uncrosslinked microparticles may be attributed to the shape or cell's ability to attach to the self-assembled microparticles, as literature indicates facile endocytosis of nanoscale hybrid microparticles. Huang *et al* have shown excellent uptake of nano-scale HA-shell PLGA-HA nanoparticles (100-200nm, labelled with coumarin-6) by MCF-7 cancer cells via the interaction with the HA-CD44 receptors, while the PLGA nanoparticle control showed notably reduced phagocytosis.[33] Similarly, HA nanoparticles with surface functionalized polyethylene glycol containing UV crosslinking capabilities (~200-300nm, to deliver drug payload) are easily taken up by SCC7 rat squamous cell carcinoma for delivery of paclitaxel.[9]

Limited endocytosis of uncrosslinked hybrid microparticles may also be a factor of surface morphology of the microparticles. Balazs *et al* discovered that highly purified sodium hyaluronate inhibits phagocytosis by macrophages, limiting particle uptake.[40] They suggested that the inhibition of macrophage uptake by sodium hyaluronate was not a factor of electrostatic charge, but rather dictated by both steric hindrance as a result of large molecular weight chains and disruption of cell-microparticle interaction adhesive surface.[40] Therefore, the large HA petal-like shell on the exterior of the uncrosslinked hybrid microparticles could discourage macrophage cells from efficient endocytosis of the uncrosslinked UArg-PEA/HA hybrid microparticles. Contrastingly, the crosslinked UArg-PEA/HA hybrid microparticles have decreased HA presence on the hybrid microparticle surface with increased availability to UArg-PEA, and hence inducing higher macrophage endocytosis. The lower negative zeta

potential data in the crosslinked UArg-PEA/HA hybrid microparticles (Table 1) also support this argument.

Proinflammatory (TNF-α) Cytokine Production

Tumor necrosis factor alpha (TNF-α) is a proinflammatory cytokine whose production *in vitro* correlates with the inflammatory activity of biomaterials *in vivo*. RAW 264.7 macrophages were incubated with four different hybrid microparticle formulations (1:1 and1:1 XL UArg-PEA/HA, 2:1 and 2:1 XL UArg-PEA/HA). Hyaluronic acid precursor (positive control) induced the highest TNF-α secretion, consistent with glycosaminoglycan/macrophage TLR receptor interaction.[41] In contrast, the UArg-PEA precursor did not induce TNF-α secretion when compared to unstimulated control cells (Figure 10). These results are consistent with the findings of Wu *et al* study of Phe-PEA and poly(caprolactone) (PCL) hybrids.[15] They reported that the chemical conjugation of Phe-PEA into poly(caprolactone) (PCL) led to a reduction in the inflammatory response by macrophages when compared to a pure PCL.[15] Wu *et al* also demonstrated reduced J774 macrophage TNF-α cytokine production in Phe-Arginine based AA-PEA copolymers when compared to commercially available PCL and PMBA polymers, indicating the muted inflammatory response characteristics of AA-PEAs.[38]

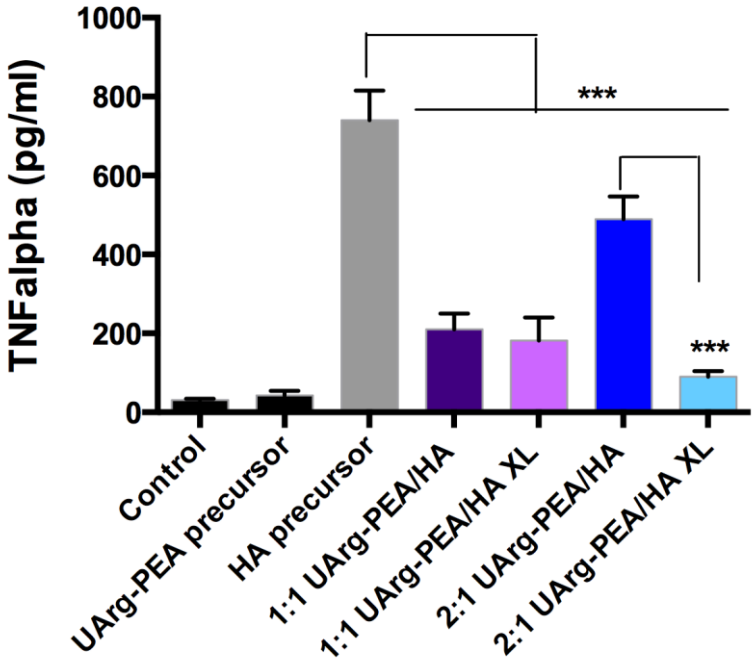

Figure 10. Microparticle-induced TNF-α production. All samples (precursors and hybrid microparticle solutions) were assayed in triplicate at 10 μg/mL incubation with macrophage cells for 24 hours. Control is macrophage on tissue culture plate (no stimulation). Values represented as average ± std. dev. Statistical significance given when $p < 0.01$, *** and $p< 0.05$, *.

Incorporating UArg-PEA into HA in the hybrid microparticles significantly reduced TNF-α stimulation when compared to the pure HA precursor alone, and the level of reduction depended on the feed ratio and crosslinking treatment. Although both feed ratio formulations (1:1 and2:1) uncrosslinked hybrid microparticles significantly reduced TNF-α release from the pure HA, the 1:1 feed ratio formulation had a far more significant reduction than the 2:1 feed ratio formulation (71% reduction at 1:1 ratio vs. 34% reduction at2:1 ratio). The effectiveness of reducing TNF-α production upon increasing UArg-PEA contents (1:1 vs.2:1 feed ratio) could be limited by macrophage access to UArg-PEA in electrostatically self-assembled structure, where an HA anionic shell masks muted inflammatory property of UArg-PEA which was trapped within the HA random coil structure.

The crosslinked 1:1 XL hybrid microparticles showed no statistically significant reduction in TNF-α production compared to the corresponding uncrosslinked hybrid microparticle at the 1:1 feed ratio formulation. UV-photocrosslinking treatment had a far more significant effect in reducing TNF-α production at the higher UArg-PEA contents, i.e., 2:1 feed ratio formulation. For example, the 2:1 XL microparticles showed 87% reductionin TNF-α production, while the uncrosslinked one at the same feed ratio formulation showed only a 51% reduction.

In the crosslinked hybrid microparticles, an increase in the UArg-PEA contents from 1:1 XL to 2:1 XL feed ratio reduced TNF-α secretion over 50%, indicating the inherently low inflammatory UArg-PEA species could become more accessible to macrophage at the 2:1 feed ratio formulation. This is likely because the more UArg-PEA contents at the 2:1 feed ratio could provide more crosslinking level and hence more disruption of the surrounding HA random coil structure, i.e., allowing more macrophage access to the cationic UArg-PEA component.

To investigate the stimulation of cytokine response, examination of precursor behaviour is key. HA biological functions largely depend on HA molecular weight.[41]For example, Neumann *et al* reported that relatively high molecular weight HA (1.2 Kda) suppresses inflammation, while low molecular weight (0.2-0.5 Kda) HA stimulates proinflammatory cytokine production. [42] HA stimulates TLRs (Toll Like Receptors, TLR4, TLR2), which trigger downstream production of inflammatory cytokines and chemokines.[43] TLR stimulation by HA is consistent with the findings of this work as high molecular weight HA (1000 Kda) stimulated the highest cytokine response.

Jones *et al* studied biomaterial induced macrophage cytokine production in great detail and discovered hydrophilic/anionic polymer materials such as PAANa (poly (ethylene terephathlate) (PET)

grafted with the sodium salt of acrylic acid) produced low levels of a potent proinflammatory cytokine IL-1β[44] (IL-1β is commonly found in pro-inflammatory responses similar to TNF-α[45]) when compared to hydrophobic (PET), hydrophilic/neutral (PET grafted with acrylamide), and hydrophilic/cationic surfaces (PET grafted with methyl iodide salt of N-[3-(dimethylamino)propyl] acrylamide). We hypothesize that, despite low proinflammatory cytokine production found by Jones *et al* for hydrophilic/anionic materials, high TNF-α stimulation of hydrophilic/anionic HA is a result of receptor interaction of naturally-occurring GAG polymers rather than adhesion effects of synthetic polymers leading to increased cytokine production. Similar to the findings of our work, Jones *et al* concluded that surface characteristics such as hydrophilicity and charge influence macrophage mediator production.[44] Paralleling surface properties, UV crosslinked UArg-PEA/HA microparticles exhibited reduced inflammatory properties, indicating feed ratio of UArg-PEA to HA, surface properties, and microparticle morphology (due to the crosslinking treatment) could influence proinflammatory cytokine production.

Nitric Oxide Assay

Nitric oxide is a reactive gas produced by macrophages that contributes to host defence and wound healing. Compared to the untreated control RAW 264.7 cells, neither the pure precursors alone (UArg-PEA and HA) nor the UArg-PEA/HA hybrid microparticles showed statistically significant NO· production at either feed ratio (1:1 or 2:1) with or without crosslinking at a concentration consistent with that assayed for cytokine production (10μg/mL) (data not shown). Therefore, UArg-PEA/HA hybrid microparticles reduce TNF-α cytokine stimulation without additional activation of the iNOS pathway. These results are consistent with the findings of Lyle *et al*, as nitric oxide production by murine macrophage cells incubated with HA (2mg/mL) against stimulation (LPS or LPS + IFN-ɣ) produced

little to no additional nitric oxide compared to untreated control, indicating low reactive nitrogen species production by HA. [32]

This lack of the effect on NO production from both precursors and their hybrid microparticles is different from other types of Arg-PEA hybrids. For example, He *et al* reported that UArg-PEA/chitosan hybrid hydrogels decreased nitric oxide production when compared to pure chitosan hydrogels[18], suggesting that the type of polysaccharides and the nature of the hybrid (i.e., hydrogels vs. self-assembled microparticles) could affect NO production level by macrophage. We conclude that hybrid materials with Arg-PEAs are excellent candidates for use in biomaterial applications due to low or reduce nitric oxide production.

Anti-inflammatory (IL-10) Cytokine Production

Figure 11 shows the beneficial anti-inflammatory IL-10 production by macrophage of the self-assembled UArg-PEA/HA hybrid microparticles and their precursors. All testing samples produced significantly higher IL-10 than the blank control. For example, pure HA precursor control induced IL-10 cytokine production many fold greater than the blank control, and is consistent with findings in other studies[45,46](Fig. 11). Biswas *et al* postulated that HA can stimulate not only inflammatory cytokine production (TNF-α), but also anti-inflammatory cytokine through CD44 receptor activation via the TIRF pathway[47], which is consistent with the elevated level of TNF-α observed through TLR stimulation with IL-10 upregulation. Brodbeck *et al* characterized similar increased anti-inflammatory response for hydrophilic anionic materials; they found increased IL-10 cytokine production using polyacrylamide and a sodium salt of poly(acrylic acid), compared to a hydrophobic neutral control (poly(benzyl N,N-diethyldithiocarbamateco-styrene).[48] They suggest that decreased macrophage fusion and increased

apoptosis on hydrophilic/anionic biomaterials correspond to decreased IL-8 and increased IL-10 production versus hydrophilic/cationic surfaces.[48] Therefore, analysis of the surface characteristics of both UArg-PEA and HA precursors and their hybrid microparticle is imperative to understanding stimulation of cellular cytokine response.

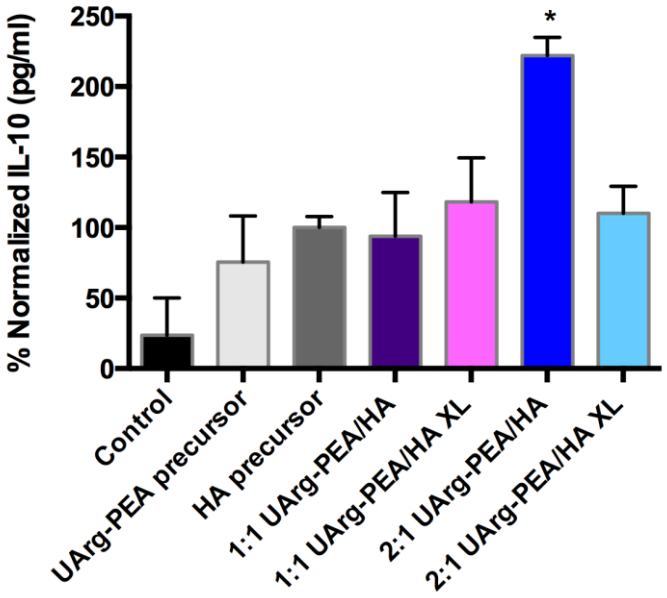

Figure 11. Microparticle-induced IL-10 production. All samples (precursors and hybrid microparticle solutions) were assayed in triplicate at 10 μg/mL incubation with macrophage cells for 24 hours. Control is macrophage on tissue culture plate (no stimulation). All values normalized to HA precursor. Values represented as average ± std. dev. Statistical significance given when $p < 0.01$, *** and $p < 0.05$, *.

In the current study, no statistical difference in IL-10 production was found among HA, UArg-PEA precursors, and their hybrid microparticles, except the 2:1 UArg-PEA/HA sample. The mean IL-10 values (excluding the 2:1 UArg-PEA/HA) ranged from 75% to 120% when normalized to HA (compared to < 25% IL-10 production of untreated control), and these data indicate the level of IL-10 cytokine production was mostly not dependent on size or/and overall surface charge of the two polymer precursors and hybrid microparticles.

The hybrid microparticles at a 2:1 UArg-PEA feed ratio elicited a statistically significant ($p < 0.05$) increase in IL-10 cytokine production when compared to HA and UArg-PEA precursors and other hybrid microparticles, suggesting that this particularly formulated feed ratio is optimal for producing IL-10 anti-inflammatory cytokine. Although the 2:1 UArg-PEA/HA microparticles could not be characterized for size/ζ-potential due to precipitation during fabrication, the increase in IL-10 production is likely attributed to decreased size and less negative surface charge compared to the 1:1 UArg-PEA hybrid microparticles. Although cell viability has been extensively studied in a variety of pure and hybrid Arg-PEA systems[19,21-26], this is the first time IL-10 cytokine production has been reported for the Arg-based PEA biomaterials.

Both UArg-PEA and hybrid UArg-PEA/HA microparticles stimulated IL-10 cytokine production equivalent to HA. Hyaluronic acid is capable of stimulating IL-10 production, essential to mitigating proinflammatory responses and promoting tissue repair.[29,49] Jones *et al* found that the use of synthetic hydrophilic/anionic PAANa grafted PET increased levels of IL-10 production[44], similar to the current study that hydrophilic and anionic HA can also stimulate IL-10 production). Much like stimulation of TNF-α pro-inflammatory cytokine production, it is postulated that, in addition to the hydrophilic and

anionic factors that stimulate IL-10 production as reported in literature[44], HA used in the present study differs from synthetic PAANa grafted PET in that HA is a natural biopolymer which has HA--receptor interactions that the synthetic polyacrylic acid salt grafted PET lacked. Therefore, the IL-10 cytokine stimulation by HA in both its pure precursor form and its UArg-PEA hybrid microparticles form is based on many factors; i.e., hydrophilic, anionic, and HA-reception interactions.

Upregulation of IL-10 production can be indicative of the phenotypic shift of macrophages from M1 (proinflammatory) to M2 (wound healing) promoting early stage tissue regeneration and repair.[50] The IL-10 cytokine data from the UArg-PEA/HA hybrid microparticles in this study indicate that the presence of UArg-PEA species does not hinder the favourable IL-10 production by HA in hybrid microparticle interactions. This is beneficial to overall wound healing as researchers have found IL-10 plays a key role in muting proinflammatory response (in particular, detrimental effects of proinflammatory cytokines such as TNF-α and IL-1β).[47,51] As shown in Fig. 8 TNF-α data, the UArg-PEA species can also have the benefit of reducing TNF-alpha proinflammatory cytokine production from the HA species. Therefore, due to the HA's inherent opposite dual proinflammatory (via TNF-alpha) and beneficial wound healing (via IL-10), the UArg-PEA/HA hybrids would create an overall beneficial synergistic effects of reduced proinflammatory cytokine and promoting production of desirable anti-inflammatory cytokine for improved wound healing.

Arginase activity Assay

The arginase activity stimulated through the interaction between macrophage cells and microparticle components depended on type of the precursors and the hybrid microparticle composition. As shown in Figure 12, the arginase activity data indicate distinct trends based on the hybrid

microparticle morphology and composition; 1) uncrosslinked hybrid microparticles stimulated significantly less [1:1 ($p < 0.01$) and 2:1 ($p < 0.05$)] arginase activity than a pure HA precursor; 2) 2:1 XL hybrid microparticles stimulated statistically higher arginase activity than the uncrosslinked at the same formulation ratio ($p < 0.01$); and 3) both pure UArg-PEA and HA precursors produced similar levels of arginase activity. Notably, both feed ratio formulations of the uncrosslinked hybrid microparticles stimulated a statistically significant reduction in arginase activity when compared to the HA control (27.5% and 23.2% for 1:1 and 2:1, respectively). No statistically significant decrease in arginase activity was observed when comparing uncrosslinked microparticles (1:1 and 2:1) to the UArg-PEA precursor, largely due to standard deviation in UArg-PEA precursor sample values. The crosslinked 1:1 UArg-PEA/HA XL hybrid microparticles induced arginase activity comparable to HA precursor, while uncrosslinked one at the same feed ratio formulation resulted in a decrease in arginase activity.

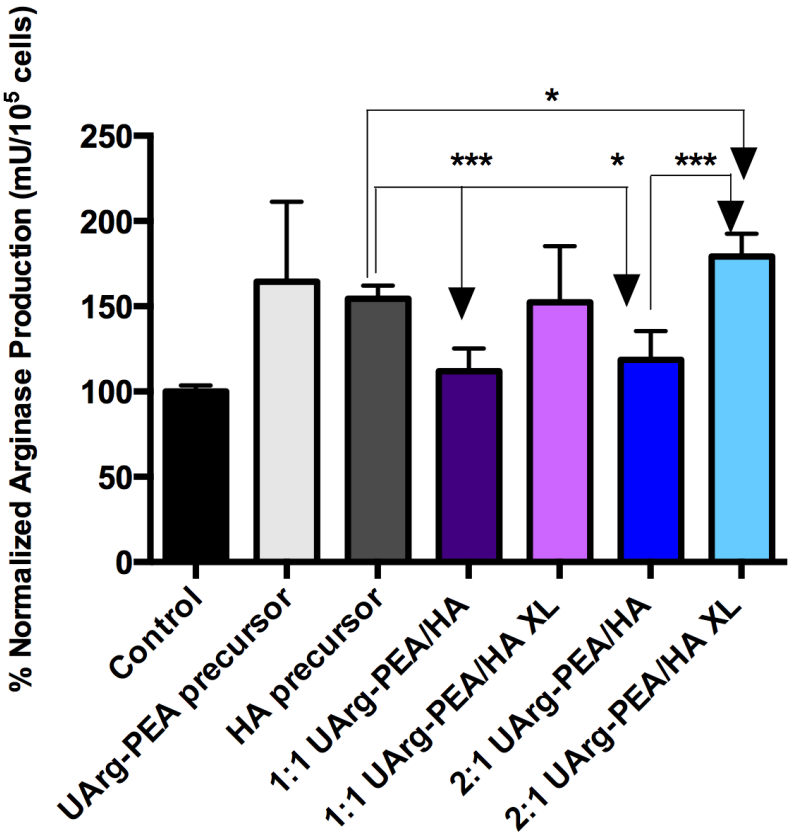

Figure 12. Microparticle induced macrophage arginase activity. All samples (precursors and hybrid microparticle solutions) were assayed in triplicate at 10 μg/mL incubation with macrophage cells for 24 hours. Values represented as average ± std. dev. Statistical significance given when $p < 0.01$, *** and $p < 0.05$, *.

The data in Fig. 12 also shows that the 2:1 UArg-PEA/HA XL hybrid microparticles induced the highest arginase activity. We hypothesize this could be a result of the increasing availability of UArg-PEA at this particular formulation to macrophage cells upon endocytosis. As shown in Fig. 9, the smaller crosslinked UArg-PEA/HA XL hybrid microparticles were endocytosed more efficiently than the uncrosslinked microparticles at the same formulation feed ratio. As L-Arginine is a potent substrate of the arginase pathway, hybrid microparticles having larger UArg-PEA contents like 2:1 formulation

potentially increase availability of arginine species to macrophage via crosslinked form, leading to increased production via the arginase pathway. A comparison of arginase data between XL and uncrosslinked microparticles at the 2:1 feed ratio clearly indicate the crosslinked (or XL) hybrid microparticle fabrication method could allow increased arginine availability or access to macrophage for its proper arginase activity. We postulate that the uncrosslinked 2:1 UArg-PEA/HA microparticles could form an anionic HA shell similar to the uncrosslinked 1:1 UArg-PEA/HA microparticles; consequently, resulting in no statistically significant increase in arginase activity due to an increase in UArg-PEA content compared with the 1:1 UArg-PEA/HA uncrosslinked microparticles. This trend suggests the HA anionic shell may mask beneficial arginine contents in UArg-PEA and hence discourage macrophage from producing arginase.

Previous research in arginase activity of hybrid polysaccharide-based/Arg-PEA biomaterials had shown similar results[18]; UArg-PEA polymers and their hybrid hydrogels with modified chitosan stimulated more arginase activity than a pure chitosan.For example, He *et al* has shown that not only a pure UArg-PEAs increased arginase activity (> 20 mU/10^5cells) over the untreated macrophage cells (< 20 mU/10^5 cells), but also the UArg-PEA/chitosan hybrid hydrogels significantly increased arginase activity (~40 mU/10^5cells) when compared to pure chitosan-based hydrogels (< 20 mU/10^5 cells).[18] Furthermore, the hydrolysed arginine-based AA-PEA precursor and hybrid hydrogel byproducts stimulated even greater arginase activity (~50 mU/10^5 cells and ~60 mU/10^5 cells, respectively) than their non-degraded counterparts, indicating hydrolyzed products of Arg-based polymers could make arginine more available to macrophages. Therefore, He *et al* suggested that the use of Arg-based polymers or their hybrids may not only sustain but prolong wound healing via arginase upregulation by

macrophage cells.[18] The Arginase activity data from the He *et al* study[18] are consistent with the findings of the current study which uses UArg-PEAs/HA hybrid microparticles, indicating UArg-PEA or its presence in hybrid microparticles can increase the stimulation of the arginase pathway, which is expected to promote M2 macrophage functionality, a beneficial phenomenon for proper wound healing. These data indicate the potential benefits for the UArg-PEA precursor and its hybrids like the current UArg-PEA/HA microparticles formulations in a wound healing environment; a future *in vivo* study would be required to validate such potential benefits in a wound healing model.

3.4 Conclusions

Using the principle of electrostatic self-assembly, cationic unsaturated arginine-based poly (ester amide) polymers (UArg-PEA) and anionic Hyaluronic acid (HA) were fabricated into micron and sub-micron hybrid particles (0.77 to 22.1 μm diameter) in a non-toxic aqueous medium. Unique morphology for each uncrosslinked (floral micron sized sphere) and -XL (sub-micron scale spheres) hybrid microparticles were observed. Rheology data indicated high viscosity from the uncrosslinked hybrid microparticle due to the HA polymer chain entanglements, while the crosslinked hybrid microparticle solutions had viscosity similar to UArg-PEA in solution.

These new UArg-PEA/HA hybrid microparticles induced low TNF-α and NO·, with excellent arginase and IL-10 levels from RAW 264.7 macrophages, consistent with low M1 and high M2 promoting ability. The crosslinked (XL) hybrid microparticles had their surface charge shifted more toward neutral (i.e., less negative) than the corresponding uncrosslinked ones. These unique morphological characteristics make the XL hybrid microparticles more easily engulfed by macrophage, and exhibit a lower inflammatory profile. In all, these new UArg-PEA/HA hybrid microparticles

exhibited excellent biocompatibility and performance *in vitro*. All results support the hypothesis that UArg-PEA-based hybrid microparticles may be the excellent candidates for reducing macrophage inflammatory response in wound healing.

AUTHOR INFORMATION

Corresponding Author

*To whom correspondence should be addressed. Tel.: (1-607) 255-1938; e-mail: cc62@cornell.edu

Author Contributions

The manuscript was written through contributions of all authors. All authors have given approval to the final version of the manuscript.

Funding Sources

This study was partially supported by the grant from the Becky Q. Morgan Foundation to Chu and its assistantship to Potuck.

ACKNOWLEDGMENT

The authors would like to thank the Becky Q. Morgan Foundation for their financial support in terms of fellowship to Potuck and research funds to Chu. The authors would also like to acknowledge Jody Lopez and Siddhartha Sinha of the Leifer Lab for their input and expertise on cell culture protocol and analysis. Many thanks to Ying Ji for her excellent TEM imaging. This work made use of the Cornell Center for Materials Research Facilities supported by the National Science Foundation under Award Number DMR-1120296.

REFERENCES

(1) Soppimath, K.; Aminabhavi, T.; Kulkarni, A.; Rudzinski W. Biodegradable polymeric nanoparticles as drug delivery devices. *J. Controlled Release* **2001**,*70*, 1-20.

(2) Alvarez-Roma´n, R.; Naik, A.; KaliaY.; Guy, R.; Fessi, H. Enhancement of topical delivery from biodegradable nanoparticles. *Pharm. Res.* **2004**, *21.10*, 1818-1825.

(3) Gou, M.; Li, X.; Dai, M.; Gong, C.; Wang, X.; Xie, Y.; Deng, H.X.; Chen, L.; Zhao, X.; Qian, Z.; Wei, Y. A novel injectable local hydrophobic drug delivery system: Biodegradable nanoparticles in thermo-sensitive hydrogel. *Int. J. Pharm. (Amsterdam, Neth).* **2008**,*359.1-2*, 228-33.

(4) *Hatakeyama, H.; Hatakeyama, T. Interaction between water and hydrophilic polymers.* Thermochim. Acta **1998**, *308.1-2*, 3-22.

(5) Iannitti, T.; Bingöl, A.; Rottigni, V.; Palmieri, B. A new highly viscoelastic hyaluronic acid gel: rheological properties, biocompatibility and clinical investigation in esthetic and restorative surgery. *Int. J. Pharm. (Amsterdam, Neth).***2013**, *456.2*, 583-592.

(6) Laurent, T.; Laurent, U.; Robert, J.; Fraser, E. The structure and function of hyaluronan: An overview. *Immunol. Cell Biol.* **1996**, *74.2*, A1-A7.

(7) Necas, J.; Bartosikova, L.; Brauner, P.; Kolar, J. Hyaluronic acid (hyaluronan): a review.*Vet. Med. (Prague, Czech Repub.)* **2008**,*53.8*, 397-411.

(8) Choi, K.; Kwon, I.; Choi, K.; Park, J.; Kim, K.;Na, J.; Min, K.; Jeong S. Self-assembled hyaluronic acid nanoparticles as a potential drug carrier for cancer therapy: synthesis, characterization, and *in vivo* biodistribution. *J. Mater. Chem.* **2009**,*19*, 4102-4107.

(9) Yoon, H.; Koo, H.; Choi, K.; Kwon, I.; Choi, K.; Park, J.; Kim, K. Photo-crosslinked hyaluronic acid nanoparticles with improved stability for in vivo tumor-targeted drug delivery. *Biomaterials***2013**, *21*, 5273-5280.

(10) Katsarava, R.; Beridze, V.; Kharadze, D.; Chu C.C.; Won, Y.; Arabuli, N. Amino Acid Based Bioanalogous Polymers. Synthesis and Study of Regular Poly (ester amide)sBased on Bis(a-amino acid) α, ω-alkylene Diesters and Aliphatic Dicarboxylic Acids. *J. Biomater. Sci., Polym. Ed.* **1999**, *37*, 391-407.

(11) Jokhadze, G.; Machaidze, M.; Panosyan, H.; Chu, C.C.; Katsarava, R. Synthesis and characterization of functional elastomeric poly(ester amide) co-polymers. *J. Biomater. Sci., Polym. Ed.* **2007**, *18.4*, 411-438.

(12) Chu, C.C.; Katsarava, R. Elastomer Functional Biodegradable Copolyester Amides and Copolyester Urethanes. US Patent, 6503538, January 7, **2003**.

(13)Tsitlanadze, G.; Machaidze, M.; Kviria T.; Djavakhishvili, N.; Chu, C.C.; Katsarava. Biodegradation of amino-acid-based poly(ester amide)s: in vitro weight loss and preliminary in vivo studies. *J. Biomater. Sci., Polym. Ed.* **2004**,*15.1*, 1-24.

(14) Deng, M.; Wu, J.; Reinhart-King, C.A.; Chu, C.C. Synthesis and characterization of biodegradable poly(ester amide)s with pendant amine functional groups and in vitro cellular response. *Biomacromolecules* **2009**,*10.11*, 3037-3047.

(15) Wu, J.; Chu, C.C. Block copolymer of poly(ester amide) and polyesters: synthesis, characterization, and in vitro cellular response. *Acta Biomater.* **2012**,*8.12*, 4314-4323.
(16) Guo, K.; Chu, C.C. Biodegradable and injectable paclitaxel-loaded poly(ester amide)s microspheres: fabrication and characterization. *J. Biomed. Mater. Res., Part B* **2009**,*89B.2*, 491-500.
(17) Li, L.; Chu, C.C. Nitroxyl Radical Incorporated Electrospun Biodegradable Poly(ester amide) Nanofibrous Membranes. *J. Biomater. Sci., Polym. Ed.***2009**, *20.3*, 341-361.
(18) He, M.; Potuck, A.; Zhang, Y; Chu, C.C. Arginine-based polyester amide/polysaccharide hydrogels and their biological response. *Acta Biomater.***2014**, *10.6*, 2482-2494.
(19) Wu, D.; Wu, J.; Chu C.C. A novel family of biodegradable hybrid hydrogels from arginine-based poly (ester amide) and hyaluronic acid precursors. *Soft Matter***2013**, *9*, 3965-3975.
(20) Zhong, C.; Wu, J.; Reinhart-King, C.A.; Chu, C.C. Synthesis, characterization and cytotoxicity of photo-crosslinked maleic chitosan-polyethylene glycol diacrylate hybrid hydrogels. *Acta Biomater.***2010**,*6.10*, 3908-3918.
(21) Wu, J.; Wu, D.; Mutschler, M.; Chu, C.C. Cationic Hybrid Hydrogels from Amino-Acid-Based Poly (ester amide): Fabrication, Characterization, and Biological Properties. *Adv. Funct. Mater.* **2012**, *22.18*, 3815-3823.
(22) Pang, X.; Wu, J.; Reinhart-King, C.A.; Chu, C.C. Synthesis and characterization of functionalized water soluble cationic poly (ester amide) s. *J. Polym. Sci., Part A: Polym. Chem.* **2010**, *48.17*, 3758-3766.
(23) Pang, X.; Wu, J.; Chu, C.C.; Chen, X. Development of an arginine-based cationic hydrogel platform: Synthesis, characterization and biomedical applications. *Acta Biomater.***2014**,*10*, 3098-3107.
(24) Yamanouchi, D.; Wu, J.; Lazar, A.; Kent, C.; Chu, C.C.; Liu, B. Biodegradable arginine-based poly(ester-amide)s as non-viral gene delivery reagents. *Biomaterials* **2008**,*29.22*, 3269-3277.
(25) Wu, J.; Mutschler, M.; Chu, C.C. Synthesis and characterization of ionic charged water soluble arginine-based poly(ester amide). *J. Mater. Sci.: Mater. Med.***2011**, *22.3*, 469-479.
(26) Song, H.; Chu, C.C. Synthesis and Characterization of A New Family of Cationic Poly(ester amide)s and Their Biological Properties. *J. Appl. Polym. Sci*. **2012**, *124.5*, 3840-3853.
(27) Anderson, J.M.; Rodriguez, A.; Chang, D.T. Foreign body reaction to biomaterials.*SeminImmunol.* **2008**, *4.20*, 86-100.
(28) Soehnlein, O.; Lindbom, L. Phagocyte partnership during the onset and resolution of inflammation. *Nat. Rev. Immunol.* **2010**, *6.10*, 427-439.
(29) Huang, T.; Hsu, H.C.; Yang, K.C.; Lin, F.H. Hyaluronan up-regulates IL-10 expression in fibroblast-like synoviocytes from patients with tibia plateau fracture. *J. Orthop. Res.***2011**, *29.4*, 495-500.
(30) Van Loon, S.L.M.; Smits, A.I.P.M.; Driessen-Mol, A.; Baaijens, F.P.T.; Bouten C.V.C. *Calcific Aortic ValveDisease*, Intech, Rijeka, Croatia **2008**.

(31) Nichols, S.P.; Koh, A.; Brown, N.L.; Rose, M.B.; Sun, B.; Slomberg, D.L.; Riccio, D.A.; Klitzman, B.; Schoenfisch, J. The effect of nitric oxide surface flux on the foreign body response to subcutaneous implants. *Biomaterials***2012**, *33.27*, 6305-6312.

(32) Lyle, D.; Breger, J.; Baeva, L.; Shallcross, J.; Durfor, C.; Wang, N.S.; Langone, J. Low molecular weight hyaluronic acid effects on murine macrophage nitric oxide production. *J. Biomed. Mater. Res., Part A***2010**, *94A.3*, 893-904.

(33) Huang, J.; Zhang, H.; Yu, Y.; Chen, Y.; Wang, D.; Zhang, G.; Zhou, G.; Liu, J.; Sun, Z.; Lu, Y.; Zhong, Y. Biodegradable self-assembled nanoparticles of poly (D,L-lactide-co-glycolide)/hyaluronic acid block copolymers for target delivery of docetaxel to breast cancer. *Biomaterials* **2014**, *35.1*, 550-566.

(34) Williams, C. G.; Malik, A.N.; Kim, T.K.; Manson, P.N.; Elisseeff. J.H. Variable Cytocompatibility of Six Cell Lines with Photoinitiators Used for Polymerizing Hydrogels and Cell Encapsulation. *Biomaterials***2005**, *26.11*, 1211-218.

(35) Schuster, M.; Turecek, C.; Kaiser, B.; Stampfl, J.; Liska, R.; Varga, F. Evaluation of Biocompatible Photopolymers I: Photoreactivity and Mechanical Properties of Reactive Diluents. *J. Macromol. Sci., Part A: Pure Appl.Chem.* **2007**, *44.5*, 547-57.

(36) Liska, R.; Schuster, M.; Inführ, R.; Turecek, C.; Fritscher, C.; Seidl, B.; Schmidt, V.; Kuna, L.; Haase, A.; Varga, F.; Lichtenegger, H.; Stampfl. J. Photopolymers for Rapid Prototyping. *J. Coat. Technol. Res.* **2007**, *4.4*, 505-10.

(37) Wu, J.; Yamanouchi, D.; Liu, B.; Chu, C.C. Biodegradable arginine-based poly (ether ester amide) s as a non-viral DNA delivery vector and their structure–function study. *J. Mater. Chem.***2012**, *22.36*, 18983-18991.

(38) Wu, J.; Chu, C.C. Water insoluble cationic poly (ester amide) s: synthesis, characterization and applications. *J. Mater. Chem. B***2013**, *1.3*, 353-360.

(39) Burdick, J. A.; Chung, C.; Jia, X.; Randolph, M.A.; and Langer, R. Controlled degradation and mechanical behavior of photopolymerized hyaluronic acid networks. *Biomacromolecules***2005**, *6.1*, 386-91.

(40) Balazs, E. A.; Forrester, J.V. Inhibition of phagocytosis by high molecular weight hyaluronate. *Immunology***1980**, *40*, 435-46.

(41) Gotoh, S.; Onaya, J.; Abe, M,; Miyazaki, K.; Hamai, A.; Horie, K.; Tokuyasu, K. Effects of the molecular weight of hyaluronic acid and its action mechanisms on experimental joint pain in rats. *Ann. Rheum. Dis.***1993**, *52.11*, 817-22.

(42) Neumann, A.; Schinzel, R.; Palm, D.; Riederer, P.; Münch, G. High molecular weight hyaluronic acid inhibits advanced glycation endproduct-induced NF-kappaB activation and cytokine expression. *FEBS Lett.***1999**,*453.3*, 283-87.

(43) Moreland, L. Intra-articular hyaluronan (hyaluronic acid) and hylans for the treatment of osteoarthritis: mechanisms of action. *Arthritis Res. Ther.* **2003**, *5.2*, 54-67.

(44) Jones, J. A.; Chang, D.T.; Meyerson, H.; Colton, E.; Kwon, I.K.; Matsuda, T.; Anderson, J.M. Proteomic analysis and quantification of cytokines and chemokines from biomaterial surface-adherent macrophages and foreign body giant cells. *J. Biomed. Mater. Res., Part A***2007**, *83A.3*, 585-96.

(45) Saperstein, S.; Chen, L.; Oakes, D.; Pryhuber, G.; Finkelstein, J. IL-1beta augments TNF-alpha-mediated inflammatory responses from lung epithelial cells. *J. Interferon Cytokine Res.***2009**, *29.5*, 273-284.

(46) Deng, B.; Wehling-Henricks, M.;Villalta, A.; Wang, Y.; Tidball, J. IL-10 triggers changes in macrophage phenotype that promote muscle growth and regeneration. *J. Immunol.***2012**, *189.7*, 3669-3680.

(47) Biswas, S. K.; Lopez-Collazo, E. Endotoxin tolerance: new mechanisms, molecules and clinical significance. *Trends Immunol.***2009**, *30.10*, 475-87.

(48) Brodbeck, W.G.; Nakayama, Y.; Matsuda, T.; Colton, E.; Ziats, N.P.; Anderson, J.M. Biomaterial surface chemistry dictates adherent monocyte/macrophage cytokine expression in vitro. *Cytokine***2002**, *18.6*, 311-19.

(49) Jiang, D.; Liang, J.; Noble, P.W. Hyaluronan as an immune regulator in human diseases. *Physiol. Rev.* **2011**,*91.1*, 221-264.

(50) Takeda, K.; Kaisho, T.; Akira, S. Toll-like receptors. *Annu. Rev. Immunol.***2003**, *21.1*, 335-76.

(51) Chang, C.; Liao, J.; Kuo, L. Arginase modulates nitric oxide production in activated macrophages. *Am. J. Physiol.***1998**,*274*, H342-H348.

Chapter 4. Ketotifen Fumarate incorporated elastomeric biodegradable Poly (ester amide) three-dimensional membranes for improved wound healing via mast cell stabilization

(In Preparation – proposed June 2015) Potuck, Alicia, Ashley Weiner, Marcus Wilkes, and C. C. Chu. Ketotifen Fumarate Incorporated Elastomeric Biodegradable Poly (ester Amide) Three-dimensional Membranes for Improved Wound Healing via Mast Cell Stabilization. Acta Biomaterialia

Abstract

Amino acid based poly(ester amide) (AA-PEA) nanoscale fibers were fabricated using electrospinning techniques with a chloroform/DMF solvent mixture, giving excellent fiber properties and deposition. Ketotifen fumarate (KF) was added to AA-PEA polymer solutions as a dopant and electrospun to give drug encapsulated fibers.Both three-dimensional amorphous electrospun fibers and two dimensional semi-crystalline solvent cast films were used to measure drug release over time, to understand how material morphology affects drug release and degradation. Sustained release of KF over a one month incubation time in PBS at 37°C (with and without enzymatic degradation) was observed. After 30 days incubation, AA-PEA electrospun fiber glass transition temperature sample Tg increased 58% on average, while the solvent cast sample Tg decreased 10%. AA-PEA electrospun fibers maintained HeLa viability and muted macrophage activation (TNF, NO) comparable to commercial control, with significant RBL-2H3 reduction of degranulation through KF release. Therefore, these new AA-PEA fibrous membrane biomaterials show excellent potential for long term sustained release of KF for uses in wound healing applications.

4.1 Introduction

In recent years, electrospinning has become a versatile technique for fabricating micro and nanoscale fibers from polymer solutions to form three dimensional fibrous membranes. This method is comprised of three main components; 1) polymer solutions loaded into capillary or syringe, 2) high voltage source, 3) collection apparatus. Fibers are formed as the solvent in the polymer solution evaporates in the electric field, depositing solid drawn fibers randomly on the collection plate.[1,2] Due to their unique morphology and properties to mimic physiological extracellular matrix composition, micro and nano-scale electrospun fibers have been extensively studied for their potential in tissue engineering and wound healing care.[3-6] Electrospun fibers can be fabricated from commercially available materials such as poly lactic acid (PLA), poly glycolic acid (PGA), and their copolymers, offering excellent biocompatibility, biodegradation (hydrolytic degradation), and mechanical properties.[7-9] Electrospun nanoscale fibers can be functionalized to deliver DNA[10], proteins[11,12], and drugs.[13-15] Moreover, Wang *et al* have demonstrated natural products such as chitosan and starch could be electrospun into fibers and used as a drug delivery system, decreasing the likelihood of pronounced foreign body response by having physiological biorecognition.[16]

Using principles of biocompatibility, biodegradation, and biorecognition, a family of polymers has been developed based on three non-toxic starting materials; naturally occurring α-amino acids, fatty diols, and dicarboxylic acids.[17-20] Amino acid-based poly(ester amide)s (AA-PEAs) have favourable characteristics of both ester and amide linkages in the polymer backbone, giving excellent mechanical properties found in aliphatic polyamides, as well as hydrolytic degradation characteristics of

polyesters.[21,22] Based on starting amino acids and synthesis variations, properties of AA-PEA polymers can be tailored to have neutral charge[18], cationic charge via incorporation of arginine amino acid offering excellent cell adhesion and viability[23-26], unsaturation for UV photocrosslinking[19,27], and pendant amine[28] or hydroxyl[29]groups for functionalization. Furthermore, based on fabrication technique, AA-PEA polymers can be made into microspheres[30], fibers[31], and hydrogels[32-35]for applied biomedical devices.

Many of the AA-PEA polymer materials (in particular the phenylalanine-based polymers) have excellent solubility in many common organic solvents such as Chloroform and DMF and can be easily made into solutions with appropriate viscosity for electrospinning.[17] Phe-based AA-PEA polymers have shown excellent cell adhesion[36] with ability to mute inflammatory response when incorporated into commercial materials.[37] Li *et al* have shown that such Phe-based AA-PEA materials create fibers of approximately 640nm in diameter[31] which can undergo enzymatic degradation *in vitro*[21] to create a sustainable biodegradable drug delivery system for nitric oxide.

All foreign body materials exert an influence on the microenvironment in which they are used. To understand this, it is crucial to analyze which types of cells and their functions are of interest. For example, mast cells are commonly found in wound sites and are implicated in contributing to all phases of wound healing; 1) inflammation, 2) tissue deposition, and 3) tissue remodelling.[38] In the early stages of wound healing, mast cells release or "degranulate" soluble mediators that, in conjunction with macrophage cells, promote wound debridement and inflammatory response.[39] One such mediator, histamine, causes inflammation, redness, and vasodilation upon release, symptoms associated with allergic reaction.[40] Studies suggest high levels of inflammation hinder wound repair and can ultimately

lead to increased collagen deposition and fibrosis.[39]Therefore, incorporating agents within biomedical devices to stabilize, or prevent mast cell degranulation, would lead to improved wound healing. Ketotifen fumarate (KF), a benzocyclohepatathiopene compound, acts as an anti-histamine and mast cell stabilizer used to treat allergies, asthma, and inflammatory conditions and has been studied in wound healing.[41,42] Ketotifen fumarate has poor oral bioavailability (50%) due to first pass metabolism by the liver, and therefore cannot be delivered easily by conventional methods.[43] Ketotifen fumarate specifically targets mast cells (leukocyte cell line) characterized to degranulate proinflammatory mediators such as histamine, cytokines, and chemotactic factors upon stimulation.[44] Research focusing on KF release from varying polymeric devices including microspheres[45], patches[43], and ocular lenses[46-48] strives to reduce mast cell inflammatory response.

Paralleling examination of mast cell behaviour, macrophage cells also heavily influence wound healing response. Macrophages have the ability to display different phenotypic behaviors; 1) M1 (classically activated), characterized for release of proinflammatory mediators such as TNF-α and IL-6, 2) M2 (alternatively activated), characterized for promoting wound healing through release of IL-4, IL-10, and stimulation of arginase.[49] Biomaterials themselves, including properties such as hydrophobicity and surface charge, dictate macrophage response.[50] Hence, this provides the opportunity to tune polymeric biomedical devices to stimulate wound healing while muting inflammatory response.

Drug encapsulation of KF within AA-PEA nanofibers utilizes advantages of excellent mechanical properties of phenylalanine-based poly(ester amide) materials while providing pendant phenylalanine groups as scission points for enzymatic degradation. This paper presents a facile method for fabrication, characterization, and biological response to nanoscale KF-doped AA-PEA fibers. Developing a novel

sustained release delivery system of ketotifen fumarate for wound healing would serve a two-fold benefit: improve the bioavailability of ketotifen fumarate and provide a site of action application for reducing inflammation in wound healing.

4.2 Methods and Materials

L-Phenylalanine, dimethylacetamide (DMAc), and 4-Nitrophenol were purchased from Alfa Aesar (Hersham, UK). Toluene was purchased from Avantor Performance Materials, Inc. (Center Valley, PA, USA). Ethyl acetate was purchased from Fischer Scientific (Fair Lawn, NJ, USA). PDLLA was a kind gift from the Frey Lab (FSAD, Cornell University) (Natureworks, LLC, Minnetonka, MN, USA). Ketotifen fumarate was purchased from Enzo Life Sciences (Farmingdale, NY, USA). Enzyme α-chymotrypsin (from bovine pancreas; ≥ 40 units/mg protein), P-toluenesulfonic acid,1,4-butanediol, sebacoyl chloride and all other chemicals were purchased from Sigma Aldrich (Milwaukee, WI, USA) and used as received.

AA-PEA Polymer Fabrication

Using previously reported methods[18], 8-Phe-4 polymer (8 referring to the methylene chain length in amide linkage, and 4 to that of ester linkage) was synthesized (Mw= 27,770 g/mol). AA-PEA synthesis occurred via solution polycondensation in DMAc from two starting monomers; p-toluenesulfonic acid salt of L-phenylalanine 1,4-diester and di-nitrophenyl sebacate. Briefly, equal molar ratio of two starting monomers were added to 500mL round bottom flask with DMAc and stirred at 70℃ for 48 hours with triethylamine as an acid scavenger. 8-Phe-4 polymer was precipitated into cold ethyl acetate for purification (24 hours at 4℃), vacuum collected, re-dissolved in chloroform, and re-precipitated in ethyl acetate (process repeated 2x more). Final polymer solid was collected using vacuum filtration, dissolved

in chloroform, and cast into Teflon mold for solvent evaporation into solid film. Fig. 1 includes the chemical structures for both 8-Phe-4 polymer (a) and Ketotifen fumarate (b).

Electrospinning of AA-PEA polymer fibers

Electrospinning stock solutions were prepared at 16 wt% 8-Phe-4 by dissolving 8-Phe-4 in a 4:1 ratio of chloroform to dimethylformamide (DMF) at room temperature for two hours. Previous work has found that decreasing the amount of chloroform does not create well-extended fibers.[31]Without using DMF as a cosolvent, chloroform alone evaporates too quickly and leads to a blocked needle for fiber formation.

Drug doped 8-Phe-4 polymer solutions were made using the same protocol described above, including 10mg/g polymer KF added to solution with stirring at room temperature for ~2 hours to ensure drug dissolution in the electrospinning solvent. For example, drug-doped 8-Phe-4 solution was made by dissolving 2.3g 8-Phe-4 in 2.3g DMF and 9.3g Chloroform in a clean glass scintillation vial. After complete polymer dissolution, 23mg of KF was added and stirred at room temperature. Both 8-Phe-4 and 8-Phe-4 + KF polymer solutions were a viscous brown solution.

8-Phe-4 polymer solutions were loaded into a 5mL glass syringe with a 26-guage needle (Cadence Science, Cranston, RI, USA). Using a syringe pump (Model 200, KD Scientific, Holliston, MA, USA), polymer solutions were spun at a flow rate of 0.5mL/hour under high voltage of 20kV (Gamma High Voltage Supply, ES 30–0.1P). Electrospinning tip to collector distance was approximately 15cm, with grounded aluminum foil serving as the collection plate.

To understand how drug release is affected by polymer morphology, 16 wt% 8-Phe-4 polymer solutions were solvent cast (with and without 10mg/g polymer KF) into Teflon molds. After complete

solvent evaporation (24 hours at room temperature in the chemical safety hood), the polymer solid was cut into ~36mg samples to use for experimentation.

Characterization of AA-PEA fibers and 2D films

IR measurements were taken using ATIR (Nicolet Magna-IR 560, Nicolet Instrument Corp., Madison, WI, USA). Thermal analysis of samples was determined using differential scanning calorimetry (DSC) (Q-Series 2000, TA Instruments, New Castle, DE, USA) using a nitrogen flow rate of 50.0 mL/min and sample size of 10mg, run at 10°C/min from 0°C to 300°C. Analysis of thermal behaviour was completed with TA Universal Analysis software (T_g and T_m). Molecular weight was measured with gel permeation chromatography (GPC, Waters Associates, Milford, MA, USA) using tetrahydrofuran (THF) as solvent eluent (1.0mL/min), standardized with polystyrene. Contact angle measurements were taken using a Rame Hart Contact Angle Goniometer/Tensiometer (Rame Hart, Succasunna, NJ, USA). Fiber diameter size was characterized using Image J software (ImageJ, NIH Image software, NIH, Bethesda, MD, USA). Plotting of assay and fiber size data was completed using Graphpad Prism 6 software (Graphpad Software Inc, La Jolla, CA, USA). UV-Vis spectroscopy (Lambda 35, Perkin Elmer, Waltham, MA, USA) measurements were taken to measure UV absorbance of KF at 300nm using a plastic disposable cuvette.

***In vitro* degradation of 8-Phe-4 KF encapsulated electrospun fibers**

In vitro biodegradation assessment of KF doped 8-Phe-4 films and fibers was quantified by placing 36mg electrospun and solvent cast samples in either 6mL phosphate buffer solution (PBS, pH 7.4 - control) or 1µg/mL α-chymotrypsin solution (PBS buffer – enzyme) at 37°C using reciprocal water

bath. Aliquots (1mL) were removed daily and used for spectroscopic analysis (measurement of triplicate independent samples at 300nm absorbance). Quantification of KF release was plotted as calculated percent cumulative release over 30 days from a standard curve of KF in PBS (0-50µg/mL). In order to ensure proper enzymatic activity, all samples were refreshed daily with PBS or enzyme solution.

Cell Culture

HeLa epithelial cells were cultured in complete DMEM (CDMEM, 10% fetal bovine serum (FBS), 10,000 IU/mL penicillin, 10,000 µg/mL streptomycin, 1mM Hepes, 200mM L-glutamine, and 100mM Sodium pyruvate) at 37°C with 5% CO_2 (cells kindly provided by the Leifer Lab, Cornell ~~Veterinary~~ College of Veterinary Medicine). After media aspiration, cells were trypsinized suspended in fresh CDMEM, counted, and plated at an appropriate density for viability quantification (50,000 cells/well of 24 well plate) and incubated for 36 hours at 37°C and 5% CO_2. All media reagents (expect FBS) were purchased from Mediatech (Manassas,VA, USA)). FBS was purchased from PAA Laboratories (Dartmouth, MA, USA).

To examine HeLa adhesion to electrospun materials, HeLa cells (50,000cells/well) were bubbled directly onto electrospun materials (or 12mm round glass coverslip control) in a 24 well plate and incubated for 24 hours at 37°C and 5% CO_2. To prepare cells for staining, each well was rinsed twice with sterile 1X PBS, fixed with 3% Paraformaldehyde for 15 minutes, permeabilized with 0.1% Triton X-100 (Alfa Aesar, Ward Hill, MA, USA) in PBS for 5 minutes, followed by rinsing twice in PBS. To stain actin filaments of HeLa cells, each sample was inverted onto a bubble of staining solution (5µL Phalloidin Alexafluor 488, 200µL PBS, 2mg BSA) (Alexafluor 488, Life Technologies, Grand Island,

NY, USA) for twenty minutes at room temperature. After a final rinsing in PBS, each sample was mounted to a glass microscope slide using Prolong Gold Mountant (contains DAPI) (Life Technologies, Grand Island, NY, USA), dried overnight, and imaged on a Leica SP5 confocal microscope using a 40x dry lens.

RAW 264.7 mouse macrophage cells were cultured in CDMEM at 37°C in 5% CO_2 (cells kindly provided by the Leifer Lab, Cornell College of Veterinary Medicine). Macrophage cells were plated at a proper concentration (100,000 cells per well) for both cytokine and nitric oxide assays.

RBL-2H3 (rat basophil leukemia) cells cultured in complete Minimal Essential Medium (CMEM, 20% fetal bovine serum (FBS) and 10μg/mL gentamicin sulfate) at 37°C with 5% CO_2 (cells kindly provided by the Baird Lab, Cornell University).

For viability, TNF-α, and NO· assays, electrospun fibers were spun directly onto sterilized 12mm round glass coverslips using 16 wt% solutions with and without ketotifen fumarate drug doping. Before cell culture, coverslips were sterilized under UV light for 30 minutes.

Biological Assays

HeLa Cell Proliferation Assay

Thirty-six hours after incubation, HeLa cells seeded on fibrous materials were assayed with CCK-8 Reagent assay kit (Sigma Aldrich, Milwaukee, WI, USA). Assay was run according to the manufacturer's protocol. Assay absorbance was read at 450nm. PLA electrospun fibers were used as a

commercial control. All samples were read in quadruplicate. Results were normalized to HeLa untreated controls.

TNF-α Cytokine Inflammation Assay

Twenty-four hours after incubation, RAW264.7 macrophage cell supernatant was removed and assayed using Biolegend ELISA Maxx Kit (Biolegend, San Diego, CA, USA). After proper dilutions, assay was run according to manufacturer's protocol. Assay plate was read using a plate reader at 450nm filter. LPS (lipopolysaccharide) (ATCC, Manassas, VA, USA) was used as a positive control (assayed at 100ng/mL), and PLA as a commercial control with all samples read in quadruplicate. Ketotifen fumarate was assayed at a concentration consistent with release from fibers over 24 hours (10µg/mL).

Nitric Oxide (NO· Assay)

Twenty-four hours after incubation, RAW264.7 macrophage cell supernatant was removed and assayed with Promega Griess Reagent system following manufacturer's protocol. All samples were run without dilution and read using plate reader 540nm (Biotek Synergy, BioTek, Winooski, VT, USA). Ketotifen fumarate (10µg/mL) was used as a positive control, while PLA electrospun fibers used as commercial control.

Degranulation Assay

Approximately 36 mg of fibrous membranes (PLA, 8-Phe-4, or KF-doped 8-Phe-4) were prepared and placed in 15mL conical tube with 3 mL Tyrodes Buffer solution (137mM NaCl, 2.7 mM KCl, 1 mM $MgCl_2$, 1.8 mM $CaCl_2$, 5.6 mM glucose, 0.4mM NaH_2PO_4, 12mM $NaHCO_3$, pH 6.5). Fibrous

membranes were then placed in an incubator at 37° for 48 hours. Supernatants were removed from these vials to assess degranulation stimulation.

RBL-2H3 cells were sensitized with 0.5 μg/mL IgE and plated in sextuplicate at a density of 5 x 10^5 cells/well and incubated overnight. The next day cells were washed two times with buffered saline solution (BSS: 135 mM NaCl, 5 mM KCl, 1 mM MgCl2, 1.8 mM CaCl2, 5.6 mM glucose, 20 mM HEPES, pH 7.4) and then incubated for 15 min with 50 μl of supernatant collected from fibers. Cells were then washed two times with BSS, and 50 μl of supernatant was again added to cells, following which β-hexosaminidase release in response to DNP-BSA was assessed as described previously.[51]

Statistical Analysis

All data presented in tables and assay results are given as mean ± the standard deviation. For each sample set, number of samples tested (n) replicates are given to provide accurate reproducible independent data analysis. Samples were analysed using one way Anova to determine significance. Statistically significant results are denoted (*) when $P < 0.05$ and (***) when $P < 0.01$.

4.3 Results and Discussion

Characterization of 8-Phe-4 Electrospun Fibers

Highly distinct well-drawn 8-Phe-4 electrospun fibers were formed using a modified protocol from previously reported work.[31] In brief, 16 wt% solutions of 8-Phe-4 were made by dissolving 8-Phe-4 solid polymer (Fig. 13a) with a 4:1 ratio of chloroform to DMF (with and without ketotifen fumarate drug doping, Fig. 13b). Contrasting the previous study[31], our current study found that increasing the

chloroform /DMF ratio from 3:1 to 4:1 was more efficient for electrospinning of these fibers, including the drug encapsulated samples. Minimal tip blockage was observed with increased chloroform content. At a 3:1 ratio chloroform to DMF ratio, DMF was not able to evaporate quickly enough leading to aggregated fiber networks.

Figure 13. Chemical Structures of (a) 8-Phe-4 poly(ester amide) (b) and Ketotifen Fumarate

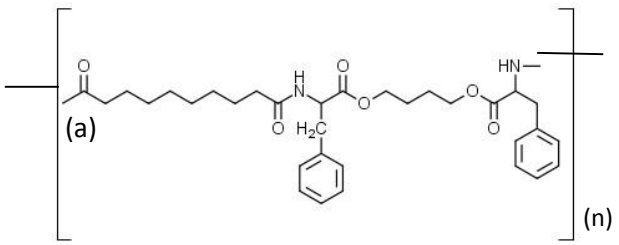

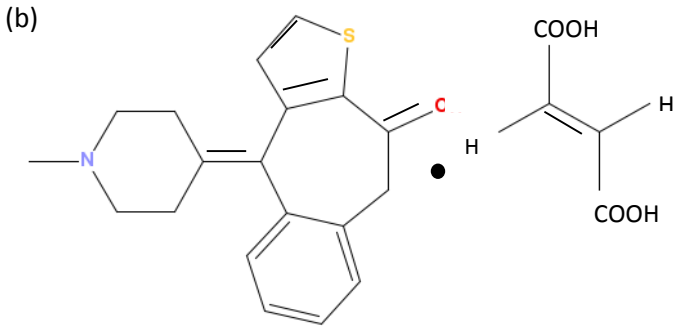

As characterized by Li *et al*, and observed in our experimental trials, increasing the amount of DMF present in the 8-Phe-4 electrospinning solution does not give well-defined fibers, as the fibers did not have adequate time to dry before depositing on the collection plate due to the relatively high boiling

point of DMF (~150°C).[31] Scanning Electron microscopy was used to verify the formation of fiber strands in both empty 8-Phe-4 (Fig. 14a) and KF-loaded 8-Phe-4 fibers (Fig. 14b).

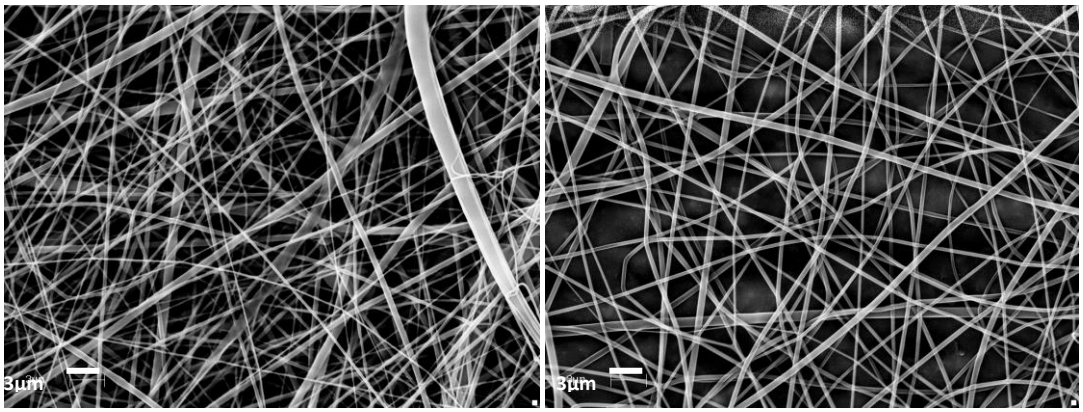

(a) (b)

Figure 14. SEM Images of 8-Phe-4 Electrospun Fibers using 4:1 chloroform to DMF volume ratio without (a) and with 10mg KF per gram 8-Phe-4 drug encapsulation (b) Images of solvent cast samples are not included as they were used solely for release comparison purposes.

The individual fiber sizes of the empty 8-Phe-4 fibers show a size distribution with an average fiber diameter of approximately 507nm (Fig. 15a). Upon encapsulation of the hydrophilic drug ketotifen fumarate (the water soluble alternative to ketotifen base), the average fiber diameter increased to 557nm (Fig. 15b). A moderate, but marked increase in fiber diameter (9%) indirectly indicates that KF was encapsulated within the interior of the fibers.

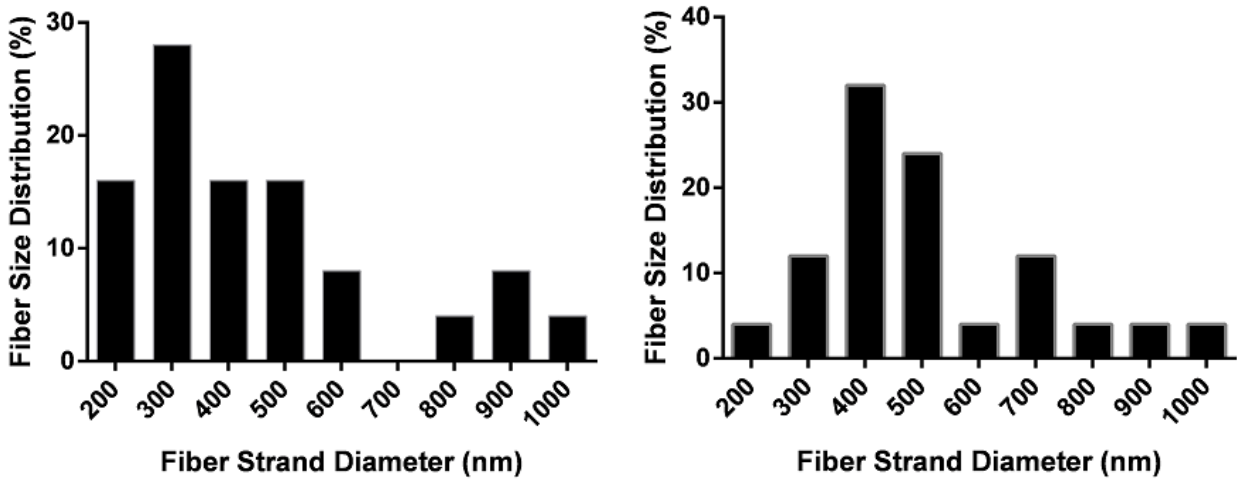

Figure 15. Fiber Size Distribution of 16 wt% (a) 8-Phe-4 Electrospun Fibers, (b) KF-doped (10mg/g polymer) 8-Phe-4 Electrospun Fibers.

Thermal Analysis of 8-Phe-4 electrospun and solvent cast samples

Thermal analysis was assessed for both electrospun and solvent cast 8-Phe-4 samples to determine the effect of polymer morphology on its thermal properties such as T_g (glass transition) and T_m (melting temperature). The effect of drug encapsulation on AA-PEA biomaterial thermal behaviour was also characterized (KF T_m approximately 198°C). 8-Phe-4 electrospun fibrous membranes had significantly smaller T_g (31.0°C) than the solvent-cast films (47.2°C), consistent with previous observed results for these 8-Phe-4 morphologies.[31] The difference in Tg can be attributed to different levels of polymer chain orientation due to different fabrication methods. A relatively higher oriented polymer molecules could maximize intermolecular force, and hence restricting chain motion and leading to a higher T_g. Electrospun fibers exhibit a lower T_g due to the limited time (microseconds) polymer chains that could travel in an electric field and permit the AA-PEA polymer chains to orient into crystalline domains before reaching the collection plate and the evaporation of solvent. The 8-Phe-4 solvent cast films have

higher T_g because of the increased time (> 16 hours) permitted for solvent evaporation. The solvent cast 8-Phe-4 polymer chains had time to orient into crystalline domains as evident in the presence of a melting temperature, i.e., limiting chain flexibility, and a higher glass transition temperature; while the 8-Phe-4 electrospun fibrous membrane are amorphous and did not have a characteristic T_m.

As established previously with commercially available materials such as poly(D,L-lactide), electrospinning of polymer solutions creates polymer matrixes with lower T_g than solvent cast materials. For example, Cui *et al* found by electrospinning poly (lactide) polymers, T_g reduced to 54.6°C from 61.7°C of the solvent cast films due to increased inner stress, orientation, and alignment as the fiber strands are electrospun under high voltage.[52] They suggest that although the overall glass transition temperature decreases after electrospinning, high degree of alignment and orientation are a result of high transition enthalpy compared to solvent cast films.[52]

8-Phe-4 electrospun glass transition temperature was also influenced by the incorporation of Ketotifen fumarate drug into the fiber core. The empty 8-Phe-4 electrospun fibers underwent glass transition at 31.0°C (Fig. 4), while the KF-encapsulated 8-Phe-4 fibers exhibited a slight increase in glass transition temperature (T_g: 35.9°C). The increase in glass transition can be attributed to decrease in segmental chain mobility of the polymer fiber due to the presence of the drug molecule which could restrict polymer chain motion as KF can generate intermolecular force between KF and 8-Phe-4 chains causing the polymer backbone to become more rigid. The physical presence of KF within the 8-Phe-4 polymer domain could also reduce the free volume of the polymer and hence leading to a higher T_g.

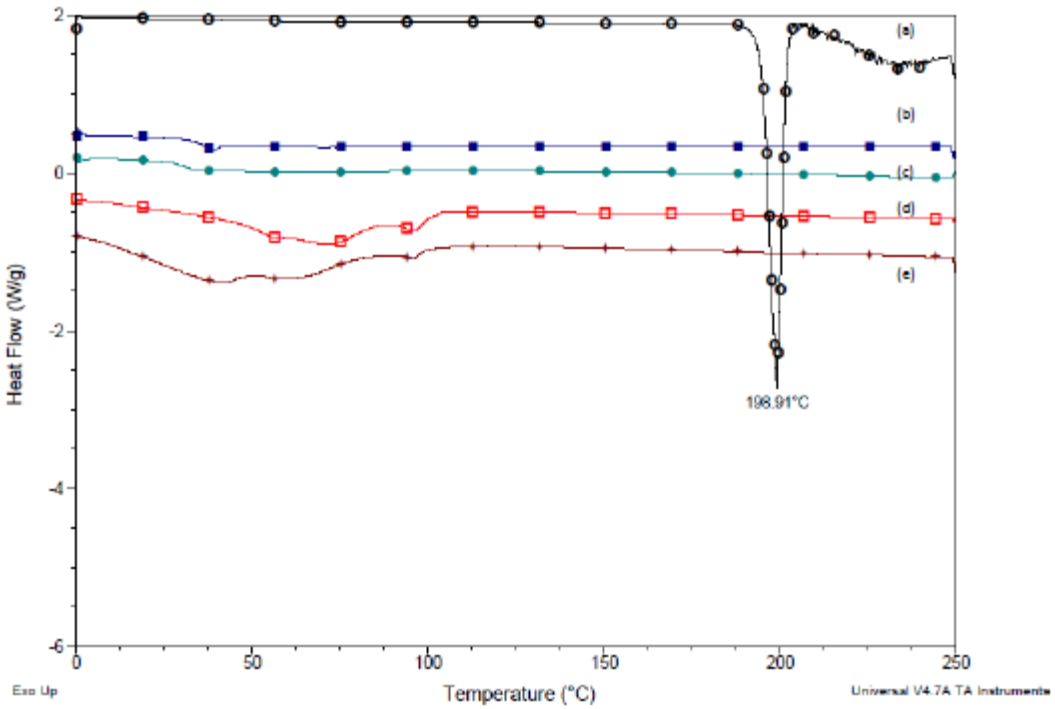

Figure 16. Thermal behavior of electrospun 8-Phe-4 (a) Ketotifen Fumarate solid drug, (b) 8-Phe-4 ES + KF (0 Day degradation), (c) 8-Phe-4 ES (0 Day degradation), (d) 8-Phe-4 ES (30 Day degradation), (e) 8-Phe-4 + KF (30 Day degradation)

To assess how polymer thermal behaviour was affected by aqueous environments, T_g measurements were taken after 30 days incubation in either physiologically relevant buffer solution or buffer solution with enzyme that targets enzymatically liable groups in AA-PEA polymers. Results indicate incubation in an aqueous environment increased T_g approximately 58% for both KF-doped electrospun 8-Phe-4 control (control is PBS buffer, no enzyme) and enzymatically degraded (PBS with α-chymotrypsin) KF-loaded electrospun 8-Phe-4 fibers (Table 2). The T_g of the solvent cast KF-loaded 8-Phe-4 films decreased approximately 10% for both control and enzymatically degraded samples (Fig. 16). As suggested by Li *et al*, Tg increase in aqueous environments for the hydrophobic 8-Phe-4 fibers can be

attributed to increased crystallinity within the polymer domains as the amorphous regions undergo segmental chain motion to more rigid, increased crystallinity domains.[31] In solvent cast samples, an increase in Tg was not observed since the crystalline domains had already formed as the solvent evaporated, resulting in little to no additional segmental motion.

Table 2. Thermal Glass transitions (T_g) and Melting Temperature (T_m) of KF-loaded 8-Phe-4 morphologies before and after 30 day *in vitro* incubation (presented as average ± std dev of triplicate samples)

		T_g (°C)	**T_m (°C)**
Materials Before release study	**Solvent Cast Film**	47.2 ° C ± 1.9°C	110.2°C ± 0.4°C
	Electrospun	35.9° C ± 0.5°C	amorphous
Materials after 30 days of enzymatic degradation	**Solvent Cast Film**	43.4 ° C ± 0.9°C	111.6° C ± 0.9°
	Electrospun	56.6 ° C ± 2.3°C	94.4° C ± 1.9°C
Materials after 30 days immersion without enzyme	**Solvent Cast Film**	42.5 ° C ± 0.6°C	111.5° C ± 0.2°C
	Electrospun	56.5° C ± 1.0°C	95.8° C ± 0.3°C

Contact Angle Goniometry of 8-Phe-4 electrospun and solvent cast samples

Contact angle measurements indicated no significant alteration in hydrophobicity between varying morphology empty (no KF) 8-Phe-4 materials including 2D polymer films (77.9°C) and 3D electrospun membranes (78.6°C) (Table 3). Furthermore, encapsulating hydrophilic drug KF within either the 2D solvent cast or 3D randomly oriented electrospun fibers did not significantly decrease the overall material contact angle, compared to the empty control (78.9°C and 78.8°C, respectively). Should KF been present in large amounts on the polymer surface, an expected decrease in the contact angle as a result of the hydrophilic drug would have been observed. This effect was not seen suggesting that KF was successfully encapsulated within the polymer fiber strands.

Table 3. Contact Angle Measurements of 8-Phe-4 polymer samples, with and without 10mg/g polymer KF encapsulation. All measurements are given as average ± std dev of triplicate samples. Angle presented is advancing angle.

Material	Contact Angle (ɵ)
Solvent Cast 8-Phe-4	**77.9 ° C ± 3.3°**
Electrospun 8-Phe-4	**78.6 ° C ± 1.2°**
Solvent Cast 8-Phe-4 with KF	**78.9 ° C ± 1.0°**
Electrospun 8-Phe-4 with KF	**78.8 °C ± 1.0°**

Infrared Analysis of 8-Phe-4 electrospun and solvent cast samples

Infrared spectroscopy was used to assess KF encapsulation within 8-Phe-4 fibrous membranes. Empty 8-Phe-4 electrospun fiber FTIR spectra show amide I (1645.1 cm^{-1}), amide II (1534.9 cm^{-1}), ester (1737.3 cm^{-1}), and NH vibration at 3285.1 cm^{-1} bands that are consistent with previous findings.[18] The FTIR spectrum of KF contains peaks for –CH thiophene stretching (3097 cm^{-1}), aromatic stretching (3000-2840 cm^{-1}), and carbonyl peaks (1650 cm^{-1} - overlap with 8-Phe-4 signal). Upon testing of KF-doped 8-Phe-4 electrospun fibers, no significant increase in absorbance for KF characteristic peaks were observed over empty 8-Phe-4 electrospun fibers, indicating the lack of increased signal suggests KF drug content was successfully encapsulated within fiber core (Fig. 17), rather than significantly present on fiber surface, which would contribute to the overall IR signal spectra.

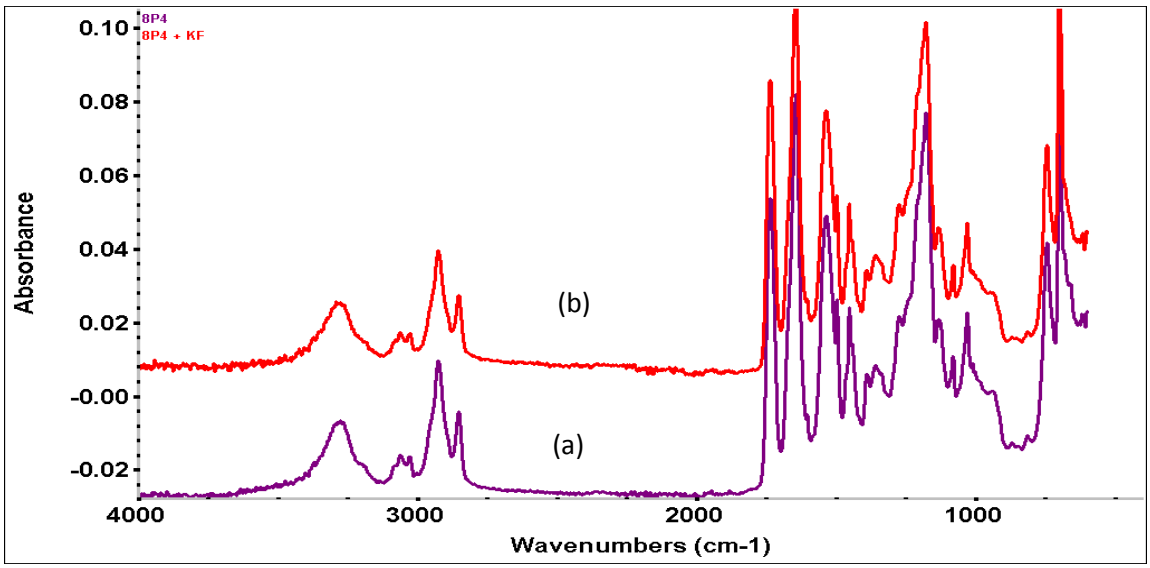

Figure 17. ATIR Spectra of 16wt% electrospun 8-Phe-4 fibers without (a) and with 10mg/g polymer KF drug encapsulation (b)

In vitro degradation 8-Phe-4 electrospun and solvent cast samples

An initial burst of 6.55% total loaded Ketotifen Fumarate was seen within the first three hours of incubation, attributed to the diffusion of KF closer to the surface of the fiber. This quantity is hypothesized to be loosely bound to the surface of the fibers or embedded in the surface, but not fully encapsulated within the interior of the fiber. KF release slowed down between the 3rd and 5th hour, after which release adopts a steadily inclining, linear trend (r^2=.9906) (Fig. 18). Release from control electrospun fibers (PBS-no enzyme) exhibited a similar trend to enzymatically-degraded electrospun samples during the first 24 hours. This release data indicates that up until the first 24 hours of incubation, hydrolytic degradation of the 8-Phe-4 is predominant, elucidating why both the sample and control exhibit similar percentages of drug release.

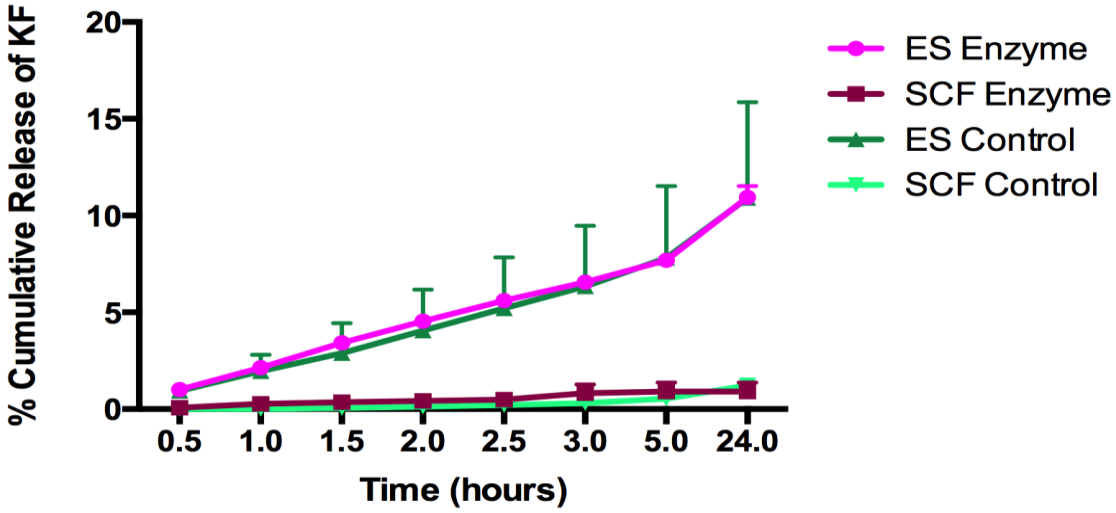

Figure 18. Graph of cumulative drug release from electrospun and solvent cast film samples with and without α-chymotrypsin degradation over the first 24 hours of incubation. ES and SCF samples contain 5mL PBS and 1mL α-chymotrypsin in their immersion media. ES and SCF controls contain 6mL PBS and no enzyme in their immersion media. ES denotes electrospun samples, while SCF denotes solvent cast films.

By day 30, about 94% of total loaded KF had been released from the electrospun fibers in enzymatic incubation media (Fig. 19). At three days incubation, KF release from control electrospun samples started to steadily increase and level off after the 9th day of incubation. At the 3rd day of incubation, enzymatically-degraded electrospun sample released 18% of the total loaded KF while the electrospun control released only 13%. Because samples in control solution do not have enzyme present to facilitate the degradation of the polymer via scission at hydrophobic amino acid residues, less polymer degradation takes place resulting in less drug released. After 3 days *in vitro* degradation, enzymatically-degraded electrospun samples show an increase of approximately 8% release every three days, while the KF-loaded 8-Phe-4 electrospun controls remain at approximately 15% of the total loaded KF released throughout the remainder of the 30 day incubation period. These results demonstrate the presence of α-chymotrypsin in incubation media is necessary for the desired sustained release of the drug. Since α-chymotrypsin is a native enzyme present physiologically, including liable groups available for enzymatic scission in AA-PEA 3D fibrous membranes provides a naturally degrading scaffold for cell migration and deposition of new extracellular matrix.

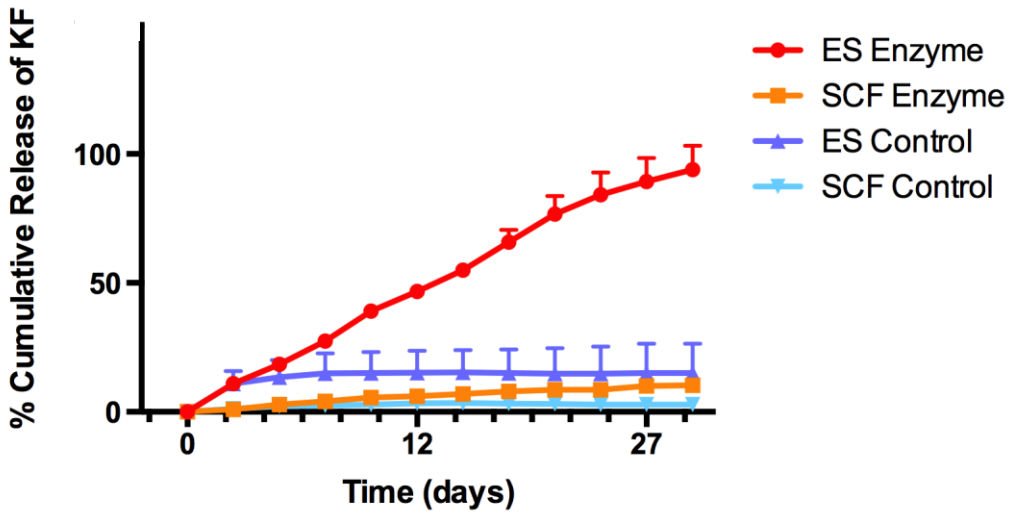

Figure 19. Graph of cumulative drug release from electrospun and solvent cast film samples over 30-day incubation period. ES and SCF samples contain 6mL α-chymotrypsin (in PBS). ES and SCF controls contain 6mL PBS with no enzyme in their immersion media. ES denotes electrospun samples, while SCF denotes solvent cast films.

Release of ketotifen fumarate from the biodegradable 8-Phe-4 fibrous membranes and solvent cast films is a function of degradation of polymer surface, as well as diffusion of the drug into the aqueous medium. Upon sufficient polymer degradation, water-soluble KF diffuses from fiber strands as matrix surface polymer degradation creates channels and pores which the drug can be released into the incubation medium. KF is thought to be released into solution media through Fickian diffusion; plotting time$^{1/2}$ vs cumulative release of ketotifen fumarate gives a linear relationship with an r^2 value of .9742 between 0-24 hours and r^2 value of .9873 from day 1 to day 30.

Difference in release trends between the electrospun and solvent cast film materials can be attributed to the differences in morphology between the 2D solvent cast films and the 3D nanofibers. Attributing to the 3D structure of the electrospun nanofibrous mats, aqueous media and enzyme can reach more

polymer surfaces at once, fully surrounding the polymer and facilitating its degradation more efficiently. Solvent cast films only have a minimal planar surface for exposure to enzyme, thereby limiting interaction with the 2D polymer surface, resulting in less 8-Phe-4 degradation and reduced KF release. Differences in morphology influence KF release from the start of incubation, as the solvent cast films reach 1% KF release after 24 hours while the electrospun materials released approximately 10%. Solvent cast films in the enzymatic incubation media had a slightly higher release than the solvent cast films without enzyme present, but do not release more than 10% of the total KF content after the one month period.

Upon *in vitro* degradation in both control (which the sample undergoes hydrolytic degradation via scission of the ester group of the polymer backbone) and under enzymatic degradation influence, electrospun material surface morphology was affected in the pseudo physiological environment. After 30 days degradation, distinct fiber strands observed from day 0 were no longer visible and gave way to a more planar surface (Fig. 20). Porosity is still maintained within the material morphology, yet the material surface has become flattened with distinct peaks and valleys. Both control and α-chymotrypsin degraded samples exhibited similar polymer morphology, with the enzymatically degraded sample displaying slightly less defined surface roughness.

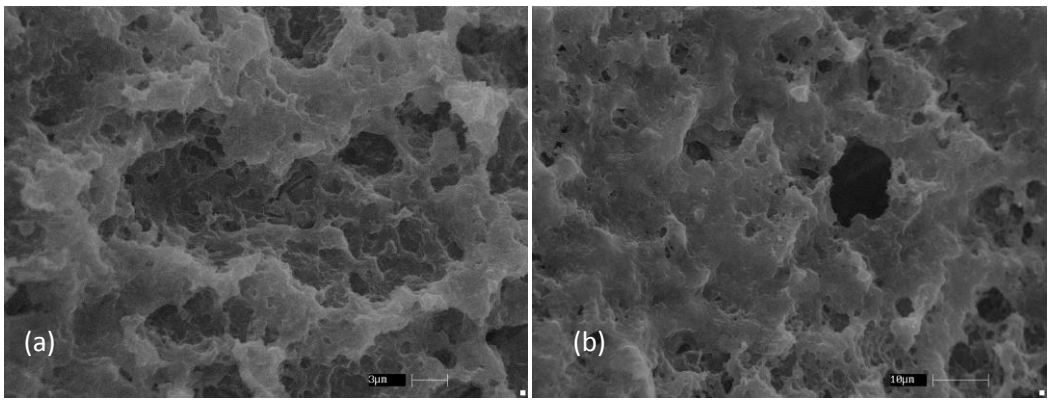

Figure 20. SEM Images of 8-Phe-4 drug doped Electrospun Fibers after 30 days incubation at 37°C without α-chymotrypsin (a) and with α-chymotrypsin (b).

Depending on the application and the duration of the device needed, KF incorporation into polymeric devices varies greatly. Due to the large proportion of mast cells in the ocular region, many KF-releasing devices target this biological caveat. For example, Xu *et al* fabricated silicone hydrogel contact lenses, followed by KF loading (suspended in PBS), and found complete cumulative release (100%) within 40 hours at physiological temperature.[46] Using commercially available lenses, Karlgard *et al* demonstrated fast release of ketotifen (~100%) via desorption from lens surface over 24 hours.[48]

Mast cell stabilizer drug release systems can also target mast cells in other parts of the body, including topical and injectable applications. Patel *et al* established controlled release of KF from ethyl cellulose/hydroxypropyl methyl cellulose/poly(ethylene glycol) scaffolds and found (based on the formulation conditions) between 47-95% KF release at physiological temperature after 24 hours.[43] Guerrero *et al* fabricated KF-encapsulated glutaraldehyde crosslinked chitosan-based microspheres and found approximately one half of the encapsulated amount of KF was released within 50 hours.[45] In ocular and additional application KF release from drug delivery systems, it becomes apparent that

release is observed over a brief timeline. Utilizing the hydrophobic properties of 8-Phe-4, electrospun fibers have the capability to extend KF release up to 30 days, producing a drug delivery device which is cost effective (less repeated material applications to patient) and improves patient compliance.

Fibrous Membrane HeLa Viability and adhesion

HeLa epithelial cells were used to quantify cell toxicity upon incubation with electrospun materials. Within electrospun scaffolds tested (PLA, 8-Phe-4, and 8-Phe-4 + KF), each fibrous membrane exhibited equivalent HeLa viability after 3 days incubation ($p > 0.05$). KF-doping of 8-Phe-4 electrospun fibers did not affect HeLa viability (Fig. 21A) compared to empty 8-Phe-4 electrospun fibers. Results indicate AA-PEA nanofibers maintain viability comparable to commercial control (~75%), and are therefore good candidates for biomedical applications.

Paralleling good viability after three days, HeLa epithelial cells also demonstrated excellent adhesion to electospun fibers (Fig. 21B). While HeLa control cells on plain glass tended to migrate into multi-cell groups and display minimal actin filament spreading, HeLa cells on electrospun fibers established excellent actin filament extension. HeLa cell actin filament extension on KF-loaded 8-Phe-4 electrospun fibers was similar to that of empty 8-Phe-4 electrospun fibers, indicating presence of drug did not adversely influence cell adhesion.

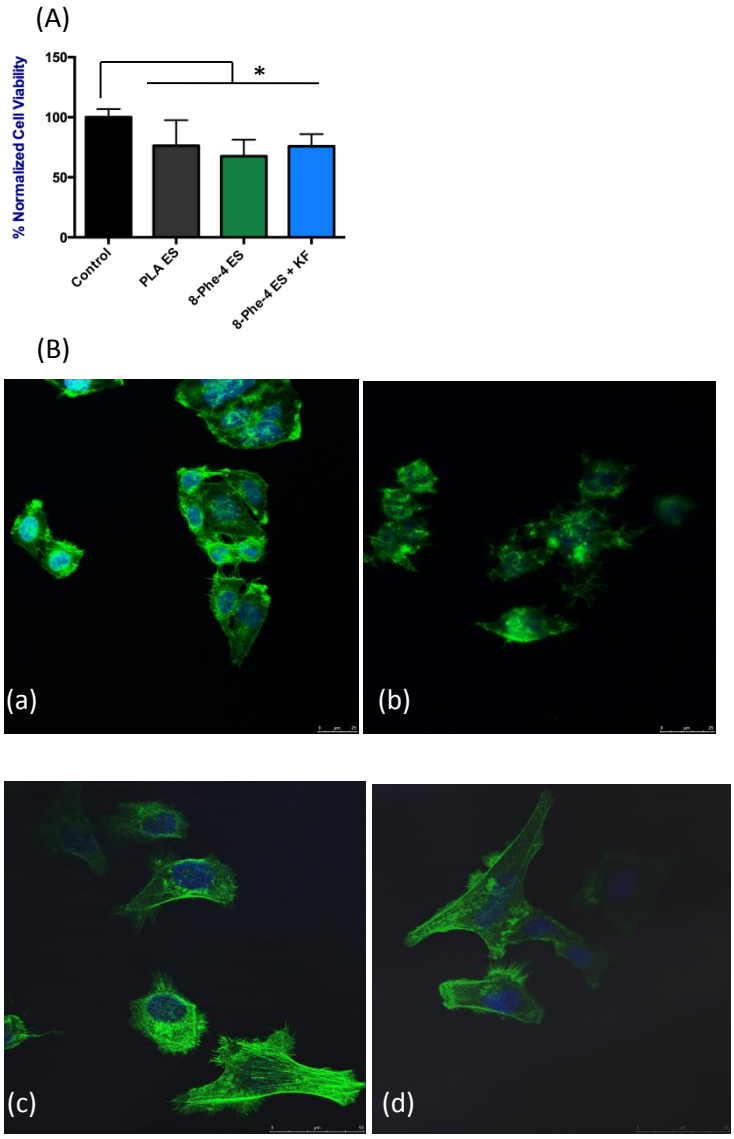

Figure 21. (A) HeLa Cell Viability Assay results for Electrospun fibers (PLA, 8-Phe-4, and 10mg/g polymer KF doped 8-Phe-4, negative control was (a) HeLa cells on 12mm round glass coverslips.). All samples (n=3) were incubated for 36hrs at 37°C and 5% CO_2 (results normalized to HeLa control). P <0.05 denoted with asterisk (*). (B) Phalloidin Staining of HeLa cells for Actin with 16wt% Electrospun fibers PLA (b), empty 8-Phe-4 (c), and 10mg/g polymer KF doped 8-Phe-4 (d). All samples were incubated for 24hrs at 37°C and 5% CO_2.

Cell adhesion and viability when incubated with nanoscale electrospun fibers is essential in tissue engineering applications for the reason that cells need a substrate to adhere to as they produce new extracellular matrix as the synthetic scaffold degrades. Kwon *et al* fabricated varying molar feed ratio electrospun fibers of poly(lactic-co-ϵ-caprolactone) (PLCL) polymers and found superb human umbilical vein endothelial cell adhesion and proliferation up to 7 days.[53] Similarly, using a fixed molar feed ratio of 75/25 PLCL, Mo *et al* successfully fabricated nanoscale electrospun fibers (0.5-1.5 μm diameter) that supported endothelial cell adhesion and proliferation up to 7 days.[54] They suggest the high level of cell interaction with nanoscale electrospun materials is directly related to the fiber's high surface to volume ratio, which mimics the environment naturally found in tissues.[54] Endothelial cells (including HeLa) are commonly used to evaluate viability and proliferation in wound healing devices as this cell type is directly involved in wound healing[55]and has been established as a go-to model.[56]

Cell Inflammation and Nitric Oxide Assay

Mouse Macrophage TNF-α Assay

Tumor necrosis factor alpha ~~NF-alpha~~(TNF-α), a proinflammatory cytokine released after mouse macrophage activation, was used to quantify macrophage activation to electrospun materials. Given its excellently characterized properties and commercial use, PLA electrospun fibers were used as a comparison (avg. fiber size 639nm, fiber dist. not shown) to the novel 8-Phe-4 electrospun fibers. LPS (lipopolysaccharide), a potent stimulation agent for macrophage pro-inflammatory cytokine production, was used as a positive control. Initial studies showed TNF-α cytokine production was elevated for Ketotifen fumarate bolus addition to macrophage cells (425% elevation) compared to untreated control.

In order to reduce proinflammatory cytokine stimulation, KF was encapsulated into AA-PEA fibers with very low inflammatory response. Both control and empty 8-Phe-4 electrospun materials induced macrophage TNF-α secretion of approximately 60pg/mL-80pg/mL (Fig. 22), which was not statistically significant from RAW cell response alone. Slow release of KF from KF-loaded 8-Phe-4 electrospun fibers did not affect macrophage TNF-α secretion (not statistically significant compared to empty 8-Phe-4 nanofibers). TNF-α cytokine production assay indicates that 8-Phe-4 electrospun materials (with and without drug doping) have excellent macrophage *in vitro* compatibility (low proinflammatory cytokine stimulation), comparable to that of commercially available materials used.

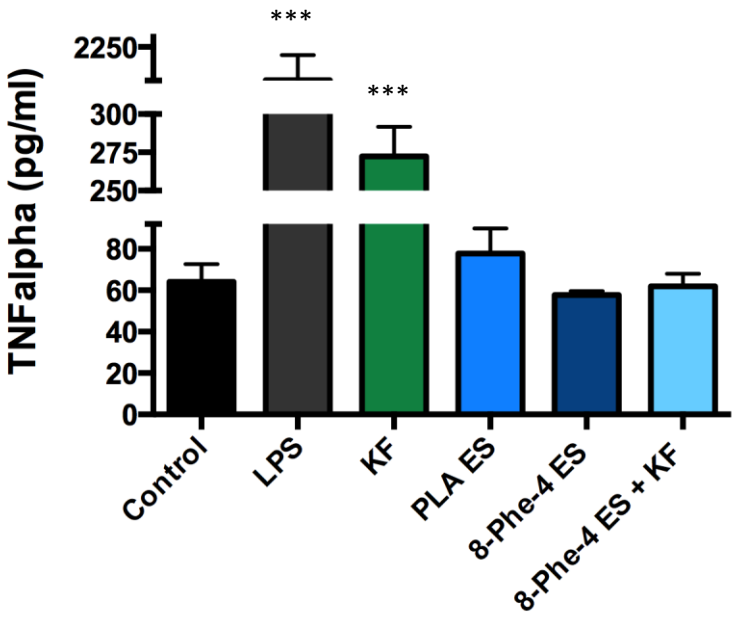

Figure 22. TNF-α Mouse Macrophage Inflammation Assay results for Electrospun fibers (PLA, 8-Phe-4, and 10mg/g polymer KF doped 8-Phe-4). All samples (n=4) were incubated for 24hrs at 37°C and 5% CO_2. LPS (lipopolysaccharide) was used as a positive control and was assayed at 100ng/mL

concentration. Ketotifen fumarate was assayed at 10μg/mL. $P < 0.01$ denoted with asterisk (***), all other samples not significantly different.

With all implantable biomaterials, devices, and drug delivery systems, the body will generate an immune response to the foreign material at the tissue/material interface including non-specific adsorption of protein and recruitment of immune and inflammatory cells.[57] In this foreign body response (FBR), macrophages can undergo fusion and activation while mast cells (and other polymorphonuclear leukocites) can be recruited and stimulated leading to an array of responses including degranulation and fibrosis as a result of fibroblast activation.[57]Because FBR can often determine the lifetime and efficiency of the device (or in this case electrospun scaffold), it is important to study immune responses to the materials used.

Mouse macrophage cells have been widely used in literature to understand cellular response to biomaterials, especially in the measurement of inflammatory response.[58,59] Anderson *et al* postulate that the overall chemical structure of the material will dictate the severity and length of foreign body response to implanted materials.[58]Materials with chemical entities amenable to physiological environments such as amino acids, ester, and amide linkages commonly found in proteins and DNA should limit the overall foreign body response and mediate inflammation, as compared to commercially available materials.[59]

Luong-van *et al* found similar results using poly(caprolactone) electrospun fibers; no statistically significant increase in macrophage inflammation occurred upon incubation with electrospun fibers.[60] Low inflammatory response can be derived from biorecognition of pendant amino acids along the

polymer backbone, with the added benefit of ester and amide linkages, gives exceptional biocompatibility while providing excellent chemical and mechanical properties, found with AA-PEA polymers[61]and in hybrid block copolymers with poly(caprolactone).[37]

Mouse Macrophage Nitric Oxide Assay

To quantify NO production upon macrophage incubation with AA-PEA electrospun samples, fiber samples were incubated RAW 264.7 mouse macrophage cells. LPS, a potent stimulatory agent for macrophage cells via M1 inflammatory stimulation, induced increased NO· production (92% elevation) compared to untreated control. After 24 hours cell seeding on the electrospun materials, very little (< 1 µM) nitric oxide was produced for any of the electrospun samples (PLA, 8-Phe-4, or KF-loaded 8-Phe-4), which was not statistically significant from the untreated control (RAW cells) (Fig. 23). No increase in NO· production was observed for addition of KF to macrophage cells.

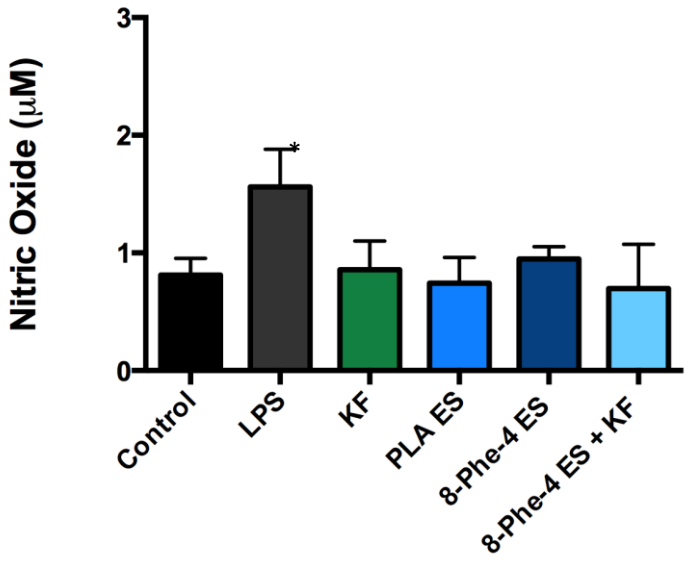

Figure 23. Nitric Oxide Mouse Macrophage Inflammation Assay results for Electrospun fibers (PLA, 8-Phe-4, and 10mg/g polymer KF doped 8-Phe-4). All samples (n=3) were incubated for 24hrs at 37°C and

5% CO_2. Ketotifen fumarate was assayed at 10µg/mL. LPS (positive control) was assayed at 100ng/mL. $P < 0.05$ denoted with asterisk (*), all other comparisons with control were not significant.

Nitric oxide (NO·) is a short lived radical known to participate in many crucial biological functions including production of reactive nitrogen species and chemotaxis of macrophage cells.[62] NO·, once released through the inducible isoform pathway (iNOS), promotes cell proliferation, collagen formation, and wound site contraction in a distinguishable wound healing model.[63] M1 macrophage activation (inflammatory response) is characterized by activation by antigen or pathogen leading to production of chemokines and proinflammatory cytokines (TNF-α) leading to production of reactive nitrogen species (NO·).[64]Since no additional TNF-α cytokine stimulation was detected, it is logical that no additional NO· stimulation was seen, as 8-Phe-4 electrospun fibers are hypothesized to not stimulate M1 macrophage inflammatory response.

Mast Cell Degranulation Assay

RBL-2H3 cells were used as a model system to probe degranulation behaviour in response to electrospun scaffolds (PLA, empty 8-Phe-4, and KF-loaded 8-Phe-4). Percent degranulation was measured after 48 hours for spontaneous release (spon – RBL cells with tyrodes buffer on tissue culture plate), antigen-stimulated release (Ag), total release, and degranulation as a result of electrospun fiber supernatants. Results show distinct trends; 1) 8-Phe-4 electrospun fibers stimulated low spontaneous degranulation, 2) KF release from electospun fibers mitigated degranulation stimulation by antigen. Looking first at spontaneous release (without antigen stimulation), PLA electrospun fibers statistically increased spontaneous degranulation ($p < 0.05$) compared to the untreated control (RBL cells on tissue

culture plate), while 8-Phe-4 electrospun fibers did not statistically increase spontaneous degranulation (Fig. 24). Upon antigen (AG) stimulation, % degranulation increased significantly for PLA electrospun fibers challenged with AG compared to spontaneous release; PLA electrospun fibers ($p < 0.05$), but an increase in % degranulation was not evident for 8-Phe-4 electrospun fibers. Antigen stimulation of IgE sensitized RBL cells is crucial in the priming and release of secretory granules.[70]

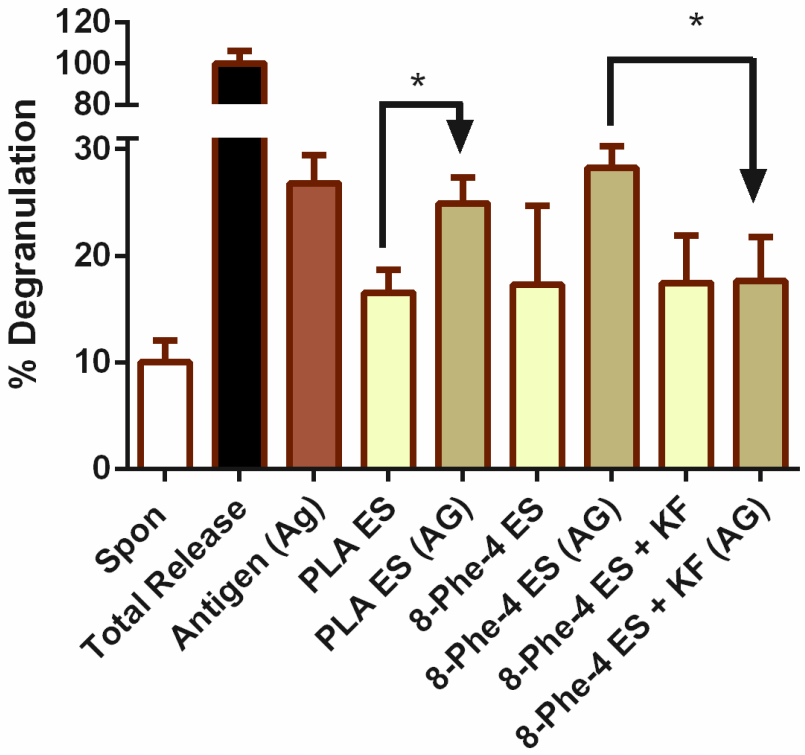

Figure 24. Mast cell model degranulation assay results for electrospun fibers (ES) (PLA, 8-Phe-4, and 10mg/g polymer KF doped 8-Phe-4). All samples (n=3) were incubated for 48hrs at 37°C and 5% CO_2 before plating supernatant with cells. Spontaneous release indicates control (RBL cells untreated), (AG) antigen stimulated cells, and total release (lysed cells). All samples are normalized to total release. $P < 0.05$ denoted with an asterisk (*) .

In the third condition tested, 8-Phe-4 electrospun fibers were doped with KF and incubated to allow KF to diffuse from the interior of the fiber into the supernatant. Compared to the spontaneous release control, KF-loaded 8-Phe-4 electrospun fibers did not statistically increase % degranulation. Furthermore, upon antigen stimulation, no statistically significant increase in degranulation was observed. This assay was completed todetermine whether the KF released from encapsulation was functional and effectively stabilized mast cell degranulation. Since degranulation was muted as a result of KF-loaded 8-Phe-4 fibers, data are consistent with our hypothesis that KF is indeed released during the first 48 hours incubation with the drug intact.

Mast cells, progenitor cells with yet unspecified function derived from bone marrow through systemic circulation, can migrate to wound sites upon stimulation.[65] Mast cells are most commonly characterized by their innate metachromatism used to visualize granules present within the cell.[66] Granules present in mast cells range from cytokines, proteases, and growth factors, which can be either influential or detrimental to the wound healing process.[65] In depth studies on the effect of such mediators have been extensively studied. For example, the effect of renin release on angiogenesis from mast cell degranulation has been an area of much research, leading to developments in diabetic retinopathy understanding and treatment.[67] Researchers are striving to understand the complex interactions of mast cells with biomaterials[68] and have extended work to electrospun scaffolds.[69] The choice of drug, ketotifen fumarate functions as a mast cell stabilizer via the IgE regulated calcium pathway to reduce mast cell degranulation and release of proinflammatory mediators in wound sites. By muting the ability of mast cells to release proinflammatory mediators such as histamine, both initial foreign body response and stimulation of fibrosis is down-regulated, leading to less inflammation and reduced scar formation.

An abundance of combination KF and polymer systems have been developed to address the very issue of mast cell stabilization. Yet, very few studies have utilized *invitro* mast cell models to assess functional KF release from biomaterials, as many focus primarily on *in vitro* release profiles, *in vivo* studies, or effect of mast cell stabilizer on mast cells. For example, Schoch *et al* have shown that concentration of KF release consistent with that tested in this work (~50μM) supress hHuman conjuntivital mast cell histamine degranulation (>90%) while maintaining excellent cell viability (70-80%).[41] Using RBL-2H3 cells and a similar protocol including cell sensitization and antigen challenge, Yanni *et al* found *in vitro* inhibition of histamine release for ketotifen (> 90%) and novel anti-histamine drug AL-4943A (> 95%).[71]

Using male winstar rats as an *in vivo* model, Guerrero *et al* delivered ketotifen encapsulated spray dried chitosan microspheres (1-1.3 μm diameter) to the intraperitoneal cavity ——and found ketotifen plasma concentration was only detected up to 24 hours, attributed to quick release of drug from microsphere.[45] Contrastingly, they found when they injected ketotifen to the intraperitoneal cavity (without polymeric carrier), maximal plasma concentration was reached after 2.4 hours.[45] Therefore, use of polymer carriers greatly extends ketotifen circulation *in vivo*.

4.4 Conclusions

Employing the widely used technique of electrospinning, 8-Phe-4 poly(ester amide) nanofibers were formed with an average fiber size of 507nm, creating a unique physiological mimic of extracellular matrix collagen fiber matrices. Anti-inflammation drug ketotifen fumarate was encapsulated successfully in 8-Phe-4 nanofibers with 94% of drug released after 30 days *in vitro* incubation at 37°C in PBS (pH

7.4). HeLa cell viability and macrophage cytokine response showed comparable levels of viability, TNF-α secretion, and NO· production between commercially available PLA, empty 8-Phe-4, and KF-loaded 8-Phe-4 electrospun materials indicating excellent *in vitro* compatibility. KF *in vitro* release from 8-Phe-4 fibers was shown to stabilize mast cell model degranulation at a physiologically relevant concentration, demonstrating potential of these materials in reduction of inflammation in wound sites.

Acknowledgements

This study was partially support by the Becky Q. Morgan Foundation. The authors would like to acknowledge Leifer Lab and Baird/Holowka Labs for their input and expertise on cell culture protocol and analysis. This work made use of the Cornell Center for Materials Research Facilities supported by the National Science Foundation under Award Number DMR – 112029.

References

1. Huang Z, Zhang YZ, Kotaki M, Ramakrishna S. A Review on Polymer Nanofibers by Electrospinning and Their Applications in Nanocomposites. Compos. Sci. Technol. 2003;63.15;2223-253.
2. Pham Q P, Sharma U, Mikos AG. Electrospinning of Polymeric Nanofibers for Tissue Engineering Applications: A Review. Tissue Eng. 2006;12.5;1197-211.
3. Zahedi P, Rezaeian I, Ranaei-Siadat S, Jafari S, Supaphol P. A Review on Wound Dressings with an Emphasis on Electrospun Nanofibrous Polymeric Bandages. Polym. Adv.Technol.2009;21.2;77-95.
4. Schiffman J D, Schauer CL. A Review: Electrospinning of Biopolymer Nanofibers and Their Applications. Polym. Rev.2008;48.2;317-52.
5. Murugan R, Ramakrishna S. Nano-Featured Scaffolds for Tissue Engineering: A Review of Spinning Methodologies. Tissue Eng. 2006;12.3;435-47.
6. Armentano I, Dottori M, Fortunati E, Mattioli S, Kenny JM. Biodegradable Polymer Matrix Nanocomposites for Tissue Engineering: A Review. Polym. Degrad. Stab.2010;95.11;2126-146.
7. Yu, DG. Electrospun nanofiber-based drug delivery systems. Health 2009;01.02; 67-75.

8. Zong, X, Kwangsok K, Fang D, Ran S, Hsiao B, Chu B. Structure and process relationship of electrospun bioabsorbable nanofiber membranes. Polymer 2002;43; 4403-4412.
9. Li W, Laurencin CT, Caterson EJ, Tuan RS, Ko FK. Electrospun Nanofibrous Structure: A Novel Scaffold for Tissue Engineering. J. Biomed. Mater. Res.2002;60.4;613-21.
10. LuuYK, Kim K, Hsiao BS, Chu B, Hadjiargyrou M. Development of a Nanostructured DNA Delivery Scaffold via Electrospinning of PLGA and PLA–PEG Block Copolymers. J. Controlled Release 2003;89.2; 341-53.
11. Kim TG, Lee DS, Park TG. Controlled Protein Release from Electrospun Biodegradable Fiber Mesh Composed of Poly(ε-caprolactone) and Poly(ethylene Oxide). Int. J. Pharm. (Amsterdam, Neth.) 2007;338.1-2;276-83.
12. Chew SY, Wen J, Yim EK, Leong KW. Sustained Release of Proteins from Electrospun Biodegradable Fibers. Biomacromolecules 2005;6.4; 2017-024.
13. Zeng J, Xu X, Chen X, Liang Q, Bian X, Yang L, Jing X. Biodegradable Electrospun Fibers for Drug Delivery. J. Controlled Release 2003;92.3;227-31.
14. Cui W, Li X, Zhu X, Yu G, Zhou S, Weng J. Investigation of Drug Release and Matrix Degradation of Electrospun Poly(-lactide) Fibers with Paracetanol Inoculation. Biomacromolecules 2006; 7.5;1623-629.
15. Kenawy E, Bowlin GL, Mansfield K, Layman J, Simpson DG, Sanders EH, Wnek GE. Release of Tetracycline Hydrochloride from Electrospun Poly(ethylene-co-vinylacetate), Poly(lactic Acid), and a Blend. J. Controlled Release 2002;81.1-2;57-64.
16. Wang Q, Zhang N, Hu X, Yang J, Du Y. Chitosan/Starch Fibers and Their Properties for Drug Controlled Release.Eur. J. Pharm. Biopharm.2007;66.8;398-404.
17. Chu, CC. Novel Biodegradable Functional Amino Acid-based Poly(ester Amide) Biomaterials: Design, Synthesis,Property and Biomedical Applications. J. Fiber Bioeng. Inform. 2012;5.1;1-31.
18. Katsarava R, Beridze V, Arabuli N, Kharadze D, Chu CC, Won CY. Amino Acid-based Bioanalogous Polymers. Synthesis, and Study of Regular Poly(ester Amide)s Based on Bis(α-amino Acid) α,ω-alkylene Diesters, and Aliphatic Dicarboxylic Acids. J. Polym. Sci., Part A: Polym. Chem. 1999;37.4;391-407.
19. Guo K, Chu CC, Chkhaidze E, Katsarava R. Synthesis and Characterization of Novel Biodegradable Unsaturated Poly(Ester-Amide)**s.** J. Polym. Sci., Part A: Polym. Chem. 2005;43;1463-1477.
20. Jokhadze G, Machaidze M, Panosyan H, Chu CC, Katsarava R. Synthesis and characterization of functional elastomeric poly(ester amide)s copolymers. J. Biomater. Sci., Polym. Ed.2007;18.4;411-438.
21. Tsitlanadze G, Machaidze M, Kviria T, Katsarava R, Chu CC.In vitro enzymatic biodegradation of amino acid based poly (ester amide)s biomaterials. J. Mater. Sci.: Mater. Med. 2004;15;185-

190.

22. Tsitlanadze G, Machaidze M, Kviria T, Djavakhishvili N, Chu CC, Katsarava R. Biodegradation of amino acid based poly(ester amide)s: *In vitro* weight loss and preliminary *in vivo* study. J. Biomater. Sci., Polym. Ed. 2004;15.1;1-24.
23. Pang X, Wu J, Reinhart-King C,Chu CC. Synthesis and characterization of functionalized water soluble cationic poly(ester amide)s. J. Polym. Sci., Part A: Polym. Chem. 2010;48;3758–3766.
24. Yamanouchi D, Wu J, Lazar AN, Kent KC, Chu CC , Liu B. Biodegradable Arginine-based Poly(ester-amide)s as Non-viral Gene Delivery Reagents. Biomaterials 2008;29.22; 3269-277.
25. Wu J, Yamanouchi D, Liu B, Chu CC. Biodegradable Arginine-based Poly(ether Ester Amide)s as a Non-viral DNA Delivery Vector and Their Structure–function Study. J. Mater. Chem. 2012;22.36;18983-18991.
26. Wu J, Mutschler MA, Chu CC. Synthesis and Characterization of Ionic Charged Water Soluble Arginine-based Poly(ester Amide). J. Mater. Sci.: Mater. Med. 2011;22.3;469-79.
27. Song H, Chu CC. Synthesis and Characterization of a New Family of Cationic Amino Acid-based Poly(ester Amide)s and Their Biological Properties. J. Appl. Polym. Sci. 2011;124.5;3840-853.
28. Deng M, Wu J, Reinhart-King CA, Chu CC. Synthesis and Characterization of Biodegradable Poly(ester Amide)s with Pendant Amine Functional Groups and In Vitro Cellular Response. Biomacromolecules2009;10.11;3037-047.
29. Deng M, Wu J, Reinhart-King CA, Chu CC. Biodegradable Functional Poly(ester Amide)s with Pendant Hydroxyl Functional Groups: Synthesis, Characterization, Fabrication and in Vitro Cellular Response. Acta Biomater. 2011;7.4;1504-515.
30. Guo K, Chu CC. Biodegradable and Injectable Paclitaxel-loaded Poly(ester Amide)s Microspheres: Fabrication and Characterization. J. Biomed. Mater. Res., Part B2009;89B.2;491-500.
31. Li L, Chu CC. Nitroxyl Radical Incorporated Electrospun Biodegradable Poly(ester Amide) Nanofiber Membranes. J. Biomater. Sci., Polym. Ed.2009;20.3;341-61.
32. Wu D, Wu J, Chu CC. A Novel Family of Biodegradable Hybrid Hydrogels from Arginine-based Poly(ester Amide) and Hyaluronic Acid Precursors. Soft Matter 2013;9.15;3965-3975.
33. Wu J, Wu D, Mutschler M, Chu CC. Cationic Hybrid Hydrogels from Amino-Acid-Based Poly(ester Amide): Fabrication, Characterization, and Biological Properties. Adv. Funct. Mater. 2012;22.18;3815-823.
34. He M, Potuck A, Zhang Y, Chu CC. Arginine-based Polyester Amide/polysaccharide Hydrogels and Their Biological Response. Acta Biomater.2014;10.6;2482-494.

35. Guo K, Chu CC. Synthesis and Characterization of Novel Biodegradable Unsaturated Poly(ester Amide)/poly(ethylene Glycol) Diacrylate Hydrogels. J. Polym. Sci., Part A: Polym. Chem.2005;43.17;3932-944.
36. Horwitz JA, Shum KM, Bodle JC, Deng M, Chu CC, Reinhart-King CA. Biological Performance of Biodegradable Amino Acid-based Poly(ester Amide)s: Endothelial Cell Adhesion and Inflammation in Vitro. J. Biomed. Mater. Res., Part A 2010;95A.2;371-80.
37. Wu J, Chu CC. Block Copolymer of Poly(ester Amide) and Polyesters: Synthesis, Characterization, and in Vitro Cellular Response. Acta Biomater. 2012;8.12;4314-323.
38. Noli C, Miolo A. The Mast Cell in Wound Healing. Vet. Dermatol.2001;12.6;303-13
39. Martin P, Leibovich SJ. Inflammatory Cells during Wound Repair: The Good, the Bad and the Ugly. Trends in Cell Biol. 2005; 15.11; 599-607.
40. Thurmond RL, Gelfand EW, Dunford PJ. The Role of Histamine H1 and H4 Receptors in Allergic Inflammation: The Search for New Antihistamines. Nat. Rev. Drug Discovery 2008;7.1; 41-53.
41. Schoch, C. Inhibition of Human Conjunctival Mast-Cell Degranulation by Ketotifen. J. Ocul. Pharmacol. Ther. 19.1 (2003): 75-81.
42. Rosenwasser LJ, O'Brien T, Weyne J. Mast Cell Stabilization and Anti-histamine Effects of Olopatadine Ophthalmic Solution: A Review of Pre-clinical and Clinical Research. Curr. Med. Res. Opin. 2005;21.9;1377-387.
43. Patel HJ, Patel JS, Patel KD. Int. J. PharmTech Res. 2009;1.4; 1297-1304.
44. Lee, D M. Mast Cells: A Cellular Link Between Autoantibodies and Inflammatory Arthritis. Science 2002;297.5587;1689-692.
45. Guerrero S, Teijón C, Muñiz E, Teijón JM, Blanco MD. Characterization and in Vivo Evaluation of Ketotifen-loaded Chitosan Microspheres. Carbohydr. Polym. 2010;79.4;1006-013.
46. Xu J, Li X, Sun F. Andevaluation of Ketotifen Fumarate-loaded Silicone Hydrogel Contact Lenses for Ocular Drug Delivery. Drug Delivery 2011;18.2;150-58.
47. Ali M, Horikawa S, Venkatesh S, Saha J, Hong JW, Byrne ME. Zero-order Therapeutic Release from Imprinted Hydrogel Contact Lenses within in Vitro Physiological Ocular Tear Flow. J. Controlled Release 2007;124.3;154-62.
48. Karlgard CCS, Wong NS, Jones LW, Moresoli C. In Vitro Uptake and Release Studies of Ocular Pharmaceutical Agents by Silicon-containing and P-HEMA Hydrogel Contact Lens Materials. Int. J. Pharm. (Amsterdam, Neth.) 2003;257.1-2;141-51.
49. Van Loon SLM, Smits AIPM, Driessen-Mol A, Baaijens FPT, Bouten CVC.The Immune Response in In Situ Tissue Engineering of Aortic Heart Valves, Calcific Aortic Valve Disease. *In Print* 2013

50. Brodbeck WG, Nakayama Y, Matsuda T, Colton E, Ziats NP, Anderson JM. Biomaterial Surface Chemistry Dictates Adherent Monocyte/macrophage Cytokine Expression In Vitro. Cytokine 2012;18.6;311-19.
51. Naal RM, Tabb J, Holowka D, Baird B. In Situ Measurement of Degranulation as a Biosensor Based on RBL-2H3 Mast Cells. Biosens. Bioelectron.2004; 20.4;791-96.
52. Cui, W, Li X, Zhu X, Yu G, Zhou S, and Weng J. Investigation of Drug Release and Matrix Degradation of Electrospun Poly(-lactide) Fibers with Paracetanol Inoculation. Biomacromolecules 2006;7.5;1623-629.
53. Kwon IK, Kidoaki S, Matsuda T. Electrospun Nano- to Microfiber Fabrics Made of Biodegradable Copolyesters: Structural Characteristics, Mechanical Properties and Cell Adhesion Potential. Biomaterials 2005;26.18;3929-939.
54. Mo XM, Xu CY, Kotaki M, Ramakrishna S. Electrospun P(LLA-CL) Nanofiber: A Biomimetic Extracellular Matrix for Smooth Muscle Cell and Endothelial Cell Proliferation. Biomaterials 2004;25.10;1883-890.
55. Katz MH, Alvarez AF, Kirsner RS, Eaglstein WH, Falanga V. Human Wound Fluid from Acute Wounds Stimulates Fibroblast and Endothelial Cell Growth. J. Am. Acad. Dermatol. 1991;25.6;1054-058.
56. Stepnowski P, Skladanowski AC, Ludwiczak A, Laczyńska E. Evaluating the Cytotoxicity of Ionic Liquids Using Human Cell Line HeLa. Hum. Exp. Toxicol. 2004;23.11;513-17.
57. Morais JM, Papadimitrakopoulos F, Burgess DJ. Biomaterials/Tissue Interactions: Possible Solutions to Overcome Foreign Body Response. The AAPS Journal 2010;12.2;188-96.
58. Mcnally A K, Anderson JM. Foreign Body-type Multinucleated Giant Cells Induced by Interleukin-4 Express Select Lymphocyte Co-stimulatory Molecules and Are Phenotypically Distinct from Osteoclasts and Dendritic Cells. Exp. Mol. Pathol.2011;91.3;673-81.
59. Tsan, M. Toll-like Receptors, Inflammation and Cancer. Semin. Cancer Biol. 2006;16.1;32-37.
60. Luong-Van E, Grøndahl L, Chua KN, Leong KW, Nurcombe V, Cool SM. Controlled Release of Heparin from Poly(ε-caprolactone) Electrospun Fibers. Biomaterials 2006; 27.9;2042-050
61. Wu J, Chu CC. Water Insoluble Cationic Poly(ester Amide)s: Synthesis, Characterization and Applications. J. Mater. Chem. B 2012;1.3;353-360.
62. Stamler J, Singel D, Loscalzo J. Biochemistry of Nitric Oxide and Its Redox-activated Forms. Science 1992;258.5090;1898-902
63. Radomski, M. W. Nitric Oxide: Biological Mediator, Modulator and Effector. Ann. Med. 1995;27.3;321-29.
64. Mantovani A, Sica A, Sozzani S, Allavena P, Vecchi A, Locati M. The Chemokine System in Diverse Forms of Macrophage Activation and Polarization. Trends Immunol. 2004;25.12;677-86.

65. Theoharides, TC, Kempuraj D, Tagen M, Conti P, Kalogeromitros D. Differential Release of Mast Cell Mediators and the Pathogenesis of Inflammation. Immunol. Rev. 2007;217.1;65-78.
66. Beaven, M. A. Our Perception of the Mast Cell from Paul Ehrlich to Now. *Eur.* J. Immunol. 2009;39.1; 11-25
67. Silver, R. B. Mast Cells: A Unique Source of Renin. Proc. Natl. Acad. Sci. U.S.A 2004;101.37;13607-3612.
68. Thevenot PT, Baker DW, Weng H, Sun M, Tang L. The Pivotal Role of Fibrocytes and Mast Cells in Mediating Fibrotic Reactions to Biomaterials. Biomaterials 2011;32.33;8394-403.
69. Garg K, Ryan JJ, Bowlin GL. Modulation of Mast Cell Adhesion, Proliferation, and Cytokine Secretion on Electrospun Bioresorbable Vascular Grafts. J. Biomed. Mater. Res., Part A2011;97A.4;405-13.
70. Yamaguchi, M. IgE Enhances Mouse Mast Cell Fcepsilon RI Expression In Vitro and In Vivo: Evidence for a Novel Amplification Mechanism in IgE-dependent Reactions. J. Exp. Med.1997;185.4;663-72.
71. Yanni JM, Stephens DJ, Miller ST, Weimer LK, Graff G, Farnell D, Lang LS, Spellman JM, Brady MT, Gamache DA. The in vitro and in vivo Ocular Pharmacology of Olopatadine (AL-4943A), an Effective Anti-Allergic/Antihistaminic Agent. J. Ocul. Pharmacol. Ther.12.4 (1996): 389-400

Chapter 5. Ketotifen Fumarate Delivery by Pluronic/Arginine-based Poly(ester amide) Hybrid Hydrogels: Fabrication, Characterization, and Biological Property

(In Preparation – proposed July 2015) Potuck, Alicia, Sarah Meyers, Marcus Wilkes, and C. C. Chu. Ketotifen Fumarate Delivery by Pluronic/Arginine-based Poly(ester Amide) Hybrid Hydrogels: Fabrication, Characterization, and Biological Property. Journal of Materials Chemistry B

Abstract

Sustained release of mast cell stabilization agent Ketotifen fumarate (KF) was achieved by delivery via hydrogel swelling using novel unsaturated arginine-based poly(ester amide) polymers (UArg-PEA)s and biocompatible Pluronic F127 polymers.Pure Pluronic and hybrid UArg-PEA/Pluronic hybrid hydrogel interior morphology, swelling ratio, weight loss, KF release, and biological properties were explored. Incorporation of arginine-based UArg-PEA into Pluronic hydrogel fabrication greatly affected mechanical (i.e. larger pore size, larger swelling ratio) and *in vitro* degradationperformance (higher enzymatic degradation rate for hybrid hydrogels). Hybrid hydrogels had greater RAW macrophage viability compared to Pluronic alone. In addition, hybrid hydrogels released KF at a slower rate than Pluronic hydrogels, indicating higher indication for sustained release. Overall, hybrid UArg-PEA/Pluronic hydrogels had higher viability, lower inflammation, and longer sustained drug release, showing their excellent potential for use *in vivo*.

5.1 Introduction

A hydrogel is characterized as polymeric material that has the capability of storing considerable amounts of water via porous microstructure formed during crosslinking of polymers, low surface tension, and soft nature that mimics human tissue.[1,2] While initially hydrogels were made from materials such as collagen or cartilage, there has been a great extension in the materials used to fabricate hydrogels including biopolymer polysaccharides such as hyaluronic acid and proteins (including elastin and fibroin), as well as commercially available materials such as PVA.[2] Hydrogels can be characterized by the material of its origin, charge of polymer or copolymers (neutral, anionic, or cationic), natural or synthetic polymers, or hybrid combinations. Hydrogels can be characterized by physical appearance either as amorphous, semi crystalline, or crystalline.[3] Furthermore, hydrogels can be classified by its method of fabrication, either by chemical methods such as UV-crosslinking or physical methods such as crosslinking due to interactions such as hydrogen bonds or hydrophobic interactions.[1] Hydrogels have many different applications, from promoting wound healing to use in repairing or regenerating organs.[4]

Well documented in literature for its excellent mechanical and physical properties, Pluronic polymers are amphiphilic thermosensitive synthetic block copolymers.[4-7] Invented and patented in 1973 by Schmolka[7], poloxomers (trade name Pluronics) have the ability to form a gel when "hydrophobic interactions between the (polypropylene oxide) moiet(ies)" occur.[8] A novel characteristic of Pluronics is the ability to capture hydrophobic compounds/drugs due to hydrophobic/hydrophobic interactions, which make these polymers excellent candidates to deliver poorly water soluble.[9]Pluronic F127, a member of the Pluronic family, is a triblock

copolymer that consists of two hydrophilic polyethylene groups and a center hydrophobic polypropylene group.[10,11]Pluronic polymers have high solubility in aqueous media, low toxicity and immunogenicity leading to its approval by the FDA for use *in vivo*.[12]

Pluronic polymers can be found in a variety of hybrid formulations and fabrication methodologies. Attributing to both hydrophilic and hydrophobic blocks in Pluronic polymers, their polymeric composition lends well to micelle formation, used heavily for entrapment of hydrophobic cancer drugs in Pluronic micelles for improved drug solubilisation.[12-15]The formation of pure Pluronic hydrogels has been extensively studied for their biocompatibility, predictable weight loss, and drug release capabilities[9,16-19], along with novel hybrid hydrogels including polysaccharide/Pluronic hybrid[8, 20], peptide/Pluronic hybrid[21], and many more.

To create hybrid hydrogels for potential benefits of compatibility and sustained drug release, a novel family of amino acid-based poly (ester amide) (AA-PEA) polymers were used. AA-PEA polymers are characterized by the use of non-toxic starting materials such as α-amino acids, fatty diols, and dicarboxylic acids[22-24] which can lead to reduced inflammation when coupled with commercially available materials such as poly(caprolactone) (PCL).[25] Copolymerization of hydrophobic Phenylalanine-based monomers with hydrophilic cationic Arginine-based monomers forming hybrid AA-PEAs have also been shown to mute inflammatory response compared to commercially available PCL.[26] AA-PEA polymers contain both ester (sites available for aqueous *in vitro* and *in vivo* degradation)[27-28] and amide (excellent mechanical properties including functional elastomeric strength)[29-30] imparting favourable qualities for biomaterial applications. In addition, modifications to the AA-PEA synthesis can be introduced

to include unsaturation in both the backbone[31-32]and pendant along the polymer chain[33], further extended to the addition of amine[34] or hydroxyl groups.[35]

AA-PEA amino acids can be varied to tailor hydrophobicity/hydrophilicity, with Arginine being of greatest interest for its cationic charge and favourable isoelectric point (10.76). Arginine-based AA-PEA materials contain a pendant $–NH_2$ group, which has been proven to have excellent water solubility (reducing toxicity of using organic solvents such as chloroform) and ability to induce cell proliferation.[32,36-37] Arginine-based AA-PEAs are also ideal for fabrication of hybrid hydrogels using commercially available materials such as PEG-DA[38], Pluronic F127[39], and polysaccharide polymers.[40-43] Wu *et al* has shown excellent compression modulus and fibroblast cell adhesion after 48 hours to Pluronic/Arginine-based hydrogels.[39]

This work seeks to use Ketotifen fumarate (KF) as an additional defense to inflammation using controlled release from impregnation in hybrid unsaturated arginine-based AA-PEA (UArg-PEA)/ Pluronic hydrogels. KF stabilizes mast cells through Fc receptor mediated IgE regulated calcium channels, with multiple medicinal applications such as treatment for asthma, atopic dermatitis, and food allergies.[43] Mast cells, from the leukocyte family, are a cell ~~line~~ typecommonly ~~found~~ associated~~in~~ withallergic reactions, stimulating inflammation via release of granules present within the cell cytoplasm including the potent inflammatory mediator histamine. KF has the potential to decrease the effect of proinflammatory cytokine synthesis (in cases of conjuntivitis), leading to reduced inflammation.[44] However, KF suffers from poor oral bioavailability, ~~leading to reduced~~ limiting effectiveness of treatment. Therefore, a direct site of

action approach would be advantageous in prolonged release and efficacy, which can be directly applied to impregnation in hydrogels.

In this paper we report Pluronic F127 and AA-PEA/Pluronic F127DA were successfully fabricated and characterized for mechanical properties such as swelling, weight loss, and KF release over time. The resultingAA-PEA/Pluronic F127DA hydrogels garner slower release of KF over time, leading to extended release versus that of Pluronic hydrogels with excellent *in vitro* compatibility and cell adhesion. KF release from pure and hybrid hydrogels also had profound reductions in mast cell degranulation, making these hydrogels an excellent candidate for potential wound healing devices.

5.2 Methods and Materials

Materials

Pluronic F127, Acryloyl chloride, 4-Nitrophenol, trypsin (from porcine pancreas, 13,000-20,000 BAEE units/mg) were purchased from Sigma Aldrich (St. Louis, MO, USA). Triethylamine and hexanes were purchased from Fischer Scientific (Fairlawn, NJ, USA). L-Arginine, fumaryl chloride, and p-Toluenesulfonic Acid monohydrate were purchased from Alfa Aesar (Hersham, UK). Ethylene glycol was purchased from Mallinckrodt Chemicals (Phillipsburg, NJ, USA). Irgacure 2959 was purchased from Ciba Specialty Chemicals (Tarrytown, NY, USA). Acetone was purchased from Avantor Performance Materials (Center Valley, PA, USA). Ketotifen fumarate was purchased from Enzo Life Sciences (Farmingdale, NY, USA).

Synthesis of 2UArg-PEA-2S and Pluronic F127DA

Arginine-based unsaturated poly(ester amide) polymer (UArg-PEA) was synthesized according to established protocol.[32] Synthesis of UArg-PEA was based solution polycondensation in DMSO of two starting monomers; 1) Di-*p*-nitrophenyl fumarate, and 2) tetra-*p*-toluenesulfonic acid of bis(L-arginine) ethane diester. Each monomer (1.0mmol) was added to a 500mL round bottom flask solvent using triethylamine as an acid scavenger (2.2mmol). Resulting solution was stirred at constant temperature (70℃) for 48 hours, precipitated in ethyl acetate, collected and dried, purified by dissolution in methanol and precipitated in ethyl acetate (purification repeated 2x more to ensure polymer purity). Final polymer (brown crystalline solid) was dried under reduced pressure for 48 hours to ensure removal of residual solvent.

Pluronic F127 diacrylate (F127DA) synthesized via chemical modification of Pluronic F127 polymer using an established protocol.[9] Briefly, Pluronic F127 (0.01mol) was dissolved in toluene with heat (40℃ for 30 minutes). Acryloyl chloride (0.005mol) and triethylamine (0.005mol) were added, and resulting polymer solution was stirred at room temperature for 16 hours. Pluronic F127DA polymer solution was filtered (remove insoluble chloride salt), precipitated in cold hexane, vacuum collected, and dried at room temperature under vacuum (Isotemp Vacuum Oven 285A, Fischer Scientific, Fairlawn, NJ, USA) (48 hours) to ensure constant weight and complete removal of solvent.

Fabrication of Pure and Hybrid Hydrogels

Fabrication protocol for pure F127DA and UArg-PEA/F127DA hybrid hydrogels has been previously reported.[39] Pure F127DA hydrogels were fabricated by dissolving 20wt% F127DA in

2mL distilled water with 1wt% Igracure 2959 photoinitator in a small glass scintillation vial at 100°C with stirring for 10 minutes. Elevated temperature was needed to achieve homogenous dissolution of F127DA and photoinitiator. F127DApolymer solution was carefully pipetted into a 20-well (1cm diameter) Teflon mold and UV photocrosslinked for approximately 6-8 minutes (Black-Ray® long wave ultraviolet lamp, UVP, Upland, CA, USA). Photocrosslinked hydrogels were purified in distilled water for 24 hours to ensure removal of unreacted monomers or photoinitiator, and dried at room temperature for 72 hours to reach constant weight.

Hybrid UArg-PEA/F127DA hydrogels were fabricated using a20:80 feed ratio of UArg-PEA/F127DA.Wu *et al* found that this feed ratio provides favourable mechanical properties with excellent cell proliferation.[39]Fabrication of hybrid hydrogels is similar to fabrication of F127DA hydrogels with the addition of UArg-PEA (16wt% F127DA, 4 wt% UArg-PEA, 1 wt% Irgacure 2959). Hybrid F127DA solution was pipetted into 20-well (1cm diameter) Teflon mold and UV photocrosslinked for 8-10 minutes. Hybrid hydrogels were purified in distilled water for 24 hours and dried at room temperature for 72 hours to ensure constant weight.

Hydrogel Characterization

UArg-PEA and chemical modification of Pluronic F127 polymer were confirmed with Infrared Spectroscopy (Nicolet Magna-IR 560, Nicolet Instrument Corp., Madison, WI, USA). Surface charge of precursor materials and fabricated hydrogels were analysed using the Zetasizer Nano ZS (Malvern, UK) with zeta potential calculated using the Smoluchowsky model.For zeta potential measurements, polymer precursors were suspended in distilled water (10mg/mL) and hydrogels were swollen in distilled water and briefly homogenized for pipetting into disposable

capillary cell. Pure and hybrid hydrogel interior morphology were confirmed with Scanning Electron Microscopy (SEM) (Leica 440, Leica Microsystems, Buffalo Grove, IL, USA). To assess weight loss of pure and hybrid hydrogels, samples were kept at physiological temperature using a recriprocol water bath (Julabo SW22, Julabo, Allentown, PA, USA). Ketotifen fumarate released quantified at 300nm using UV-Vis spectroscopy (Lambda 35, Perkin Elmer, Waltham, MA, USA).

Imaging of hydrogel morphology

Pure and hybrid F127DA hydrogels were prepared for SEM imaging via established protocol.[40] After complete swelling of pure and hybrid hydrogels in distilled water (excess distilled water,48 hours), swollen hydrogels were placed directly into liquid nitrogen for 3 minutes. After complete freezing, hydrogels were transferred to a 15mL centrifuge tube for lyophilisation for 48 hours at reduced pressure (0.045 mbar) and temperature (-50°C) using Labconco Freeze Dry system (Labconco, Kansas City, MO, USA). Dry hydrogels were mounted on aluminium stubs and sputter-coated with Au/Pd for 30 seconds in preparation for imaging. Average hydrogel pore size was calculated using ImageJ software (NIH, Bethesda, MD, USA).

***In vitro* hydrogel biodegradation**

To evaluate F127DA and UArg-PEA/F127DA hybrid hydrogel weight loss based on enzymatic degradation, hydrogels were placed in 15mL centrifuge tubes with 0.1mg/mL trypsin (in 1X PBS) and incubated at 37°C until predetermined time points (1-7 days). To calculate weight loss, hydrogels were removed, media decanted, and frozen at -20°C followed by 48 hours

lyophilisation to reach a constant dry weight. Weight loss % was calculated using the following formula:

$$W_L = ((W_I - W_D)/ W_{D)} \times 100$$

where W_L= weight loss percent, W_I= initial dry weight at time 0, and W_D = weight of enzymatically degraded sample at time (t). Data is presented an average ± std.dev of three independent samples.

Swelling ratio analysis

To assess the ability of F127DA and UArg-PEA/F127DA hydrogels to swell in aqueous media from a dry state, pure F127DA and hybrid UArg-PEA/F127DA hydrogels were placed in a 15mL centrifuge tube with either (1X PBS – control) or with Ketotifen fumarate drug doping (0.2 wt% in 1X PBS) at room temperature. All hydrogel samples types were tested in triplicate.The swelling ratio was calculated from weight gain after time (t). Briefly, at predetermined time points (10-90 minutes), F127DA or UArg-PEA/F127DA hybrid hydrogels were removed from media (control or KF-doped) and weighed using an analytical balance. The swelling ratio for each hydrogel type and media composition was calculated using the formula:

$$W_S = ((W_H - W_I)/W_I) \times 100$$

where W_S= hydrogel swelling ratio, W_H= hydrated weight of hydrogel at time (t), and W_I= initial dry weight of hydrogel. Data presented is an average ± std. dev of three independent samples.

In vitro Ketotifen fumarate drug release

To quantify Ketotifen fumarate drug doping of F127DA andUArg-PEA/ F127DA hybrid hydrogels, dry hydrogels were placed in 0.2 wt% (in 1X PBS at room temperature) Ketotifen

fumarate solution for 24 hours to reach complete equilibrium swelling. KF-doped F127DA and UArg-PEA/ F127DA hydrogels were placed in either 10mL control (1X PBS) or enzyme (0.1mg/mL trypsin in 1X PBS) in 15mL tubes at 37℃. At predetermined time points, aliquots of aqueous media were removed and absorbance read at 300nm. Sample solutions were refreshed at each time point and % Cumulative ketotifen release calculated using a linear regression of a KF standard curve. Data presented in an average ± std. dev of three independent samples.

Cell viability

RAW264.7 ~~RAW~~ macropahge cells (kindly provided by Leifer Lab, Cornell Veterinary Medical College) were grown in complete DMEM (CDMEM, 10% fetal bovine serum (FBS), 1mM Hepes, 200mM L-glutamine, 10,000 IU/mL penicillin, 10,000 µg/mL streptomycin, and 100mM Sodium pyruvate) at 37°C with 5% CO_2. All media reagents (except FBS) were purchased from Mediatech (Manassas,VA, USA). FBS was purchased from PAA Laboratories (Dartmouth, MA, USA).

To assess toxicity of F127DA andUArg-PEA/F127DA hybrid hydrogels, RAW264.7 cells were plated at an appropriate density (100,000 cells/well) directly onto pure and hybrid hydrogels (immersed in cell media for 24 hours to ensure equilibrium swelling) placed into the bottom of a 24-well plate. After 24 hours RAW264.7 cell incubation with hydrogel material at 37℃ and 5% CO_2, cell prolifertionwas measured using Cell Counting Kit-8 (~~CCk~~CCK-8 Reagent, Sigma Aldrich, Milwaukee, WI, USA). CCK-8 reagent was added to each well at a ratio of 10µL reagent/ 100µL CDMEM and incubated at 37℃ for 2 hours. An aliquot of media was removed from each well, transferred to a new plate, and absorbance was measured at 450nm. RAW264.7

viability was normalized to untreated control and represented at average ± std. dev of quadruplicate samples.

Proinflammatory cytokine (TNF-α) assay

To assess proinflammatory cytokine production, supernatants were removed from incubation of macrophage cells with hydrogels (100,000 cells/well in 24-well plate, incubated 24 hours at 37℃ and 5% CO_2) and assayed according to manufacturer's protocol (Mouse TNF Elisa Maxx Standard kit, Biolegend, San Diego, CA, USA). Cells on tissue culture plate were used as a negative control, while LPS (Lipopolysaccharide) (ATCC, Manassas, VA, USA) was used as a positive control (assayed at 100ng/mL). TMB substrate (color developing agent) was purchased from KPL (Gaithersburg, MD, USA) and 2N $H_2SO_4$was used to stop the reaction. Absorbance was read at 450nm and concentration calculated using linear regression in Graphpad Prism 6 (Graphpad, La Jolla, CA, USA) using a standard curve.

Mast Cell Stabilization

RBL-2H3 rat basophil leukemia cells (kindly provided by Baird/Holowka Lab, Cornell University) were grown in complete EMEM (Eagles Minimum Essential Media) (CEMEM, 15% fetal bovine serum (FBS), 1mM Hepes, 200mM L-glutamine, 10,000 IU/mL penicillin, 10,000 µg/mL streptomycin, and 100mM Sodium pyruvate) at 37°C with 5% CO2.

Mast cell stabilization via KF was assayed using *in situ* measurement of RBL-2H3 mast cell degranulation according to a published protocol.[45] RBL-2H3 cells were plated at a density of 50,000 cells/well in a 96-well plate and treated according to protocol. Aliquots of aqueous media (hydrogels either pure or KF-doped immersed in 500µL CMEM) was removed after 48 hours

and assayed according to protocol. Total % degranulation was measured against untreated RBL-2H3 cells and total degranulation (cell lysis using 0.1% Triton X-100) and normalized to control.

Statistical Analysis

All data represented is given as an average ± standard deviation for (n) replicate independent samples to provide accurate sample behaviour. Where appropriate, samples were tested for significance using one-way ANOVA and Tukey's honest significant difference post-hoc. Statistically significant samples are denoted (*) when $p < 0.05$, (***) when $p < 0.01$.

5.3 Results and Discussion

Fabrication of F127DA andUArg-PEA/F127DA hydrogels

F127DA and UArg-PEA/F127DA hybrid hydrogels were fabricated using UV-induced radicalization of unsaturated double bonds present in both UArg-PEA and F127DA polymer precursors to create crosslinking sites for hydrogel formation using an established protocol.[39] Both polymer precursors (UArg-PEA and F127 DA) are soluble in aqueous media with slight heating to facilitate complete dissolution. Viscous hydrogel precursor solution (either pure or hybrid) was easily pipetted into a Teflon mold to form circular hydrogels during UV-photocrosslinking. Pure F127DA hydrogels formed uniform and mechanically stable hydrogels after approximately 6-8 minutes under UV exposure, while hybrid UArg-PEA/F127DA hydrogels were crosslinked for an additional two minutes to ensure crosslinking of UArg-PEA in hydrogel solution. Wu *et al* suggest that longer exposure to UV light is needed for hybrid hydrogels as the unsaturated >C=C< bond in AA-PEA polymer requires longer time than acrylate groups in F127DA to completely crosslink.[39]

Immediately following UV photocrosslinking, pure and hybrid hydrogels were placed in excess distilled water for purification (24 hours minimum). The purification step was necessary to remove polymer precursors or photoinitiator that has not been crosslinked into the overall hydrogel microstructure. Both hydrogel formulations (pure F127DA and hybridUArg-PEA/F127DA) consistently formed hydrogels whichcould be dried or soaked in aqueous media (Figure 25 A, B) for hydrogel swelling.

Characterization of F127DA and F127DA/UArg-PEA hybrid hydrogels

Surface Charge (ζ-potential)

Both precursor polymers and fabricated hydrogels were analysed to determine the surface charge that cells would come into contact with upon incubation using ζ-potential. Both commercially available Pluronic F127 and modified F127DA polymers displayed negatively-charged ζ-potentials. Anionic ζ-potential in commercially available Pluronic F127 (-9.57 ± 2.00 mV) can be ascribed to the presence of end-capped hydroxyl groups. F127DA modified polymers are capped with diacrylate groups, but still maintain a negative surface charge (-5.42 ± 1.21 mV) potentially through carbonyl resonance with the acrylate group attached. Contrastingly, UArg-PEA polymer precursor exhibits a positive ζ-potential (+11.2 ± 0.83 mV) (Figure 25C). Since the guanidine group of Arginine is protonated at physiological conditions, the guanidinium cation provides a pendant positive charge to UArg-PEA polymers. Upon fabrication into hydrogels, pure F127DA negative ζ-potential was reduced, with a surface charge close to neutral (-1.22 ± 0.26 mV) as the carbonyl group could no longer undergo resonance with the saturated diacrylate group to produce the anionic oxygen. Interestingly, hybrid UArg-PEA/F127DA

hydrogels had an overall cationic surface charge (10.58 ± 2.16 mV), due to the positive charge from UArg-PEA polymers.

In comparison to studied Pluronic polymer-based biomedical devices, Chung *et al* found a ζ-potential of -26 ± 1 mV for Pluronic F127/poly(lactic glycolic) acid nanoparticles (diameter ~150nm), with increased negativity in ζ-potential upon coating with anionic heparin (-41 ± 2 mV) for use in therapeutic angiogenic applications.[46] Similarly, Carstensen *et al* studied fat emulsions in distilled water including a series of Poloxamers (trade name Pluronic®) and found the surface charge varied from -11.1 to + 3.2 mV, measuring a surface charge of Pluronic F127 as -8.1 mV.[47] Cationic surface charge can also influence material and cell behaviour as evidence by Wu *et al*.[36] They found by increasing the ratio of cationic saturated Arg-PEEA (arginine poly(ether ester amide)s) to DNA in nanoparticle formulations for non-viral gene delivery vectors, ζ-potential increased with increasing Arg-PEEA/DNA feed ratio (-3 to +4 mV) up to 1000.[36]

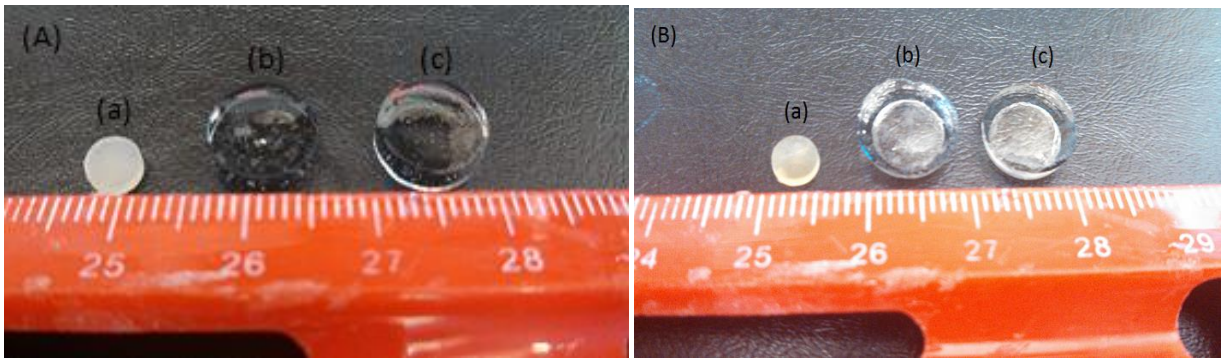

(C)

Material	Diameter (mm,dry)	Diameter (mm,swollen)	ζ-Potential (mV)
Pluronic F127	---	---	-9.57 ± 2.00
Pluronic F127DA	---	---	-5.42 ± 1.21

UArg-PEA	---	---	11.20 ± 0.83
Pure F127DA hydrogel	6.85 ± 0.23	16.98 ± 0.65	-1.22 ± 0.25
Hybrid UArg-PEA/F127DA hydrogel	7.07 ± 0.07	18.07 ± 0.32	10.58 ± 2.16

Figure 25. Pure F127DA (A) and UArg-PEA/ F127DA (B) hybrid hydrogels in a dry (a), swollen in saline (b), and swollen in saline + KF (c) state. Scale bar represents inches. (C) Table 1. Properties of pure F127DA and hybrid UArg-PEA/F127DA hydrogels. All samples tested (quadruplicate samples, in distilled water) represented as avg. ± std. dev.

Use of UArg-PEA in hybrid UArg-PEA/F127DA hydrogel offers a favourable cationic microenvironment for cell adhesion and attachment. Wu *et al* fabricated UArg-PEA/F127DA hybrid hydrogels and found increased cell proliferation after 48 hours on hybrid hydrogels versus pure F127DA hydrogels (without cationic surface) using Detroit 539 fibroblasts, further noting decreased cell adhesion and alterations in morphology for pure F127DA hydrogels.[39] Expanding beyond AA-PEA materials, De Rosa *et al* incubated both neutral base polymer hydrogels (polyhydroxyethylmethacrylate, pHEMA) and cationic hybrid hydrogels (pHEMA-co-METAC, methylacryloyloxyethyltrimethyl ammonium chloride) with human primary fibroblasts and found significantly increased fibroblast adhesion and spreading on the cationic hydrogel versus that of pHEMA.[48] Similarly, Sosnik *et al* utilized cationic METAC to modify four-arm poloxamine (poly(ethylene oxide) and poly(propylene oxide) polymer) hydrogels and found, using human umbilical vein endothelial cells, hybrid cationic poloxamine-METAC hydrogel significantly improved cell attachment leading to confluent monolayers, contrasting pure poloxamine

hydrogels which provided a poor environment for cell attachment.[49] Therefore, integration of cationic charge from UArg-PEA polymers into Pluronic hydrogels offers excellent potential for improved cell attachment.

Infrared Spectroscopy

UArg-PEA contains carbonyl bands at 1647-1650cm^{-1} (amide I), 1535-1542cm^{-1} (amide II), 1735-1745cm^{-1} (ester) and slight NH vibrations at 3290cm^{-1}. Since F127DA polymers do not contain nitrogen species, amide peaks I and II were used to characterize integration of UArg-PEA. Although muted due to large feed ratio of F127DA (80:20 F127 to UArg-PEA), amide I and II peaks are present in hybrid hydrogels and absent in pure F127DA hydrgels, indicating successful fabrication of hybrid F127DA/UArg-PEA hydrogels(Figure 26B). Chemical modification of Pluronic F127 to F127DA was confirmed with unsaturated ester/acrylate peak (Figure 26A) at 1725cm^{-1}.[9]

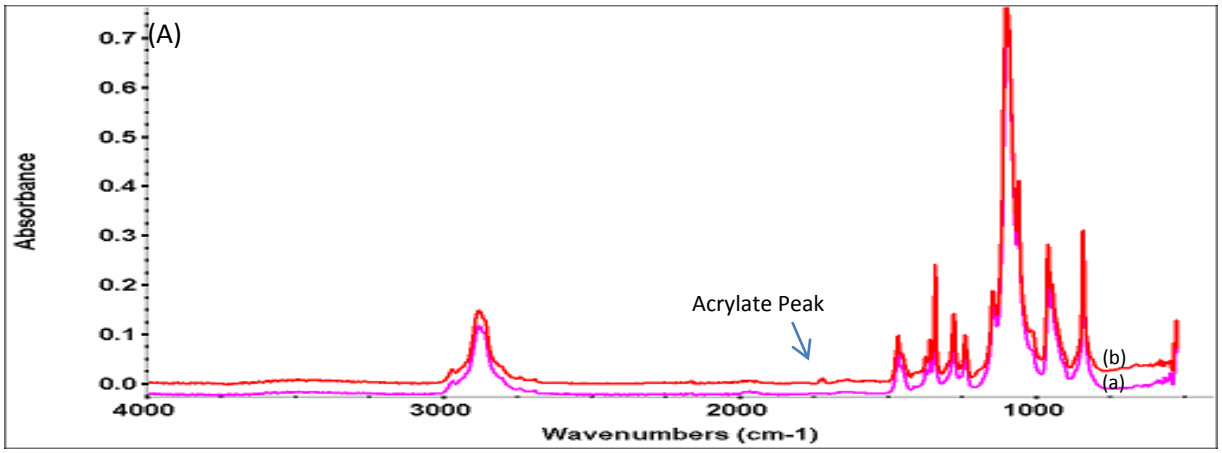

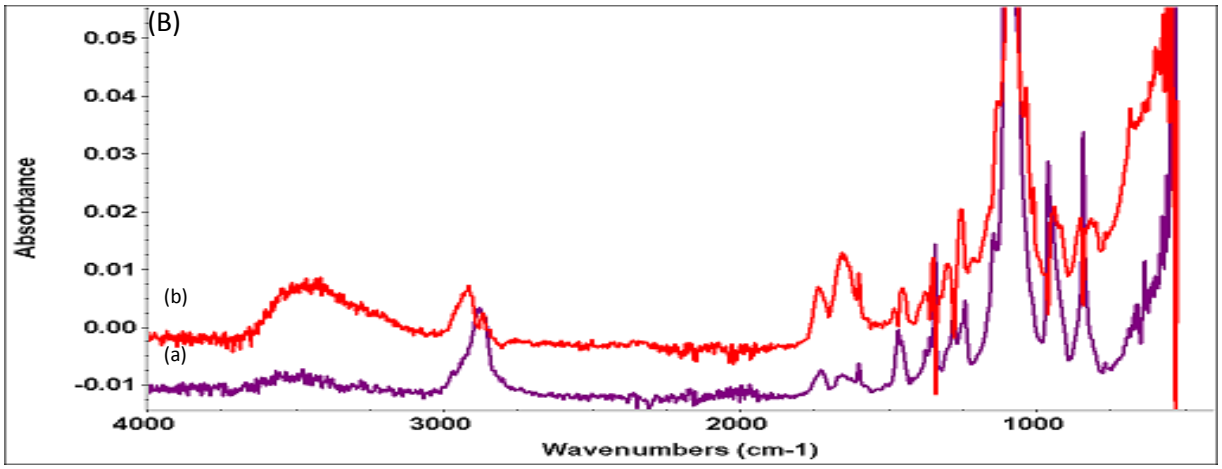

Figure 26. FTIR spectra of (A) Pluronic F127 (a) and Pluronic F127DA chemical modification (b), and (B) Pure F127DA hydrogel (a) and UArg-PEA/ F127DA hybrid hydrogel (b).

SEM Imaging

Scanning Electron Microscopy was used to determine qualitative average pore size and cross-sectional interior hydrogel morphology. Each hydrogel was flash frozen in liquid nitrogen from an equilibrium swollen state and lyophilized in order to preserve pores created upon swelling in aqueous media. F127DA and UArg-PEA/F127DA pore characteristics were tested before (day0– no *in vitro* degradation) and after enzymatic degradation (day 7 – 0.1mg/mL trypsin). Day 0 F127DA and UArg-PEA/F127DA hybrid hydrogels had similar pore size diameter,10.95 ± 5.65 µm and 10.31 ± 4.52µm, respectively (Figure 27 a, b). F127DA pore walls were much more pronounced than hybridUArg-PEA/F127DApore walls, consistent previous findings.[39]Similarly, trademark fibrous networks and visible UArg-PEA polymer nodes characteristic of hybrid hydrogels are present in UArg-PEA/F127DA hybrids, indicating 20:80

feed ratio UArg-PEA/ F127DA creates analogous pores and morphology to that of previous findings by Wu *et al*.[39]

To mimic *in vivo* degradation conditions, hybrid UArg-PEA/F127DA and pure F127DA hydrogels were incubated with enzyme to assess the degradative effect on pore size and morphology. Pure F127DA hydrogel pore size increased from 10.95 ± 5.65μmfrom day 0 to 35.50 ± 12.90μm diameter at day 7 when incubated at physiological temperature (37°C) (Figure 27a,b). UArg-PEA/F127DA hybrid hydrogel pore size increased significantly after 7 days *in vitro* enzymatic degradation (from 10.31 ± 4.52μm to 54.50 ± 6.74 μm diameter) (Figure 27c,d). We postulate that since Pluronics do not readily undergo hydrolysis, pore size increase is a result of ester hydrolysis of the Pluronic-acrylate linkage. Since these linkages are directly involved with crosslinking density, scission of these bonds could attribute to loosening of crosslinking density leading to larger pore sizes. This hypothesis is consistent with the findings of Kim *et al* who synthesized modified HA(Hyluronic Acid)/F127DA hybrid hydrogels and found that hybrid hydrogel incubation at physiological temperature accelerated the ester hydrolysis of the pluronic-acrylate bond leading to hydrogel degradation.[50]

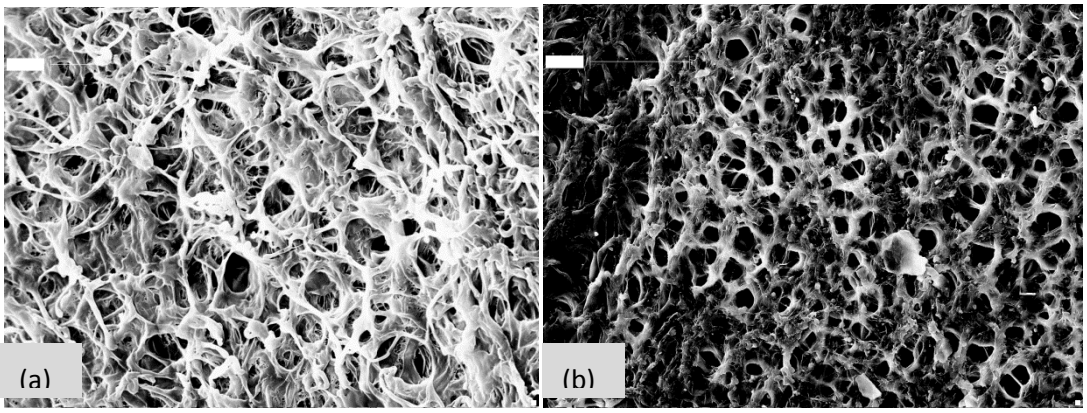

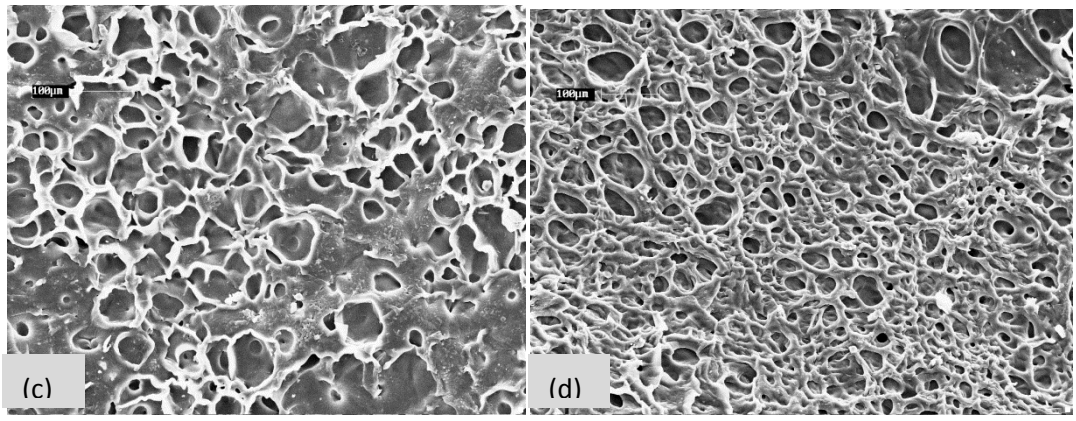

Figure 27. SEM Imaging of Pure and hybrid hydrogels at 0 days *in vitro*degradation (a) F127DA, (b) UArg-PEA/ F127DA hybrid hydrogel, and after 7 days *in vitro*degradation in 0.1mg/mL trypsin solution (c) F127DA, (d)UArg-PEA/F127DA hybrid hydrogel.

In a synergistic effect with ester hydrolysis of pluronic-acrylate bonds, increased hybrid hydrogel pore size and loosening of pore microstructure can be directly attributed to trypsin influence. Trypsin, a serine family proteolytic enzyme, has high tryptic affinity for targeting the C-terminus of arginine amino acids.[51]Since arginine pendant groups in UArg-PEA are susceptible to degradation from trypsin, increased effects from trypsin are seen in UArg-PEA/ F127DA hydrogels, but absent in pure F127DA hydrogels.

In Vitro weight loss

F127DA pure hydrogel did not show an appreciable weight loss after 7 days *in vitro* degradation (0.1mg/mL trypsin 1X PBS at 37℃) (< 10%). F127DA hydrogels had large variability in weight loss % under enzymatic degradation (1-7 days)which could be attributed to variances in starting dry weight or protein adsorption to/in F127DA hydrogel. Conversely, UArg-PEA/F127DA hybrid hydrogels underwent significant*in vitro* weight loss due to presence of

arginine in UArg-PEA susceptible to enzymatic digestion into smaller, water soluble polymer chains. Between 0-3 days no statistically significant weight loss due to trypsin degradation of UArg-PEA/F127 was evident. After 4 days, enzymatic degradation of hybrid hydrogels became dominant with weight loss % increasing with incubation time from 5 (4% increase) to 6 (5% increase) to 7 (14% increase) days (Fig. 28). Therefore, between 0-4 days, hydrolytic degradation of ester linkages in aqueous media was the main driving force of degradation. After 4 days in vitro incubation with trypsin, scission of pendant arginine groups in UArg-PEA dominated of degradation in hybrid hydrogels.

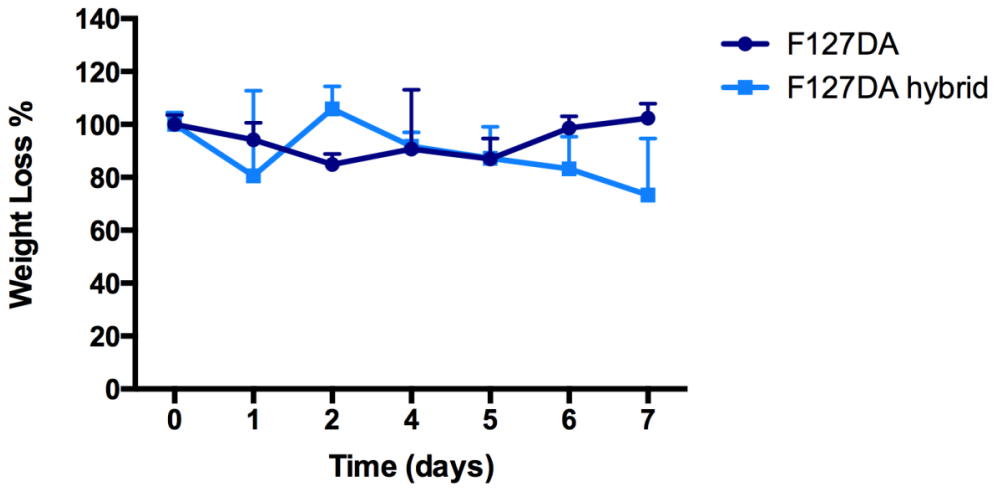

Figure 28. *In vitro*biodegradation weight loss of F127DA and UArg-PEA/F127DA hybrid hydrogels after *in vitro*biodegradation in trypsin (0.1mg/mL) at 37℃, triplicate samples (avg. ± std. dev).

Inherent in the concept and design of hydrogels, these materials are susceptible to *in vitro* and *in vivo* degradation for invasion cells into the microstructure and formation of new structural extracellular matrix as hydrogel biodegradation occurs. Hydrogels are degraded *in vivo* by a

multitude of proteins, enzymes, etc. while *in vitro* degradation is commonly modelled using aqueous environments (hydrolytic degradation) or enzymatic environments (trypsin, α-chymotrypsin, arginase, etc). Weight loss analysis was used to characterize a time frame which the hydrogel loses weight under the influence of *in vitro* degradation. Our study examined weight % retention of both pure and hybrid hydrogels under trypsin degradation to analyse the effect of trypsin degradation specifically targeting arginine UArg-PEA in hybrid hydrogels.

In comparison, F127DA/methyacrylated HA hybrid hydrogels synthesized by Kim *et al* maintained weight retention similar to our pure F127DA hydrogels (<10% weight loss) under hydrolytic degradation.[51] They observed slight degradation only after a lag time of 5 days incubation, with 90% of hydrogel weight remaining up to 40 days *in vitro* incubation at physiological temperature.[51] Pang *et al* demonstrated that using allyl-glycine modified phenylalanine-based AA-PEAs and either diacrylated Pluronic or poly(ethylene glycol) polymers, hybrid hydrogels could be fabricated that readily undergo enzymatic degradation (0.2mg/mL α-chymotrypsin at 37℃) with increasing degradation (70% for 8-Phe-4-AG-4-50-GPEG and 55% for 8-Phe-4-AG-4-25-GPEG) with increasing AA-PEA content.[52]Further, Wu *et al* found increasing UArg-PEA content in HA-AEMA/UArg-PEA hybrid hydrogels facilitated faster weight loss *in vitro* due to higher UArg-PEA targeting under trypsin degradation.[40] Therefore, F127DA/UArg-PEA hydrogels show excellent potential for wound healing by utilizing characteristics of UArg-PEA chemical structure to facilitate biodegradation for synthesis of new extracellular matrix by cells native to healing wound.

Macrophage *In vitro* Viability

RAW264.7 macrophage cell toxicity upon incubation hybrid UArg-PEA/F127DA and pure F127DA hybrid hydrogels was assayed after 24 hours. UArg-PEA/F127DA hybrid hydrogels resulted in statistically significant ($p < 0.05$) higher RAW264.7 viability compared to pure F127DA hybrid hydrogels (Fig. 29 (a)). Higher viability in UArg-PEA/F127DA hybrid hydrogels can be attributed to biocompatibility found in AA-PEA polymers, with increased viability linked to cellular recognition of AA-PEA bioanalogous polymer chemical structure.[32,36,37]

UArg-PEAs, a member of arginine-based poly(ester amide) polymers (AA-PEAs), has been well-studied and characterized to have excellent cell viability and adhesion with many different cell types. Song *et al* studied rat aortic smooth muscle cell (A10 SMC) cytotoxicity using saturated arginine-based AA-PEAs and found excellent viability after 48 hours using both low and high polymer concentrations (15μg/100μl and 1500μg/100μl) for use as soluble transfection agents.[32] Similarly, using A10 SMCs, Wu *et al* found excellent cell viability using a series of saturated arginine-based AA-PEAs with varying methylene chain length in the polymer backbone at many different polymer-DNA ratios (500-6000) with superb DNA delivery capabilities (~100%).[36] Using bovine aortic endothelial cells (BAEC) as a model for cytotoxicity, Pang *et al* characterized excellent cell viability (comparable to untreated control) using a family of water soluble and functional arginine-based AA-PEAs using allyl glycine and oligoethylene glycol for potential functionalization via pendant unsaturated >C=C< bonds.[33]

Furthermore, upon incorporation into hydrogel compositions, UArg-PEA excellently increases cell viability compared to pure control. For example, Wu *et al* found that upon

encapsulation of BAEC cells into hydrogels, cell viability was higher for hybrid UArg-PEA/F127DA hydrogels after 14 days compared to the pure F127DA hydrogel, citing the beneficial aspects of both the bioanalogous AA-PEA polymers as well as the cationic nature of the arginine-based AA-PEA for promoting cell viability.[39] Furthermore, the same group found statistically significant increased HeLa cell viability after 48 hours using hybrid UArg-PEA/HA-AEMA (AEMA, aminoethyl methacrylate)hybrid hydrogels compared to pure HA-AEMA hydrogels, again rationalizing increased cell viability to favourable cell interaction with the novel cationic UArg-PEA component present in hybrid hydrogels.[40] Use of RAW264.7 macrophage expands the library of cell types previously studied with these materials and ~~further~~ validates their excellent in vitro biocompatibility. Further, since macrophage cells play key role in foreign body response to implanted biomaterials and wound healing (including both anti and pro-flammatory cytokine production and wound debridement), it is imperative to study this cell behaviour as well.[53]

Macrophage proinflammatory cytokine stimulation

When comparing macrophage stimulation of TNF-α production, hybrid UArg-PEA/F127DA hydrogels produced a statistically significant ($p < 0.05$) reduction in cytokine production compared to pure pluronic F127DA hydrogels. Hybrid UArg-PEA/F127DA stimulated 40% less TNF-α cytokine than pure F127DA hydrogels (Fig. 29(b)). This is a pioneer study, as proinflammatory cytokine assays have not previously been studied for hybrid AA-PEA/F127DA hydrogels. Lipopolysaccharide (LPS) was used as a positive control, as LPS is known to stimulate high levels of macrophage TNF-α cytokine production.[54]

With all implantable devices that enter the body, a stimulated response known as foreign body response (FBR) is generated based on material topography, chemical composition, and cellular activation. FBR consists of three main components; non-specific protein adsorption, immune, and inflammatory cell stimulation to protect the body from the foreign materials.[55] In particular, examination of inflammatory cell stimulation is imperative as persistent inflammatory activation can lead to chronic inflammation, a detriment to the wound healing process.[55]

One example of inflammatory cell activation is macrophage production of proinflammatory cytokine TNF-α. Macrophage cells are drawn to the implanted device (in this case hydrogel) through many chemoattractive agents including chemokines, as well as mast cell degranulation and release of histamine.[56] Macrophages become adherent to the foreign biomaterial and (in the process of attempting to phagocytose~~ing~~ the biomaterial) release proinflammatory mediators such as TNF-α, IL-6, and IL-1.[56]In vitro measurement of TNF-α provides insight into the extent of macrophage activation to hydrogel biomaterials to assess potential for *in vivo* use.

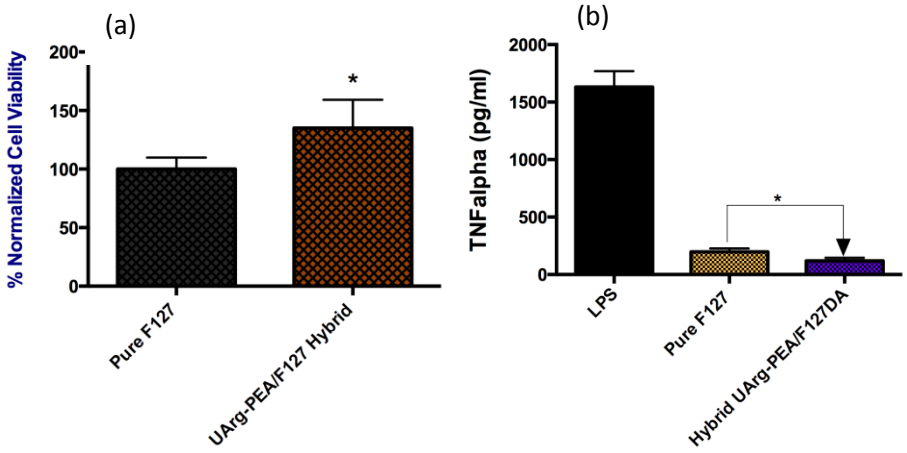

Figure 29. RAW264.7 macrophage cell viability (a) and proinflammatory cytokine (b) on F127DA and UArg-PEA/F127DA hybrid hydrogels. Hydrogels were incubated with macrophage cells (100,000 cells) for 24 hours at 37℃ and 5% CO_2. Viability (avg. ± std. dev of quadruplicate samples) normalized to pure F127 hydrogels. Statistical significance represented as $p < 0.05$ (*) and $p < 0.01$ (***).

The levels of macrophage cytokine production in response to pure pluronic F127DA and hybrid UArg-PEA/F127DA hydrogels are in excellent agreement to those found in literature. Jain-Gupta *et al* fabricated pluronic p85 for use as outer membrane vesicles in delivery of vaccine and found, after 24 hours incubation with J774 murine macrophages, TNF-α levels between 200-400 pg/mL for pure pluronic p85 polymers (varying concentration) with TNF-α stimulation by LPS greater than 1000 pg/mL.[57]Similarly, Kim *et al* examined the immunological effect of pluronic f-68 nanoparticles (~5nm diameter) on RAW264.7 mouse macrophage stimulation after 15 hours and found, after LPS challenge, no additional TNF-α cytokine production compared to the media control[58], indicating no stimulation of proinflammatory cytokine response from pluronic nanoparticles. Paralleling these results to UArg-PEA inflammatory performance, Wu *et al* discovered hybrid phenylalanine-arginine based poly(ester amides) had very little inflammatory response (<< 100 pg/mL TNF-α) compared to commercially available

poly(caprolactone) and poly(*n*-butyl methyacrylate) (both > 100 pg/mL TNF-α) after 48 hours incubation with mouse J774 macrophages.[59] Therefore, both pluronic and arginine AA-PEA materials show tendencies to create very low inflammation implantable devices.

Swelling Ratio Analysis

Within the first ten minutes of swelling in aqueous media, results show UArg-PEA/F127DA hybrid control hydrogel had greater swelling ratio than the F127DA control (338% vs 297%). At the initial reading (10 minutes),pure F127DA hydrogel in drug doped solution had the lowest swelling ratio, although not statistically significant, compared to the UArg-PEA/F127DA hybrid and controls (240%). This trend could be attributed to unfavorable interactions of hydrophilic KF in solution with hydrophobic F127DA hydrogel. Increased rate of swelling for hybrid UArg-PEA/F127DA hydrogels can also be attributed to larger pore size as a result of longer time needed during crosslinking to facilitate excitation and saturation of UArg-PEA C=C double bonds as crosslinking sites resulting in an overall lower cross linking density as compared to the control.[39]Furthermore, incorporation of UArg-PEA into hydrogel fabrication (UArg-PEA/F127DA hybrid) increases the hydrophilicity of the hydrogel network from the addition of arginine, therefore leading to a higher swelling ratio compared to more hydrophobic pure F127DA (Fig. 30).

After 60 minutes, F127DA KF-doped hydrogel swelling ratio was considerably less as compared to control and hybrid hydrogels, swelling to 594% of its original size. The remaining hydrogels including F127DA control (709%), UArg-PEA/F127DA control (821%), and UArg-PEA/F127DA KF-doped (848%) showed higher swelling ratios, with hybrid KF doped hydrogel

presenting the greatest swelling. After 60 minutes, swelling ratio began to plateau. At each time point analyzed, hybrid F127DA/UArg-PEA hydrogels had a higher swelling ratio compared to F127DA for both control and KF-doped swelling.

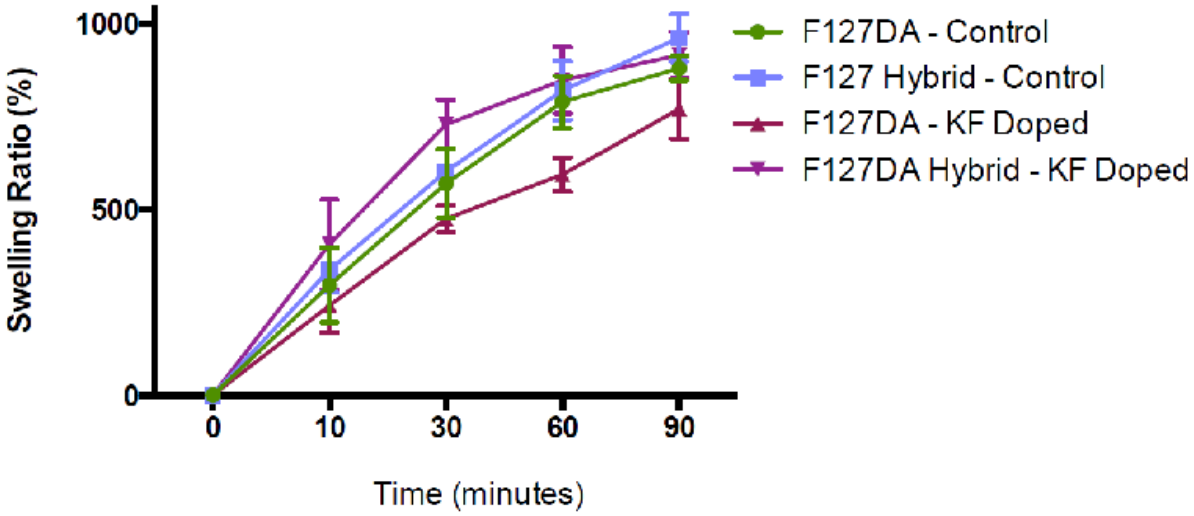

Figure 30. Swelling ratio of F127DA and UArg-PEA/F127DA hybrid hydrogels in control (PBS) or KF doped solution (0.2wt% in PBS), triplicate samples (avg. ± std. dev)

Consistent with the findings of this study, work done by Wu *et al* characterized swelling ratio of pure F127DA and hybrid UArg-PEA/F127DA hybrid hydrogels and found very fast initial (24 hours) swelling ratios for both pure and hybrid hydrogels (deionized water, room temperature) leading up to equilibrium swelling (Q_{eq}) after 20 hours of 1785± 74% for 2-UArg-2s/F127DA hybrid hydrogels compared to that of 1144± 17% for pure F127DA hydrogels.[39] Pang *et al* characterized swelling behavior for hybrid materials composed of allylglycine modified arginine-based AA-PEA/diacrylated poly(ethylene glycol) (PEG) hydrogels, finding higher Q_{eq} for hybrid arginine AA-PEA/PEGDA hydrogels as a result of increased hydrophilicity from arginine

present in AA-PEAs.[60] Consistent with the study of this work, Wu *et al* described Arg-PEA/HA-AEMA hybrid hydrogel swelling at physiological pH and found extremely fast swelling behavior with pure HA-AEMA hydrogels swelling 400% within 1 hour with hybrid Arg-PEA/HA-AEMA hydrogels swelling up to 530%.[40] Consistent with the findings of this work, and that of Wu *et al* and Pang *et al*, incorporation of arginine plays a significant role in swelling behavior.[39,40,60]

Guo *et al* found a similar trend using hydrophobic unsaturated phenylalanine-based AA-PEA/acrylated poly(ethylene glycol) hybrid hydrogels; upon swelling at room temperature in distilled water, an initial burst of swelling was observed of around 500% for pure and hybrid hydrogels (< 24 hours), followed by Q_{eq} at around 20 hours.[38] Contrasting hydrophilic arginine, they found that when using unsaturated phenylalanine AA-PEAs in hybrid hydrogels, increased hydrophobicity from the AA-PEAs decreased Q_{eq} from 2400± 800% for pure PEGDA hydrogels to 600-700± 200% for hybrid hydrogels.[38] Pang *et al* found, using allylglycine modified phenylalanine-based AA-PEAs with diacrylated Pluronic or poly(ethylene glycol) hybrid hydrogels, a prominent burst release was evident within the first 8 hours (approximately 90% of Q_{eq}) with decreased Q_{eq} for increasing hydrophobic AA-PEA feed ratio in all cases.[52]

Ketotifen Release from F127DA and UArg-PEA/F127DA hydrogels

KF-doped pure F127 and hybrid UArg-PEA/F127DA hydrogels incubated in either control (PBS) or under enzymatic degradation (0.1mg/mL trypsin) were used to assess *in vitro*release of KF over time. Both pure F127 and hybrid UArg-PEA/ F127DA hydrogel KF release plateaued after 1 day (25% and 18% respectively) indicating drug released was near the surface and easily diffused from surface pores (Fig. 31). Little release after 1 day in control

solution for either hydrogel type was observed (< 1%). Hybrid UArg-PEA/F127DA hydrogels released KF at a slower rate than F127DA in control solution. This may be attributed to the electrostatic interaction of arginine present in UArg-PEA polymer with KF, to trap KF within the hydrogel to prolong release. Guerrero *et al*extensively studied poly(D,L-Lactide) (PLA) and poly(D,L-Lactide-co-Glycolide) (PLGA) microspheres (formed via spray-drying) encapsulating KF and found a unique polymer-drug relationship that heavily dictated drug release.[61] In particular, they proposed that due to the higher electronegativity of the carbonyl oxygen present in ketotifen, polarity causes hydrogen bonding interactions between the carbonyl group of ketotifen and carboxylic groups present in PLA and PLGA degradation products.[61] Similar interactions could occur with the pendant amine groups along arginine-based UArg-PEA, creating a dipole-dipole interaction trap to slow the release of KF from hybrid hydrogels. The hypothesis of slowed release of KF from hybrid hydrogels due to hydrogel-drug interactions is consistent with the findings of this work; despite larger pore size and faster swelling ratios, KF release from hybrid hydrogels is slower in both control and enzymatically degraded samples.

F127DA and UArg-PEA/F127DA hybrid hydrogels incubated in enzymatic media exhibited greater KF release compared to control solution. Pure F127DA hybrid hydrogel cumulative KF release (over 7 days) rose from 25% to 33%, compared to PBS control. UArg-PEA/F127DA hybrid hydrogel cumulative KF release increased from 18% to 24%, compared to PBS control. An increase in KF release as a result of trypsin degradation can be ascribed to scission of ester linkages in F127DA and UArg-PEA polymers. All hydrogel species (control or enzyme incubated) released KF in a burst effect behaviour within the first 24 hours, yet only pure

and hybrid F127DA hydrogels incubated with trypsin continued to release KF (33% increase and 30% increase in release compared to control).

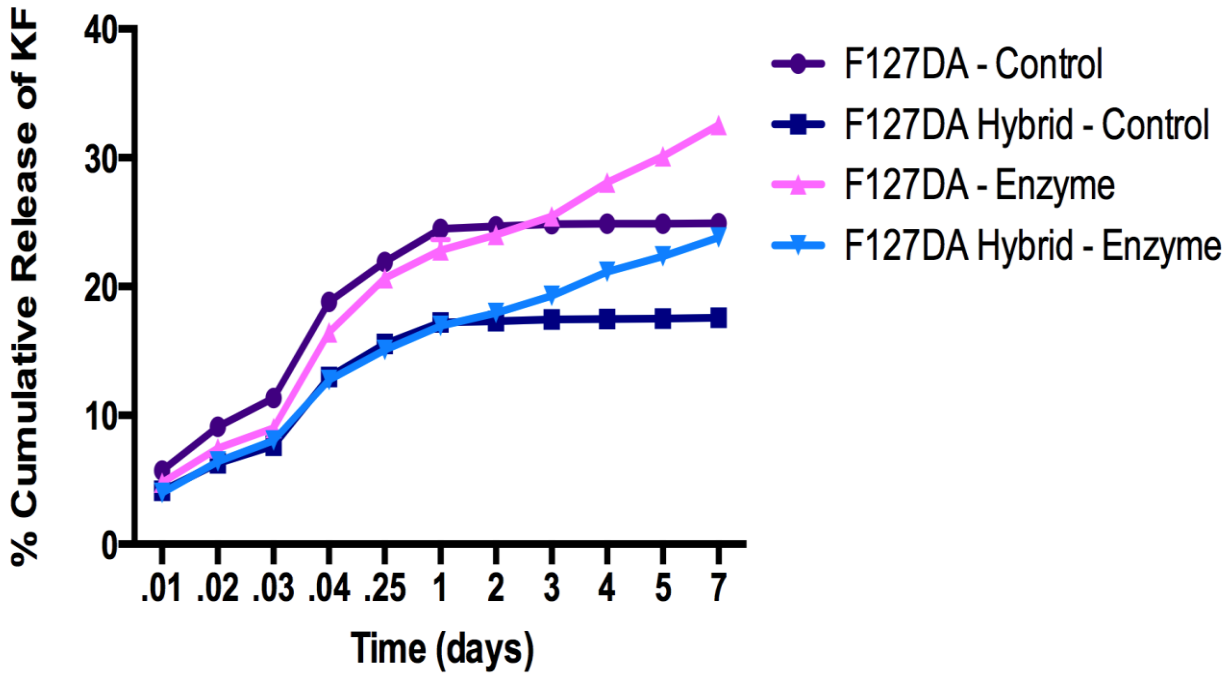

Figure 31. *In vitro* KF release from F127DA and UArg-PEA/ F127DA hybrid hydrogels in either control (PBS) or enzyme (0.1mg/mL trypsin in PBS) solution at 37℃. All measurements are an average ± std. dev of independent triplicate samples (error bars present but not visible).

Given poor oral bioavailability, ketotifen fumarate delivery *in vivo* is optimized to site of action delivery. KF sustained delivery can be found in many different formulations including tablets[62,63], transdermal patches[64], but are most commonly found in ophthalmological applications using KF doping of contact lenses for allergic reactions associated with conjunctivitis.[65,66]Focusing first on hydrogel as KF polymeric carriers, both polymer composition of the carrier and KF release rate vary greatly in literature. Ali *et al* studied KF release from

molecularly imprinted hydrogels (For example, poly(AA-co-AM-co-HEMA-co-PEG200DMA)) and found zero order release kinetics (release at a constant rate independent of drug concentration) with release dependent on hydrogel functionalization, leading up to a maximal 5 day release.[67] In a similar manner, Tieppo et al discovered KF imprinted onto Poly(HEMA-co-AA-co-AM-co-NVP-co-PEG200DMA) contact lens incubated in artificial lacrimal solution consisted of an initial burst release of KF (< 10 hours) followed by a steady release up to 100 hours.[68] They found that using imprinted hydrogel materials extended drug release (85% over 24 hours) compared to non-imprinted KF doped hydrogels (100% over 6 hours).[68] Karlgard *et al* studied a wide range of commercially available contact lens compositions and found contact materials with larger hydrophilicity (90 vs 85 μg/lens) and ionic character (103 vs 77 μg/lens for non-ionic) increased KF release rate compared to those with lower water content.[69]

Furthermore, KF release can be influenced by polymer carrier morphology. For example, Patel *et al* studied KF release from transdermal patches (Eudragit L-100/Ethyl Cellulose/Hydroxypropyl methyl cellulose) during a 24 hour in vitro release study and established zero order KF release kinetics with over 90% KF from the most hydrophilic polymer matrix.[63] Beyond patches, Guerrero *et al* showed KF could successfully be encapsulated into micron-sized spheres composed of PLA and PLGA and degraded *in vitro* (phosphate buffer, 37℃) with sustained release (after an initial burst release at < 15 minutes) with lower total KF release at 350 hours for more hydrophobic PLA (57%) as compared to hybrid PLGA (67.4%).[61]

Mast Cell Stabilization

Mast cells are most easily recognized for presence of metachromatic granules which contain many well-studied mediators including heparin (anticoagulant), histamine and TNF (inflammatory stimuli), IL-4 (wound healing and collagen production), and a multitude of others.[70] Through degranulation of granules within mast cell membranes, many proinflammatory mediators are released including histamine, cytokines, chemotactic factors that act on vasculature, tissue, and inflammatory cells leading to inflammation in wound sites.[71] Ketotifen fumarate acts to reduce mast cell degranulation through blocking of Fc receptor mediated IgE regulated calcium channels, resulting in drastically muted inflammatory response.[72] Moreover, stabilization of mast cells has been found to reduce fibrosis and wound contracture, leading to improved wound healing.[72] Therefore, biomedical systems that effectively deliver KF to wound sites are advantageous to reduce drug loss in hepatic metabolism, reduce inflammation, and reduce fibrosis in scar formation.

To assess the capability of pure F127DA and UArg-PEA/F127DA hybrid hydrogels to release KF resulting in mast cell stabilization, purified and dried F127DA and UArg-PEA/F127DA hydrogels were swollen in control (DMEM) or KF-doped solution (0.2 wt% KF in DMEM) and assayed for RBL cell degranulation. Spontaneous degranulation of RBL cells on tissue culture plate is used as a control (denoted "spon"). Triton X-100 was used for cell lysis and granule content normalization was calculated from granule content. All RBL cells were treated withanti-DNP–IgE FcεRI receptor antibody overnight before running the degranulation assay. Percent degranulation was determined for spontaneous degranulation, after antigen (AG) cell sensitization, and upon KF-doping of hydrogels. % Degranulation data show; 1) Hybrid

hydrogels stimulated increased spontaneous degranulated compared to pure F127DA control, 2) Antigen stimulation (in all cases except hybrid KF [AG]) increased % degranulation, 3) Release of KF in antigen stimulated hydrogel samples resulted in significantly decreased degranulation.

Spontaneous degranulation (no antigen or KF) of control, pure F127DA, and hybrid UArg-PEA/F127DA hybrid hydrogels established a direct correlation to degranulation and incorporation of UArg-PEA into hydrogel composition. Compared to the control, both pure F127DA hydrogels ($p < 0.05$) and hybrid UArg-PEA/F127DA hydrogels ($p < 0.01$) increased spontaneous % degranulation (Fig. 32). We hypothesize the small increase in % degranulation for pure F127DA hydrogels (from 10% to 21%) may be attributed to foreign body response to F127DA polymers, considering the possibility of residual monomer or initiator present eliciting response. UArg-PEA/F127DA hybrid hydrogel spontaneous degranulation was more highly elevated compared to the untreated control (from 10% to 47%). Rise in spontaneous degranulation therefore must be a factor of incorporation of cationic arginine-based AA-PEAs into hydrogel chemical composition. As found by Zheutlin *et al*, *in vitro* rat mast cell degranulation is influenced to release at high levels (> 30%) using arginine-rich cationic polypepetides through IgE-independent mechanisms.[73] We postulate that therefore an increase in % degranulation for hybrid UArg-PEA/F127DA hydrogels could be a result of cationic UArg-PEA stimulation of RBL cells.

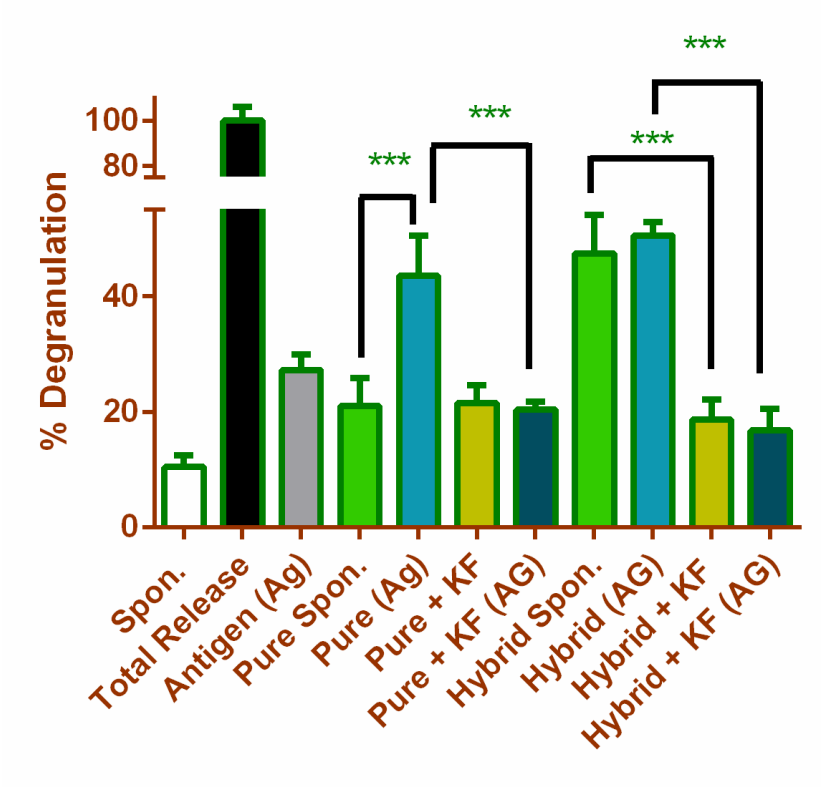

Figure 32. RBL cell degranulation assay using F127DA and UArg-PEA/F127DA hybrid hydrogels (results normalized to total release, triplicate samples). AG indicates antigen sensitized RBL cells and KF indicates KF doping of hydrogels. Unless specified with (AG), samples measured spontaneous RBL degranulation without sensitization. Statistical significance is represented as $p < 0.01$ (***), all other values are not significant.

Antigen stimulated samples statistically increased % degranulation release compared to the spontaneous release control including pure F127DA (AG) ($p < 0.01$) and hybrid UArg-PEA/F127DA (AG) ($p< 0.01$). Hybrid UArg-PEA/F127DA + KF (AG) hydrogels were the only antigen stimulated samples that did not statistically increase % degranulation compared to the spontaneous release control. Within each sample subset, antigen stimulation of pure F127DA hydrogels statistically increased % degranulation ($p< 0.01$), while antigen stimulation of hybrid

UArg-PEA/F127DA hydrogels did showed n statistical significance over spontaneous release. Absence of increased antigen stimulation could be a result of the already stimulated degranulation caused by hybrid spontaneous release.

Upon KF doping of hydrogels assayed with antigen stimulated cells, % degranulation decreased significantly for both pure F127DA and hybrid UArg-PEA/F127DA hydrogels compared to antigen sensitized cells assayed using hydrogels without drug doping. Addition of KF doping to Pure 127DA (AG) results in a 114% decrease in % degranulation, compared to Pure F127DA (AG) alone ($p < 0.01$). Similarly, KF doping of hybrid UArg-PEA/F127DA hydrogels results in a 200% decrease in % degranulation, compared to UArg-PEA/F127DA (AG) alone ($p < 0.01$). Release of KF from hydrogels plated with antigen stimulated RBL cells reduced % degranulation to a level equivalent of spontaneous release. These results verify that KF release from hybrid hydrogels is efficacious in stabilizing mast cells from degranulation.

Naal *et al* established the protocol for methylumbelliferyl-*N*-acetyl-β-D-glucosaminide cleavage by β-hexosaminidase as a facile fluorogenic method for high-throughput assessment of environmental assessment of chemical agents, including mast cell stabilizing agents.[45]This method has the ability to quantify both spontaneous and antigen stimulated RBL cell degranulation. As noted by Paul *et al* and used by Naal *et al*, antigen binding to IgE sensitized RBL cells is crucial in stimulating RBL degranulation.[45, 74] Antigen stimulation of RBL cells is dependent on the Fc receptor binding of the targeted antigen-antibody pair, resulting in signal transduction and degranulation of mediators.[74] Antigen stimulation of RBL cells was necessary

to quantify the stabilization effect of KF that may not have been visible using spontaneous release.

Schoch *et al* has demonstrated excellent human conjunctival mast cell viability (70-80%) and degranulation inhibition (>90% histamine inhibition) over a wide range of ketotifen fumarate concentrations (10^{-11} to 10^{-5} M) after 15 minutes incubation with antigen sensitized cells.[75] Combining the stabilization effect of KF with polymer drug delivery systems, Guerrero *et al* used PLGA microspheres (~1μm diameter) fabricated by spray-drying to establish *in vivo* rat model ketotifen fumarate release from polymer carriers.[61] After intraperitoneal administration to rats, they found maximal drug release at 24 hours from PLGA-based microspheres (39.4μg/mL) measured from blood plasma with little/no inflammatory response.[61]

5.4 Conclusions

Pure F127DA and hybrid F127DA hybrid hydrogels were successfully fabricated and characterized for mechanical and degradation properties. Incorporation of arginine-based poly(ester amide) polymers facilitated presence of cationic arginine within hydrogel for electrostatic interactions with both cell membranes and KF and allowed for targeted trypsin degradation of pendant arginine groups along AA-PEA backbone. Due to inherent formation of pores created during UV-photocrosslinking of carbon-carbon double bonds present in both F127DA and hybrid F127DA, pure and hybrid F127DA hydrogels were able to swell in both control and drug-doped solutions to create a porous gel microstructure (up to ~900% dry weight).

Pure F127DA and hybrid UArg-PEA/F127DA hydrogels were also investigated for biological properties including cell viability and mast cell stabilization. UArg-PEA/ F127DA hybrid

hydrogels facilitated greater macrophage viability compared to F127DA control hydrogels, indicating hybridization using arginine-based poly(ester amide) polymers increases cell in vitro biocompatibility. F127DA and F127DA hybrid hydrogels were further functionalized to deliver ketotifen fumarate to mast cells for stabilization from release of proinflammatory mediators. Due to drug-cationic UArg-PEA interactions, release of KF was prolonged compared to more hydrophobic pure F127DA. Attributing to the presence of KF, RBL cell degranulation was significantly reduced for antigen stimulated assay samples, thus reducing the amount of proinflammatory mediators released and resulting in overall improved wound healing.

Acknowledgements

The authors would like to thank the Becky Q. Morgan Foundation for their financial support in terms of fellowship to Potuck and research funds to Chu. Authors would like to thank the Leifer and Baird/Holowka Labs for providing cells and valuable consulting and discussion. This work made use of the Cornell Center for Materials Research Facilities supported by the National Science Foundation under Award Number DMR-1120296.

References

1 K. Y. Lee and D. J. Mooney, *Chemical Reviews***101.7**, 1869 (2001).
2 S. Vlierberghe, P. Dubruel and E. Schacht, *Biomacromolecules***12.5,** 1387 (2011).
3 A. Hoffman, *Advanced Drug Delivery Reviews***54,** 3 (2002).
4 A.V. Kabanov, E. V. Batrakova and V. Y. Alakhov, *J. of Controlled Release*. **82.2-3**, 189 (2002).
5 E.V. Batrakova and A. V. Kabanov, *J. of Controlled Release***130.2**, 98 (2008).
6 P. Alexandridis, T. Nivaggioli and T. A. Hatton, *Langmuir***11.5**, 1458 (1995).
7 I.R. Schmolka, *JBMR***6.6**, 571 (1972).

8 K.M. Park, S.Y. Lee, Y.K. Joung, J.S. Na, M.C. Lee and K.D. Park, *Acta Biomaterialia***5**, 1956 (2009).
9 J.B. Lee, J.J. Yoon, S.D. Lee and G.T. Park, *J. Biomater. Sci., Polym. Ed.* 15 (2004) 1571-83.
10 N. Pandit, T. Trygstad, S. Croy, M. Bohoroquez, and C. Koch, *J. Colloid Interface Science***12**, 213 (2000).
11 L. Li, L. H. Lim, Q. Wang, and S. P. Jiang, Polymer **49.7**, 1952 (2008).
12 S.D. Desai and J. Blanchard, *J. Pharmacological Science***87**, 226 (1998).
13 Z. Sezgin, N. Yuksel and T. Baykara, *European J. of Pharmaceutics and Biopharmaceutics***64.3**, 261 (2006).
14 N. Rapoport, *Progress in Polymer Science***8-9**, 962(2007).
15 Wei, J. Hao, S. Yuan, Y. Li, W. Juan, X. Sha and X. Fang, *International J. of* Pharmaceutics **376.1-2**, 176 (2009).
16 F. Ye, A. Yaghmur, H. Jensen, S. W. Larsen, C. Larsen and J. Østergaard, *European J. of Pharmaceutical Sciences***43.4**, 236 (2011).
17 Y. Liu, W. Lu, J. Wang, X. Zhang, H. Zhang, X. Wang, T. Zhou and Q. Zhang, *J. of Controlled Release***117.3**, 387 (2007).
18 S.M. Shishido, A. B. Seabra, W. Loh and M. G. Oliveira, *Biomaterials***24.20**, 3543 (2003).
19 S.F. Khattak, S. R. Bhatia and S. C. Roberts, *Tissue Engineering***11.5-6**, 974 (2005).
20 Y. Lee, H. J. Chung, S. Yeo, C. Ahn, H. Lee, P. B. Messersmith and T. G. Park, *Soft Matter***6.5**, 977(2010).
21 K. Chun, J. B. Lee, S. H. Kim andT. G. Park, *Biomaterials***26.16**, 3319 (2005).
22 R.Katsarava, V.Beridze, N.Arabuli, D.Kharadze, C.C.Chu and C.Y.Won, *J. Polym.Sci. Part A:Polym.Chem***37.4**, 391 (1999).
23 J. Horwitz, K. M. Shum, J. C. Bodle, M. Deng, C.C. Chu and C. A. Reinhart-King, *J. of Biomedical Materials Research Part A*. **95A.2**, 371 (2010).
24 G. Jokhadze, M. Machaidze, H. Panosyan, C. C. Chu and R. Katsarava, *J. of Biomaterials Science Polymer Edition***18.4**, 411 (2007).
25 X. Pang and C.C. Chu, *Biomaterials* **31.14**, 3745 (2010).
26 J. Wu and C.C. Chu, *Acta Biomaterialia***8.12,** 4314 (2012).
27 M. Machaidze, T. Kviria, N. Djavakhishvili, C.C.Chu and R.Katsarava, *J. Biomater. Sci., Polym. Ed.***15**, 1 (2004).
28 G. Tsitlanadze, T.Kviria, C.C.Chu and R. Katsarava, *J. Mater Sci. Materials in Medicine* **15.2**, 185 (2004).
29 K. Guo and C. C. Chu, *Biomacromolecules***8.9**, 2851 (2007).
30 S.H. Lee, I. Szinai, K. Carpenter, R. Katsarava, G. Jokhadze, C.C. Chu and M.K. Hong, *Coronary artery disease***13**, 237 (2002).
31 K. Guo, C. C. Chu, E. Chkhaidze and R. Katsarava, *J. of Polymer Science Part A: Polymer*

Chemistry **43.7**, 1463 (2005).
32 H. Song and C.C. Chu, *J. Appl. Polym. Sci.***124.5**, 3840 (2012).
33 X. Pang, J. Wu, C. Reinhart-King and C.C. Chu, *J. of Polymer Science Part A: Polymer Chemistry* **17**, 3758 (2010).
34 M. Deng, J. Wu, C.A. Reinhart-King and C.C. Chu, *Biomacromolecules* **10.11**, 3037 (2009).
35 M. Deng, J. Wu, C.A. Reinhart-King and C.C. Chu, *Acta Biomaterialia***7.4**, 1504 (2011).
36 J. Wu, D. Yamanouchi, B. Liu and C.C. Chu, *J. of Materials Chemistry***22.36**, 18983 (2012).
37 J. Wu, M. A. Mutschler and C. C. Chu, *J. of Materials Science: Materials in Medicine***22.3**, 469 (2011).
38 K. Guo and C. C. Chu, *J. of Polymer Science Part A: Polymer Chemistry* **43.17**, 3932 (2005).
39 J. Wu, D.Q. Wu, M. Mutschler and C.C.Chu, *Adv. Funct. Materials***22**, 3815 (2012).
40 D.Q. Wu, J. Wu and C.C. Chu, *Soft Matter***9.15**, 3965 (2013).
41 M. He, A. Potuck, Y. Zhang and C.C. Chu, *Acta Biomaterilia* **10.6**, 2482 (2014).
42 C. Zhong, J. Wu, C.A. Reinhart-King and C.C. Chu, *Acta biomaterialia***6 .10**, 3908 (2010).
43 A. Lambiase, A. Micera, and S. Bonini, *Current Opinion in Allergy and Clinical Immunology***9.5**, 454 (2013).
44 A. Martín**,** J. Urrets-Zavalia**,** A. Berra**,** A. Mariani**,** N. Gallino**,** E. Demel**,** J. Gagliardi**,** C. Baena-Cagnani**,** E. Urrets-Zavalia and H. M. Serra, ***BMC Ophthalmology* 3, 1 (2003).**
45 R. Naal, R. M., J. Tabb, D. Holowka and B. Baird, *Biosensors and Bioelectronics***20.4**, 791(2004).
46 Y. Chung, S. Kim, Y. Lee, S. Park, K. Cho, S. H. Yuk, G. Tae andY. H. Kim, *J. of Controlled Release***143.3**, 282 (2010).
47 H. Carstensen, R. H. Muller and B. W. Muller, *Clinical Nutrition***11**, 289 (1992).
48 M.D. Rosa, M. Carteni, O. Petillo, A. Calarco, S. Margarucci, F. Rosso, A. D. Rosa, E. Farina, P. Grippo and G. Peluso, *J. of Cellular Physiology***198.1**, 133 (2004).
49 A. Sosnik and M. V. Sefton, *J. of Biomedical Materials Research Part A*. **75A.2**, 295 (2005).
50 M.R. Kim and T.G. Park, *J. Controlled Release***80**, 69 (2002).
51 J.V. Olsen, *Molecular & Cellular Proteomics* **3.6**, 608 (2004).
52 X. Pang and C.C. Chu, *Polymer***51.18,** 4200 (2010).
53 P. Martin and S. J. Leibovich, *Trends in Cell Biology***15.11**, 599 (2005).
54 J.Xaus, M. Comalada, A. F. Valledor, J. Lloberas, F. López-Soriano, J. M. Argilés, C. Bogdan, and A. Celada, *Blood***95.12**, 3823 (2000).
55 J.M. Morais, F. Papadimitrakopoulos, and D. J. Burgess, *The AAPS Journal***12.2**, 188 (2010).
56 J.M. Anderson, A. Rodriguez, and D. T. Chang, *Seminars in Immunology***20.2,** 86 (2008).
57 N. Jain-Gupta, A. Contreras-Rodriguez, R. Vemulapalli, S. G. Witonsky, S. M. Boyle, and N. Sriranganathan, *FEMS Immunology & Medical Microbiology***66.3**, 436 (2012).
58 H.G. Kim, S. Jo, S. Yeon, K. H. Kim, J. W. Chung, T. W. Park, Y. Byun, E. H. Lee, Y. I. Park, and Y. W. Jung, *Macromolecular Research***21.12**, 1355 (2013).

59 J. Wu, and C. C. Chu, *J. of Materials Chemistry B***1.3**, 353 (2012).
60 X. Pang, J. Wu, C. C. Chu and X. Chen, *Acta Biomaterialia***10.7**, 3098 (2014).
61 S. Tayel, I. I. Soliman and D. Louis, *AAPS PharmSciTech***11.2**, 679 (2010).
62 M.A. Rahman, A. Khalipha and B. Opu, *International J. of Drug Delivery***3**, 513 (2011).
63 H.J. Patel, J. S. Patel and K. D. Patel, *International J. of PharmTech Research***1.4**, 1297 (2009).
64 J. Xu, X. Li and F. Sun, *Drug Delivery***18.2**, 150 (2011).
65 M. Kidd, *British Journal of Ophthalmology***87.10**, 1206 (2003).
66 S. Guerrero, E. Muñíz, C. Teijón, R. Olmo, J. M. Teijón, and M. D. Blanco, *J. of Pharmaceutical Sciences***97.8**, 3153 (2008).
67 M. Ali, S. Horikawa, S. Venkatesh, J. Saha, J. W. Hong and M. E. Byrne, *J. of Controlled Release***124.3**, 154 (2007).
68 A. Tieppo, C.J. White, A.C. Paine, M.L. Voyles, M.K. McBride and M.E. Bryne, *J. ControlledRelease***157**, 391 (2012).
69 C. Karlgard, N. Wong, L. Jones and C. Moresoli, *International J. of Pharmaceutics***257.1-2**, 141 (2003).
70 C. Noli and A. Miolo, *Veterinary Dermatology***12.6**, 303 (2001).
71 K. Amin, *Respiratory Medicine***106.1**, 9 (2012).
72 C. Behm, K. A. Hildebrand and D. A. Hart, *Wound Repair and Regeneration***16.2**, 226 (2008).
73 L. Zheutlin, S. Ackerman, G. Gleich and L. Thomas, *J. of Immunology***133.4**, 2180 (1994).
74 W.E. Paul and A.H. Seden, *Cell***76**, 241(1994).
75 C. Schoch, *J. Ocular Pharmacology and Therapeutics***19.1**, 75 (2003).

Chapter 6. Assessment of Chemical and Morphological Effects of Amino Acid-based Poly(ester amide) Fabrication on Macrophage Inflammatory Stimulation

Abstract

A series of amino acid based poly(ester amide) (AA-PEA) 2D films and 3D fibers were fabricated using solvent evaporation deposition and electrospinning techniques. Monomer amino acids were chosen to vary AA-PEA polymer key parameters in understanding the inticate biomaterial/cell surface interaction and stimulation, including chemical properties such as thermal transitions linked to crystallinity and atomic mobility, hydrophobicity/hydrophilicty, and physical parameters such as 2D vs 3D scaffolds to determine if overall topography influenced macrophage stimulation. Preliminary results indicate surface charge (anionic or cationic play a large role in influencing macrophage proliferation, while hydrophobicity/hydrophilicty may play a smaller, more secondary role. Moreover, surface charge also heavily influenced macrophage proinflammatory cytokine stimulation response (M1 classically activated stimulation), with anionic materials stimulating an increase in proinflammatory cytokine TNF-α. Translating across morphologies, macrophage adhesion to 3D porous membranes did not significantly increase proinflammatory response. Overall, macrophage proliferation, adhesion, and proinflammatory response can be directly linked to biomaterial chemical and physical properties to influence the optimal materials used in biomedical applications.

6.1 Introduction

Extensive leaps have been made in the past decades to create more innovative and efficient biomedical devices to safely and effectively deliver pharmaceutical agents to patients. Each innovation brings forth new and exciting methods for creating safer, more biocompatible advancements that aid in wound healing and patient compliance. One of the simplest methods of increasing biocompatibility and improved wound care is the use of 2D films as coatings. The use of thin films allows for an inert and durable ultra thin layer on the surface of biomedical devices. These coatings serve many purposes including surface protection and cellular adhesion[1] and antimicrobial properties[2,3], among many others. Coatings can be based on synthetic materials[4], or naturally-derived products[5,6]for enhanced biocompatibility. Overall, 2D films should have no immunogenicity, excellent cellular viability, and favourable non-toxic degradation products.

One of the most studied developments are the use of microspheres, micron-sized particles for site-of-action delivery of drug.[7,8,9] Microspheres can be formulated for syringe injection, nasal injection, impregnated in scaffolds, etc. Beyond conventionally studied poly lactic acid (PLA), poly glycolic acid (PGA) and its copolymer (PLGA) (commercially available FDA approved polymers), researchers are also harnessing the biocompatibility of naturally occurring materials such as hyaluronic acid and alginate to fabricate microspheres.[10,11] Taking a step further, microspheres can also be used as a drug carrier for a multitude of proteins, DNA, and pharmaceutical agents.[12,13]

In addition to film coatings and microspheres, nanoscale fibers have come to the forefront of biomedical engineering and wound healing. This upward trend of fibers in biomedical devices can be attributed to its unique morphological characteristics. Nanoscale fibers can be fabricated using high voltage electrospinning. This technique is based on the principle of fibers being drawn from a syringe into a high electric field, after which individual fiber strands are randomly deposited onto a grounded collection plate. Electrospun fibers are used as an excellent biomimetic model of fibers commonly found in the extracellular matrix, and can be constructed with an expansive of both synthetic and natural materials.[14,4]

A well-studied novel family of polymers referred to as amino-acid based poly(ester amide)s (AA-PEA)'s were used. AA-PEA's are unique in the fact that their synthesis is comprised of non-toxic starting materials; 1) amino acid, 2) fatty diol, and 3) dicarboxylic acid.[15,16,17] AA-PEA polymers share enhanced properties of ester linkages for hydrolytic degradation sites, and amide linkages for outstanding mechanical stability. Moreover, AA-PEA polymers degrade via enzymatic degradation (α-chymotrypsin for hydrophobic amino acids) and hydrolytic degradation of ester linkages to non-toxic degradation products.[18] By varying fabrication techniques, AA-PEA polymers can be utilized to create varying morphologies such as spheres, electrospun fibers, and hydrogels.[13,19,20] Beyond morphologies of AA-PEA materials, introduction of various amino acid in synthesis pathways makes it possible to introduce charge within the polymer structure.[21, 22, 23]

The goal of this article is to present characterization of AA-PEA chemical and morphological fabrication variances and their influences on macrophage biomaterial inflammatory response. Using various fabrication techniques, 2D films, nanoscale electrospun fibers, and reservoir-type microspheres

were fabricated into distinct morphologies, eliciting varied macrophage inflammatory response. Studying macrophage behaviour upon stimulation by distinct morphologies, invaluable insight into biomaterial performance in wound sites will be provided.

6.2 Materials and Methods

Materials

Polyvinyl alcohol (PVA), L-Arginine, and ethyl acetate were purchased from Sigma Aldrich (Milwaukee, WI, USA). 4-Nitrophenol, P-toluenesulfonic acid monohydrate, adipoyl chloride, sebacoyl chloride, and dimethylacetamide (DMAc) were purchased from Alfa Aesar (Hersham, UK). Triethylamine, chloroform, dodecanedioyl chloride, and isopropyl alcohol, and Triton-X 100 were purchased from Fischer Scientific (Fairlawn, NJ, USA). PDLLA (Natureworks LLC, Minnetonka, MN, USA) was a kind gift from the Frey Lab (FSAD, Cornell University). Prolong Gold mountant was purchased from Life Technologies (Grand Island, NY, USA).

Synthesis of AA-PEA polymers has been well studied and characterized.[15,16,18] Briefly, AA-PEA polymers of varying methylene chain length (X-Phe-4, where X=4,8,10) were synthesized using solution polycondensation in DMAc (dimethylacetamide) for 48 hours at 70°C before precipitation and purification in ethyl acetate. Two monomers were first synthesized; 1) p-toluenesulfonic acid salt of L-phenylalanine butane-1,4-diester, and 2) di-p-nitrophenyl (X)–ate (where X= adipate (4), sebacate (8), or dodecanate (10)). Resulting polymers were denoted using methylene chain length (X-Phe-4, where X= methylene chain length between amide groups, and 4 indicating methylene chain length between

ester linkages. X-Phe-4 have no charged pendant amino groups, therefore do no exhibit an overall surface charge (neutral).

In addition to varying amide group methylene chain spacers (4,8,10), differing pendant amino acid groups were introduced to add sites for surface charge. To do this, the feed ratio of p-toluenesulfonic acid salt of L-phenylalanine butane-1,4-diester was reduced to 75% of the routine for 8-Phe-4, while 25% feed ratio p-toluenesulfonic acid salt of L-Arginine butane-1,4-diester was incorporated. The final polymer (overall cationic surface charge) had a final polymer chain structure of –(8-Phe-4)$_{.75}$(Arg-4)$_{.25}$, and simplified further to 8P4A4. Anionic surface charge was introduced via chemical modification of Lysine pendant chains at the same feed ratio as arginine-modified AA-PEA polymers (kind gift of Dr. Dequn Wu), and further denoted as 8P4L4.

Fabrication of varying morphologies

2D AA-PEA films

AA-PEA 2D films were fabricated by first dissolving AA-PEA solid polymers in chloroform in clean scintillation vials at a 5 wt% ratio. Polymers were allowed to solubilize completely for ~2hrs at room temperature. After such time, clean Pasteur pipets were used to deposit approximately 200µl polymer solution onto a 12mm glass circular coverslip. Polymer coated coverslips were allowed to evaporate solvent for a minimum of 12 hours in chemical safety hood.

After complete evaporation of solvent, AA-PEA coated coverslips were immersed in excess sterile distilled water for a minimum of 24 hours to ensure removal of any residual starting material. All samples were then dried, and UV sterilized before used in cell culture.

AA-PEA 3D fibrous membranes

AA-PEA 3D nanoscale fibers were fabricated according to literature.[19] In brief, 16 wt% solution of 8P4 in a 4:1 chloroform/DMF was created in a small glass scintillation vial. Polymer solution was taken up into glass syringe and placed in syringe pump. A metal collection was used to collect fibers on 12mm glass coverslips. Polymer was released from needle at a rate of 0.001mL/min under 20kV voltage. Collection was allowed to proceed for approximately 20 minutes, or until coverlsips were well coated with fibers. All fibers were UV sterilized and rinsed in sterile cell culture media until constant weight before used in cell culture.

Chemical and Morphological Analysis

Glass transition of AA-PEA samples were determined using differential scanning calorimetry (Q-Series 2000, TA Instruments, New Castle, DE, USA) using a nitrogen flow rate of 50.0 mL/min and sample size of approximately 5mg, run at 10°C/min from 0°C to 90°C. Analysis of polymer transitions were completed with TA Universal Analysis software (included with instrument). Size and surface charge (zetapotential) of microspheres was analysed using Malvern Zetasizer Nano-ZS (Worcestershire, UK). Morphology of 2D films, microsphere samples, and fibers were visualized with scanning electron microscopy (SEM Leica 440, Leica, Wetzlar, Germany). Before imaging, samples were solution deposited onto clean Al stubs, allowed to dry at room temperature, and coated with Au/Pd for 30 seconds under 25kV voltage. Hydrophobicity of polymeric films and fibers were evaluated using using Rame Hart Contact Angle Goniometer/Tensiometer (Rame Hart, Succasunna, NJ, USA).

Cell Culture

RAW264.7 mouse peritoneal macrophage cells were grown in 5% CO2 and 37°C in complete complete DMEM (CDMEM, 10% fetal bovine serum (FBS), 1mM Hepes, 200mM L-glutamine,

10,000 IU/mL penicillin, 10,000 µg/mL streptomycin, and 100mM Sodium pyruvate) at 37°C with 5% CO_2. All media reagents (except FBS) were purchased from Mediatech (Manassas,VA, USA). FBS was purchased from PAA Laboratories (Dartmouth, MA, USA). Macrophage cells were kindly provided by the Leifer Lab (Cornell College of Veterinary Medicine).

To assess toxicity of F127DA andUArg-PEA/F127DA hybrid hydrogels, RAW264.7 cells were plated at an appropriate density (100,000 cells/well) directly onto pure and hybrid hydrogels (immersed in cell media for 24 hours to ensure equilibrium swelling) placed into the bottom of a 24-well plate. After 24 hours RAW264.7 cell incubation with hydrogel material at 37℃ and 5% CO_2, cell prolifertionwas measured using Cell Counting Kit-8 (~~CCk~~CCK-8 Reagent, Sigma Aldrich, Milwaukee, WI, USA). CCK-8 reagent was added to each well at a ratio of 10µL reagent/ 100µL CDMEM and incubated at 37℃ for 2 hours. An aliquot of media was removed from each well, transferred to a new plate, and absorbance was measured at 450nm. RAW264.7 viability was normalized to untreated control and represented at average ± std. dev of quadruplicate samples.

Cellular Imaging

Macrophage (RAW 264.7) Confocal imaging

For AA-PEA 2D films and fibers, in a 24-well plate in cell culture hood, UV-sterilized 12mm circular glass coverslips were placed in the bottom of the wells, after which macrophage cells were incubated at the appropriate density (10,000 cells/well) and were allowed to settle 1 hour. For microspheres, after cellular adhesion to the glass coverslip, fluorescently-tagged microspheres were

added for a total solution concentration of 10µl/mL. Samples were then allowed to incubate for a total incubation time of 24 hours. AA-PEA films were coated onto autoclaved microscope slides, isolated into distinct circular patterns using a wax pen, and purified using the same methodology as aforementioned. Macrophage cells were incubated directly onto polymer films, and stained and fixed in the same manner as fibers and microspheres.

At conclusion of predetermined incubation time, media was aspirated from each well, followed by rinsing with excess HBSS (Hanks Buffered Salt Solution). To fix cells, 3% pParaformaldehyde was added to each well (enough to completely cover the cells), and allowed to rest in cell culture hood for 30 minutes. Paraformaldehyde was then aspirated, followed by rinsing with excess 1x PBS, repeated three times. To permeabilize cell membranes, 0.1% Triton-X 100 (in 1x PBS) was added, and allowed to incubate for 5 minutes (permabilization used for cells stained with F-actin only, not for Cell Mask Deep Red plasma membrane dye) (Life Technologies, Grand Island, NY, USA). For samples stained for F-actin filaments, before DAPI mounting, an additional step was needed. Cells were immersed into a solution of Alexa Fluor 488 Phalloidin (1% BSA in 1X PBS, 5µl Alexa Fluor/200µL BSA solution) (Life Technologies, Grand Island, NY, USA) for 30 minutes.After rinsing again with 1x PBS, samples were removed from well-plate, excess water gently removed, and inverted on a small bubble of Prolong Gold mountant (includes DAPI) on microscope slide. Coverslips were allowed to cure for minimum 24 hours in the dark for confocal microscopy imaging.

Cytotoxicity Assay

AA-PEA sample cytotoxicity was assessed using cCell counting kit-8 (CCK-8) (Sigma Aldrich, Milwaukee, WI, USA). Briefly, macrophages at appropriate density (100,000 cells/24-well plate) were

incubated for 24hrs with AA-PEA materials. After such time, CCK-8 reagent was added to each well at a ratio of 10µl reagent/100µl media and allowed to incubate for approximately four hours. Aliquots of cell supernatant were removed and placed in 96-well plate, and read at 450nm. Results were normalized to untreated RAW264.7 control.

TNF-α Cytokine Assay

Twenty-four hours after incubation, cell supernatants were removed from incubation with AA-PEA materials (100,000 RAW cells/24-well plate) and assayed according to manufacturer's protocol using Biolegend Elisa Maxx Mouse TNF-α Elisa kit (Biolegend, San Diego, CA, USA) for quantification of macrophage inflammatory response. Color developing agent TMB substrate was purchased from KPL (Gaithersburg, MD, USA). The assay was completed by addition of 2N H_2SO_4, and the assay plate was read at 450nm. Quantification of TNF-α stimulation was calculated from a linear regression using Prism software.

Macrophage Nitric Oxide Assay

Twenty-four hours after incubation, cell supernatants were removed from incubation with AA-PEA materials (100,000 RAW cells/24-wellplate) and assayed to quantify nitric oxide production. Nitric oxide stimulation of macrophage cells by AA-PEA materials was assessed using Griess Reagent Assay (Promega, Madison, WI, USA). Briefly, 50µl of cell supernatant was added to a 96-well plate, to which 50µl sulfanilamide solution was added, and allowed to incubate protected from light for 10 minutes. Next, 50µl NED reagent (N-1-napthylethylenediamine) was added, and again incubated in the dark for 10 minutes at room temperature. The plate was read at 540nm, and concentration of sodium nitrite production calculated from linear regression using Prism software.

Statistical Analysis

Statistical significance in tables and assay results are given as the average ± the standard deviation. Number of replicates tested (n) are given to provide reproducible independent data analysis. Statistically significant samples are denoted (*) when $p < 0.05$, (***) when $p < 0.01$. All samples were evaluated using one way Anova with Tukey HSD analysis in R software.

6.3 Results and Discussion

AA-PEA 2D films

Studying 2D polymer films is of great importance to understanding foreign body response as many implantable devices are coated to increase implant amenability and mitigate inflammatory response. By understanding which polymer characteristics mute or stimulate macrophage inflammatory response, biomaterials can be tailored to optimize mechanical properties, while reducing unwanted stimulatory responses. To begin, a series of 2D polymer film Phenylalanine-based AA-PEA materials were synthesized and analyzed for mechanical properties and biological stimulation. In this experimental group, two parameters were varied; 1) Hydrophilicity/hydrophobicity leading to changes in glass transition temperature (Tg), and 2) Charge on surface (via incorporation of charged amino acids) (Fig. 33). Poly(lactic acid) was chosen as a commercial control due to its proven compatibility and FDA approval as a viable biomaterial. To assess mechanical performance, two tests were used; 1) DSC (differential scanning calorimetry (DSC) to determine polymer rigidity, and 2) Contact angle goniometry to assess polymer Hydrophilicity/hydrophobicity.

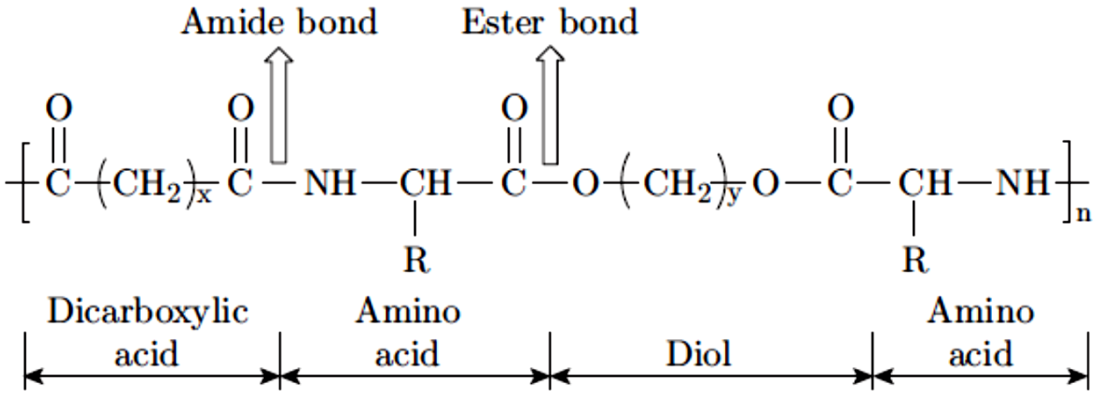

Figure 33. Chemical structures of AA-PEA polymers varying methylene chain length (x), diol (y), and varying pendant amino acid groups of AA-PEA polymers (R). Figure courtesy of Dr. C.C. Chu.

AA-PEA polymers were synthesized using varying methylene chain length diacid precursors, which introduces flexibility to AA-PEA polymer chains. Longer chains (i.e. 10-Phe-4) offers higher polymer chain mobility, therefore leading to a lower glass transition than the model 8-Phe-4 polymer. Contrastingly, synthesis of 4-Phe-4 reduces polymer flexibility by decreasing methylene chain length spacers, resulting in higher chain rigidity and glass transition temperature. Tg of AA-PEA solid polymers in the X-Phe-4 series decrease 24% and 6% respectively as X is increased from 4 to 8 and 8 to 10.

Similarly, introduction of hydrophilic amino acids (Arginine, Lysine in 8-Phe-4 – X-4) to the polymer chain correspondingly decreases the glass transition temperature (Fig. 34). Charged AA-PEA polymers were built from a model 8-Phe-4 polymer (which has been shown to have excellent mechanical properties and biocompatibility). Both Arginine and chemically-modified Lysine side chains offer increased pendant chain flexibility and decreased chain packing, therefore resulting in a lower overall polymer glass transition temperature.

Macrophage (and many cells including cancer cells) are sensitive to subtleties in physiological microenvironment, thus examining polymer hydrophobicity/hydrophilicity in stimulating macrophage cells will aid in understanding what material parameters are most likely to cause foreign body response and adverse effects to implanted devices. To do this, contact angle goniometry was used. Contact angle measurements were directly correlated to the amount of methylene chains in the AA-PEA backbone, as well as the amino acid used for polymer synthesis. Looking directly at neutrally-charged Phenylalanine-based PEA materials (X-Phe-4), hydrophobicity increased with increasing X value from 4 to 10 (49%). This is correlated to increased number of hydrophobic methylene chains along the backbone, between ester and amide linkages. In addition, by incorporating hydrophilic amino acids into the random solution polymerization (Arginine and Lysine), hydrophobicity correspondingly decreased as a result of hydrophilic (electrostatic and hydrogen bonding) interactions with the water droplet on the surface of the polymer film (19% and 9% decrease for Arginine and Lysine, respectively compared to model 8-Phe-4).

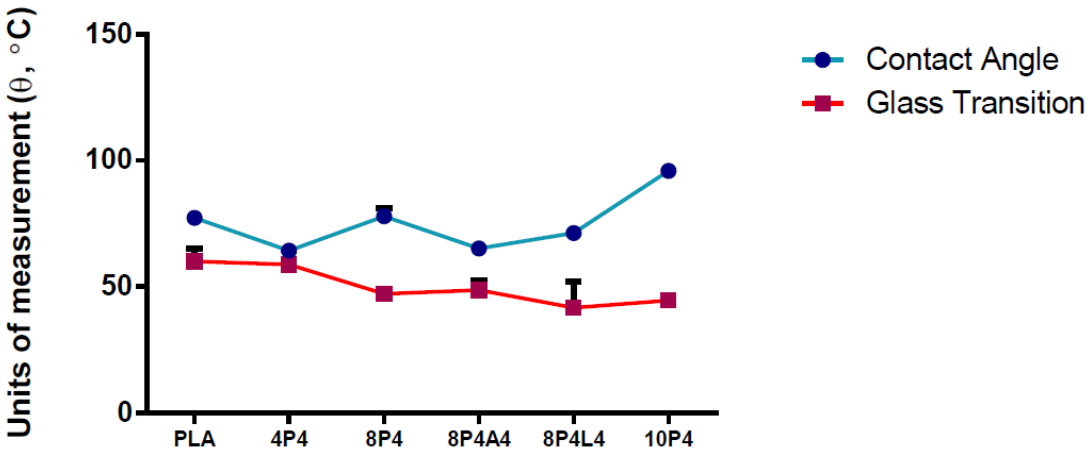

Figure 34. Mechanical properties of varying chemical structure AA-PEA polymers. All values are represented as avg. ± std. dev of three independent samples. Glass transition temperature is given in ℃ (red line), and contact angle represented as advancing angle θ (blue line).

Scanning electron microscopy was used to ensure even surface coating for a smooth surface free of defects that may affect degradation or macrophage response. All AA-PEA solution cast films exhibited an even and smooth coating free of any pitting or roughness (Fig. 35). Contrastingly, due to higher solution viscosity at equivalent weight percent to AA-PEA materials, PLA solution cast 2D films had a much more pronounced surface morphology (including divots where bubbles had formed).

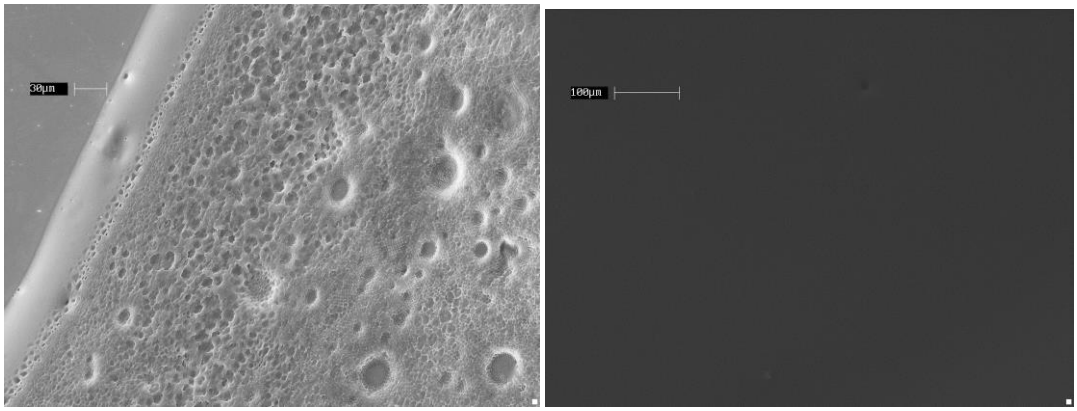

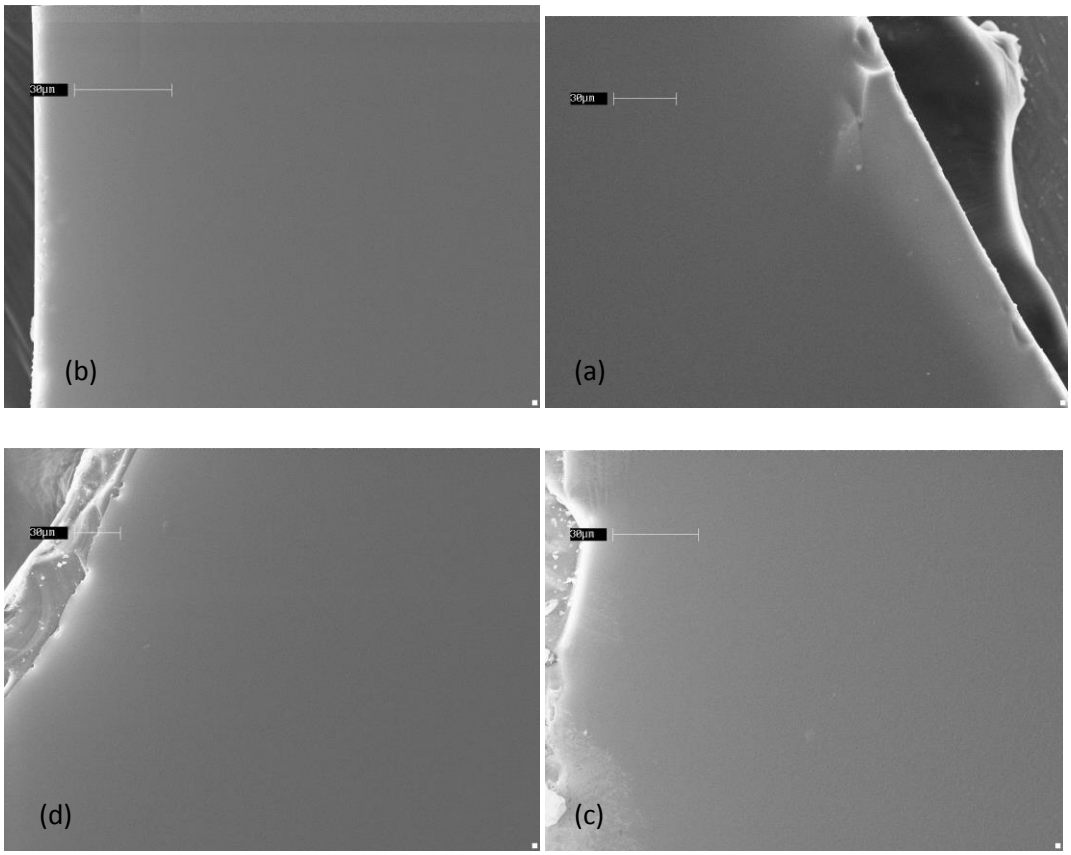

Figure 35. SEM images of 5 wt% 2D polymer film morphology, (a) PLA, (b) 4-Phe-4, (c) 8-Phe-4, (d) 8-Phe-4-Arg-4, (e) 8-Phe-4-Lys-4, (f) 10-Phe-4. Samples solution cast on 12mm round glass coverslips and imaged near an edge to show polymer layer more clearly.

AA-PEA film Biological Response

Macrophage Viability

In order to understand macrophage response to 2D polymer films, cytotoxicity, TNF-α ELISA and Nitric Oxide production assays were used. Using Poly (lactic acid) as a commercial control, macrophage cytotoxicity upon incubation with AA-PEA 2D polymer films was measured. PLA demonstrated excellent proliferative *in vitro* biocompatibility with macrophage cells (Fig. 36(a)), while neutral AA-

PEA 2D polymer films (X-Phe-4, X=4, 8) showed no statistically significant decrease in macrophage viability (compared to untreated control). Contrastingly, 10-Phe-4 elicited a statistically significant decrease in viability ($p < 0.01$) compared to untreated control. Macrophage viability is not affected when neutral polymers are moderately hydrophobic (4-Phe-4 and 8-Phe-4), but become less viabile when incubated on the highest hydrophobicity polymer (10-Phe-4).

RAW264.7 viability was slightly elevated upon incubation with cationic film (8-Phe-4-Arg-4), but the response is not statistically different from the untreated control or the PLA commercial control. Modifying the polymer to contain anionic charge (8-Phe-4-Lys-4) results in a decrease in viability compared to untreated control ($p< 0.01$) and its neutral 8-Phe-4 polymer family member ($p < 0.05$). Minor changes in cytotoxicity can be directly attributed to overall characteristics of the macrophage; cell membranes are negatively-charged as a result of the phospholipid membrane, therefore favorable electrostatic interactions can occur with 8-Phe-4-Arg-4, and repulsive interactions with 8-Phe-4-Lys-4, leading to more highly activated macrophages upon incubation with anionic AA-PEA films.

Macrophage TNF-α Pro-inflammatory cytokine production

Tumor necrosis factor-α (TNF-α) is a pro-inflammatory cytokine released into soluble media from macrophage cells upon stimulation. Upon TNF-α assay, all neutrally-charged material did not have a statistically significant increase in TNF-αcompared to PLA commercial control (Fig. 36(b)). Starting with the neutral X-Phe-4 materials, no statistically significant effect on TNF-α production could be seen with increase in methylene chain length when X= 4,8,10 in X-Phe-4. Therefore, material stiffness and hydrophobicity do not play a large role in macrophage stimulation. Compared to untreated control, the

anionic 8-Phe-4-Lys-4 film stimulated the greatest cytokine production(403% increase) compared to untreated control (Fig. 36(b)). Contrastingly, the cationic 8-Phe-4-Arg-4 2D polymer films showed very little TNF-α production (~50% decrease compared to untreated control). This trend can be attributed to the favorable cell membrane electrostatic interaction to pendant arginine amino groups and larger hydrophilicity of the polymeric material.

Anderson *et al*, researchers at the forefront of understanding complex macrophage interactions with biomaterials suggest four key parameters in understanding the longevity of implantable biomaterials: material-dependent monocyte/macrophage adhesion mechanisms, adhesion signaling, apoptosis induced by adhesion failure, and chemokine/cytokine networks.[24]Athough immense time and effort is spent to elegantly design and synthesize polymer materials for biomedical applications, some degree of macrophage activation is observed at the biomaterial/adhered cell interface linking to material dependent adhesion signaling. In a proinflammatory environment such as M1 classically activated macrophage activation, macrophages secrete many components that can be linked to host inflammation such as cytokines (TNF-α), proteases, proteins, and bioactive lipids that result in fever, tissue damage, and vasodilation associated with swelling, therefore resulting in unfavorable outcomes for the patient.[25]Therefore, in order to create biomaterials that are stable over long periods of time without adverse effects, understanding proinflammatory macrophage adhesion signaling patterns is of paramount concern.

In the same vein as the work done in this study, Jones *et al* studied the proteomic quantification of cytokines released from macrophages adhered to varying chemical composition polymer films (PET, polyethylene terephthalate/hydrophobic; BDEDTC, poly(styrene-co-benzyl N,N-

diethyldithiocarbamate)/hydrophobic; PAAm, polyacrylamide/hydrophilic neutral;PAANa, sodium salt of poly(acrylic acid)/hydrophilic anionic; and DMAPAAmMEI, methyl iodide of poly[3-(dimethylamino)propyl]acrylamide)/hydrophilic cationic).[26]Of interest, these researchers examined the release of proinflammatory mediator MIP-1β (macrophage inflammatory protein) and found after 3 days, hydrophilic anionic polymers (PAANa) induced the highest *in vitro* stimulation of human monocyte MIP-1β, consistent with the findings of this work.[26] In the same study, Jones *et al* also examined another proinflammatory cytokine (IL-1β) in a 3 day in vitro experiment and found in general that hydrophilic polymers stimulated higher proinflammatory cytokine response (PAAm, PAANa, DMAPAAmMEI) versus hydrophobic polymers with hydrophilic neutral polymers stimulating the highest response (PAAm).[26]These researchers suggest that reduced macrophage adhesion to hydrophilic neutral materials is the root cause for higher activation, leading to higher levels of cytokine release.[26]Similarly, Rodriguez et al found that surface chemistry dictated cytokine response, finding that after 4 days in vivo implantation in Sprague-Dawley rats, TNF-α production was produced at the highest level for silicone rubber compared to polyurethane, and PET.[27] In this case, the authors indicated that few macrophage cells were adherent to the silicone rubber substrate, linking to the hypothesis that TNF-α is the driving force for apotosis in non-adherent cells.[27]

Comparing to the work of this study, we also found that anionic materials stimulate proinflammatory cytokine response, while contastingly, we found that cationic materials did not promote proinflammatory cytokine. This may be attributed to two main factors; 1) the charge density of cationic monomer to hydrophobic monomer in 8-Phe-4-Arg-4 is 1:4, therefore the low response could be attributed to a low ratio of surface charge compared to DMAPAAmMeI materials, 2) increased

compatibility of macrophage cells to the pseudo protein structure, mitigating a higher level of proinflammatory response. Overall, hydrophobic AA-PEA polymers showed a moderate increase in proinflammatory cytokine response, while charged AA-PEAs displayed the most drastic changes, suggesting high macrophage sensitivity to surface charge/chemistry.

Macrophage Nitric Oxide Production

Uncharged AA-PEA films (X-Phe-4) exhibited increased nitric oxide production when X >4, corresponding to less rigid materials with greater hydrophobicity. Stimulation of nitric oxide production was more prominent with varying charge amino acid AA-PEA films (8-Phe-4-Lys-4 and 8-Phe-4-Arg-4) than the neutral series of materials (8-Phe-X series). Anionic AA-PEA 2D polymer films stimulated statistically significant NO· productioncompared to its neutral base polymer (8-Phe-4), aligning with macrophage stimulation exhibiting decreased viability and increased TNF-α secretion (Fig. 36(c)). Similarly, cationic AA-PEA 2D films stimulated nitric oxide production similar to uncharged 8-Phe-4, attributed to availability of pendant arginine amino acid groups for stimulation of the iNOS pathway to promote nitric oxide production. Since both TNF-α and nitric oxide are present in the M1 classically activated macrophage cascade, it is important to draw parellels between release profiles of these two components. Logically, an increase in stimulation of TNF-α production should also result in an increase in nitric oxide production. This is clearly evident for anionic 8-Phe-4-Lys-4 materials. Although not stimulating a high TNF-α response, cationic 8-Phe-4-Arg-4 materials did show an increase in nitric oxide production, again, most likely linked to surface chemistry stimulation of the iNOS pathway.

Nitric oxide (denoted NO·) production was used as a method to characterize M1 classically activated macrophage response to 2D AA-PEA polymer films.Nitric oxide is a reactive nitrogen

intermediate produced upon stimulation of the iNOS pathway, commonly associated with M1 inflammatory phenotype macrophage activation. Therefore, commercial and novel polymeric 2D polymer films ideally should not induce exogenous NO· production, inherently leading to improved wound healing.

Macrophage IL-10 production

Equally as important and valid as examining M1 classically activated proinflammatory response mediators such as TNF-α and nitric oxide, looking at the M2 alternatively activated pathway stimulation offers insights into potential directions of which biomaterials stimulate a reponse more commonly associated with wound healing rather than wound irritation. Of the materials tested (hydrophobic, cationic, anionic), only the hydrophobic commercial control (PLA) and moderately hydrophobic 8-Phe-4 polymers stimulated a statistically significant IL-10 cytokine response ($p < 0.05$) over the untreated control (RAW264.7 cells on tissue culture plate) (Fig. 36(d)). All others did not show an increase in IL-10 production compared to the untreated control. Therefore, unlike TNF-α and nitric oxide in M1 classical activation pathway, M2-type activation is not as heavily influenced by surface charge. In this arena, surface hydrophobicity was indicated as a more influential factor.

Comparing to results found in literature, Jones *et al* found after 3 days *in vitro* incubation with human monocyte cells PAAm hydrophilic neutral materials had the highest IL-10 production (pg/cell x 10^5), a trend that continued out to 10 days.[26] On average, human monocyte cells were producing 170pg/mL per cell IL-10 cytokine during the 3 day study.[26] Consistent with the samples tested in this found, Jones *et al* found that at 3, 7, and 10 days, hydrophilic anionic materials did not induce IL-10 production.[26]In the same field of research, Brodbeck *et al* also concluded that, using human monocyte *in*

vitro total RNA quantification analysis, hydrophilic neutral (PAAm) and hydrophilic anionic (PAANa) stimulated IL-10 production at multiple time points over 10 days, while a noteable decrease in IL-10 cytokine stimulation was observed for hydrophilic cationic (DMAPAAmMeI).[28] Akin to TNF-α data trends, lack of increased rises in IL-10 production to charged AA-PEAs (8-Phe-4-Arg-4 and 8-Phe-4-Lys-4) could be a results of the overall charge density in the polymer chemical structure (25% charge to hydrophobic 8-Phe-4). Therefore, in order to have a more direct side by side comparison, AA-PEAs with a larger charge density can be used in future study to determine if the trends observed by literature[26,28] are consistent with this series of AA-PEA materials.

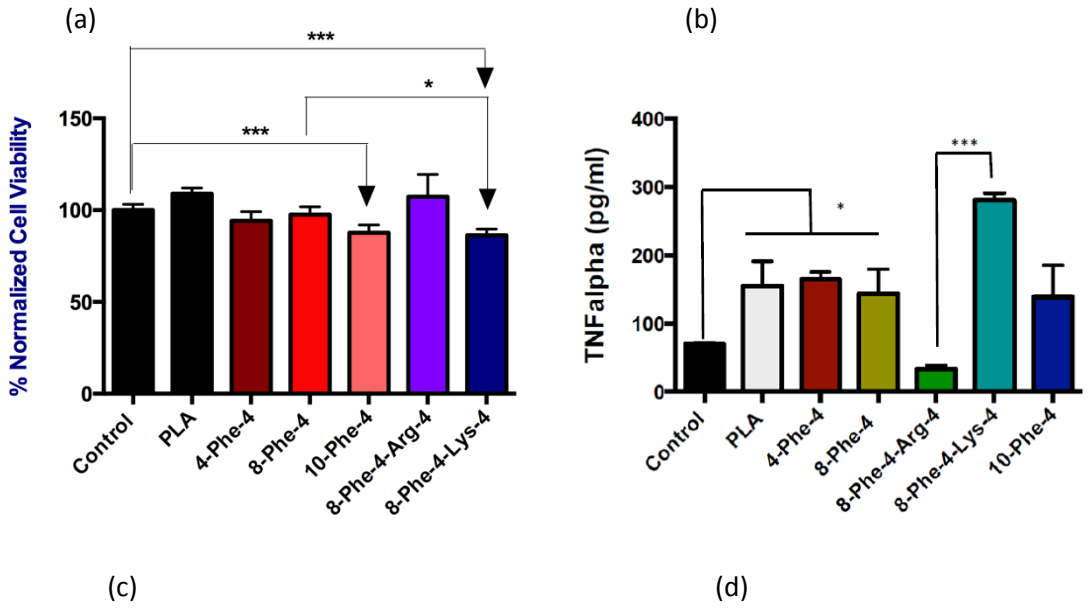

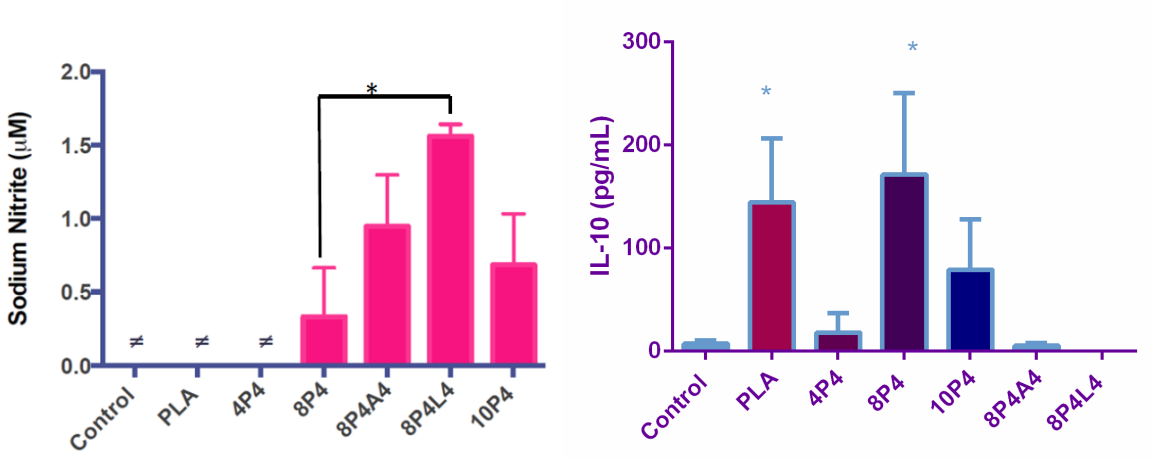

Figure 36. Mouse Macrophage biological stimulation of 2D AA-PEA polymer films, (a) Cytotoxicity assay, (b) TNF-alpha cytokine inflammation assay, (c) Nitric Oxide production assay, (d) IL-10 anti-inflammatory cytokine assay. All samples were tested represented as avg ± std. dev of independent quadruplicate samples. (≠) indicates sample assay falling below bottom standard on calibration curve. Statistical significance is given as $p < 0.05$ (*), and $p < 0.01$ (***). All other samples are considered not significant unless annotated.

Macrophage Adhesion

In order to assess polymer biocompatibility with cells, including macrophage cells, one can assess cytokine and mediator release (as discussed above), but in order to gain a more complete and biologically relevant picture, cell adhesion must be examined to determine if adhesion factors are determining cytokine release patterns. Understanding macrophage adhesion to materials is of utmost importance because as cells adhere to the biomaterial surface, many mediators such as reactive nitrogen and oxygen species as well as enyzmes that lower the pH and degrade the surface, thereby reducing the lifetime of the implant. RAW264.7 macrophage adhesion was indeed influenced by chemical and atomic

variations in 2D AA-PEA polymer films. Hydrophobic PLA, 8-Phe-4, and 10-Phe-4 all had excellent macrophage adhesion (Fig. 37 (a,c,d)) with observable podosomal stretching (assessed qualitatively using F-Actin Phalloidin staining) onto the surface. Compared to the hydrophobic commercial control PLA, 8-Phe-4 2D polymeric film promoted some cell aggregation, but a larger degree of single cell podosomal stretching (Fig. 37 (g,h)). Moderately charged 4-Phe-4 and charged surfaces displayed a reduced number of macrophage adhesion with low observable podosomal stretching. Between cationic 8-Phe-4-Arg-4 and 8-Phe-4-Lys-4, 8-Phe-4-Lys-4 visually appears to have more cells adhered. A low visual content of cells adhered to cationic 8-Phe-4-Arg-4 may be attributed to the fact that the material displayed some opacity after cell culture, resulting in increased difficulty in confocal imaging.

A leading hypothesis in the field of macrophage/biomaterial interactions is the premise that surface chemistry can dictate macrophage stimulation. According to Jones *et al*, in an *in vitro* human monocyte study, the concluded that hydrophobic and hydrophilic/charged surfaces did in fact support monocyte adhesion.[26] At all time points (3-10 days), they observed a steep decrease in cell adhesion to hydrophilic/neutral surfaces, while hydrophobic surfaces remained at the top of the total adherent cells range.[26]This data suggest that macrophage cells are inherently capable of sensing their local microenvironemt, stimulating differently for varying surface hydrophoboicity and charge.

In an elegant study completed by Brodbeck *et al*, an in vivo Sprague-Dawley model was used to quantify which polymer material characteristic that most strongly influenced macrophage adhesion. They found that between 7-21 days *in vivo* implantation, macrophage adhesion statistically decreased on hydrophilic neutral (PAAm) and hydrophilic anionic (PAANa) polymer films, coupled with a corresponding increase in apoptotic cells.[29] Due to decreased adhesion and increased apoptosis,

hydrophilic neutral (PAAm) and hydrophilic anionic films displayed reduced macrophage fusion compared to hydrophobic (PET, BDEDTC) and hydrophilic cationic films (DMAPAAmMeI).[29]The authors postulate that the low number of adhered cells can be linked to the amount and types of adsorbed proteins to the hydrophilic anionic (PAANa) material, as this material may not promote sufficient number of oriented ligands in the protein layer.[29]Therefore, biomaterial polymers designed for coatings to which macrophages may adhere must balance the delicate scales of disfavoring macrophage adhesion, while not at the same time causing apoptosis.

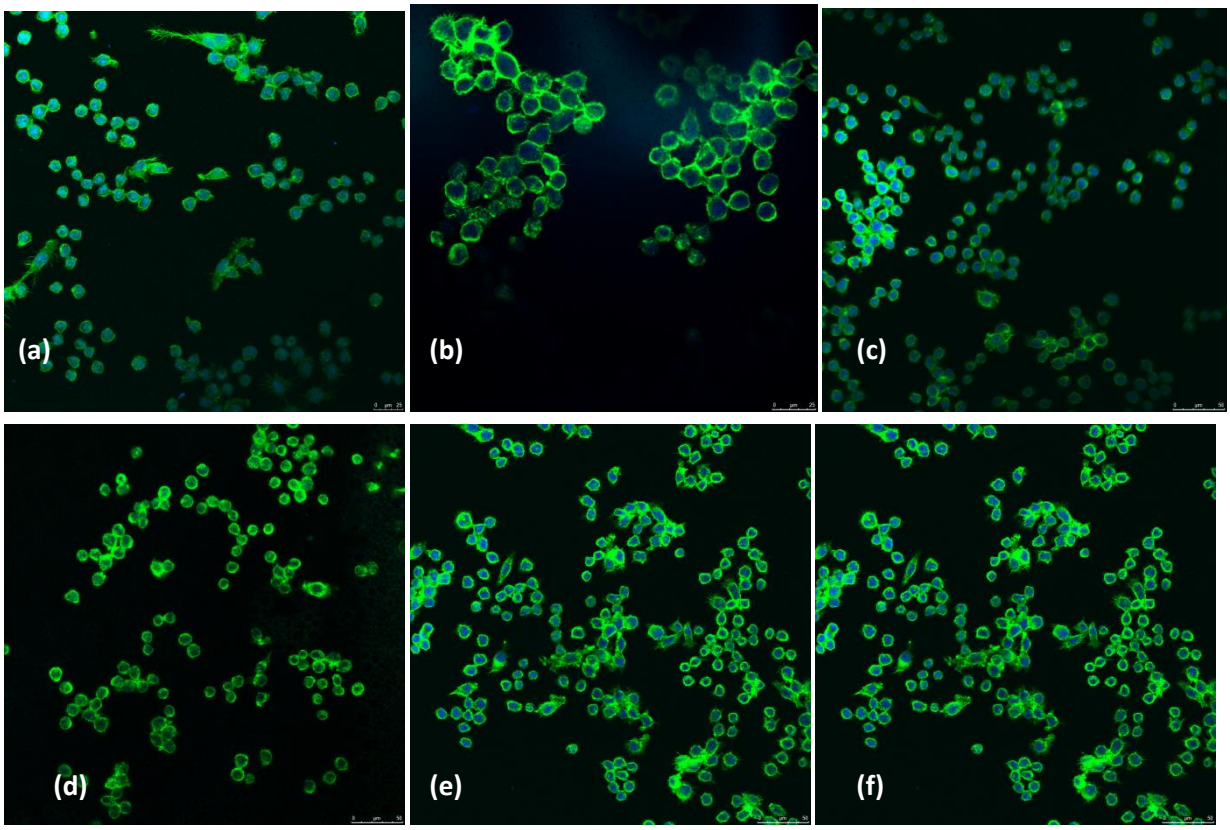

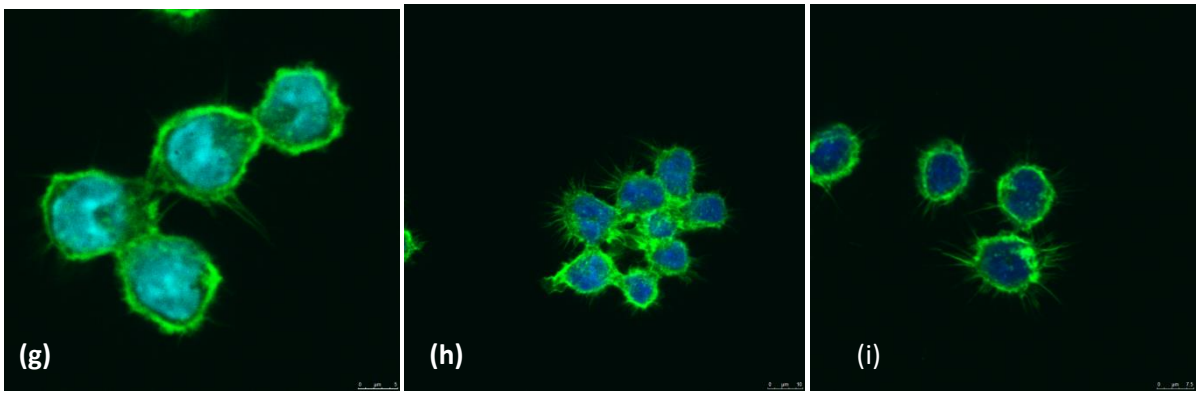

Figure 37. Fluorescent microscopy – macrophage adhesion and morphology upon incubation with AA-PEA 2D films, (a) PLA, (b) 4-Phe-4, (c) 8-Phe-4, (d) 8-Phe-4-Arg-4, (e) 8-Phe-4-Lys-4, (f) 10-Phe-4, and zoom of adhesion on (g) PLA, (h) 8-Phe-4, and (i) 10-Phe-4. Macrophage nuclei are stained with DAPI (blue), and F-actin filaments with Phalloidin (green).

6.4 Conclusions

Overall, in a series of AA-PEA 2D polymer films with varying hydrophobicity (X-Phe-4) and charged amino acid content (8-Phe-4-X-4), little effect on macrophage viability was found based on increasing hydrophobicity ($p < 0.01$ for 10-Phe-4). Macrophage incubation with cationically-charged 8-Phe-4-X-4 polymers did not statistically affect macrophage viability when compared to neutral 8-Phe-4 polymer, while a statistically significant decrease in viability was found for anionically-charged 8-Phe-4-X-4 polymers when compared with neutral 8-Phe-4 ($p < 0.05$). No increase in TNF cytokine production corresponding to increased polymer hydrophobicity was observed for neutral X-Phe-4 polymers, while cytokine stimulation dependence on amino acid content was a strong factor. Cationically-charged 8-Phe-4-Arg-4 polymers statistically decreased cytokine production, while anionically-charged 8-Phe-4-Lys-4

stimulated cytokine production when compared to neutral 8-Phe-4. Moreover, a statistically significant increase in nitric oxide was observed for anionic 8-Phe-4-Lys-4 materials compared to hydrophobic 8-Phe-4, paralleling M1 proinflammatory stimulation observed in conjunction with increased TNF-α cytokine production.

Contrasting high M1 proinflammatory response sensitivity to surface charge, only hydrophobic PLA and 8-Phe-4 produced a statistically significant production of IL-10, commonly found with M2 wound healing responses. Similarly, macrophages adhered well to all materials, favoring hydrophobic materials for higher levels of podosmal stretching. Therefore, based on the culmination of cytotoxicity, TNF-α, nitric oxide, IL-10, and adhesion, it becomes clear that hydrophobic (8-Phe-4) or cationic (8-Phe-4-Arg-4) AA-PEAs are excellent candidates for macrophage biocompatibility, displaying comparable or lower levels of cytotoxicity, TNF-α, nitric oxide, IL-10, and adhesion.

References

1. Tessier, P.y., L. Pichon, P. Villechaise, P. Linez, B. Angleraud, N. Mubumbila, V. Fouquet, A. Straboni, X. Milhet, and H.f. Hildebrand. Carbon Nitride Thin Films as Protective Coatings for Biomaterials: Synthesis, Mechanical and Biocompatibility Characterizations.*Diamond and Related Materials* 12.3-7 (2003): 1066-069.
2. Chapman, Robert G., Emanuele Ostuni, Michael N. Liang, Gloria Meluleni, Enoch Kim, Lin Yan, Gerald Pier, H. Shaw Warren, and George M. Whitesides. Polymeric Thin Films That Resist the Adsorption of Proteins and the Adhesion of Bacteria.*Langmuir* 17.4 (2001): 1225-233.
3. Vasilev, Krasimir, Jessica Cook, and Hans J. Griesser. Antibacterial Surfaces for Biomedical Devices.*Expert Review of Medical Devices* 6.5 (2009): 553-67.
4. Karp, Jeffrey, Molly Shoichet, and John Davies. Bone Formation on Two-dimensional Poly(DL-lactide-co-glycolide) (PLGA) Films and Three-dimensional PLGA Tissue Engineering Scaffolds in Vitro. *J Biomed Mater Res A* 64.2 (2003): 388-96
5. Hong, Helen, and Jan P. Stegemann. 2D and 3D Collagen and Fibrin Biopolymers Promote Specific ECM and Integrin Gene Expression by Vascular Smooth Muscle Cells. *Journal of Biomaterials Science, Polymer Edition* 19.10 (2008): 1279-293

6. Ahmad Khan, Tanveer, and Kok Khiang Peh. A Preliminary Investigation of Chitosan Film as Dressing for Punch Biopsy Wounds in Rats. *J Pharm Pharmaceut Sci* 6.1 (2003): 20-26
7. Okada, Hiroaki. Biodegradable Microspheres in Drug Delivery.*Critical Reviews in Therapeutic Drug Carrier Systems* 12.1 (1995): 1-99.
8. Brannon-Peppas, Lisa. Recent Advances on the Use of Biodegradable Microparticles and Nanoparticles in Controlled Drug Delivery.*International Journal of Pharmaceutics* 116.1 (1995): 1-9
9. Freiberg, S., and X.x. Zhu. Polymer Microspheres for Controlled Drug Release. *International Journal of Pharmaceutics* 282.1-2 (2004): 1-18.
10. Lim, S.T., G.P. Martin, D. J. Berry, and M.B. Brown. Preparation and Evaluation of the in Vitro Drug Release Properties and Mucoadhesion of Novel Microspheres of Hyaluronic Acid and Chitosan. *Journal of Controlled Release* 66.2-3 (200): 281-92.
11. Herran, C. Leigh, and Yong Huang. Alginate Microsphere Fabrication Using Bipolar Wave-based Drop-on-demand Jetting.*Journal of Manufacturing Processes* 14.2 (2012): 98-106
12. Determan, Amy S., Jennifer R. Graham, Katherine A. Pfeiffer, and Balaji Narasimhan. The Role of Microsphere Fabrication Methods on the Stability and Release Kinetics of Ovalbumin Encapsulated in Polyanhydride Microspheres.*Journal of Microencapsulation* 23.8 (2006): 832-43
13. Guo, Kai, and C.C. Chu. Biodegradable and Injectable Paclitaxel-loaded Poly(ester amide)s Microspheres: Fabrication and Characterization. *Journal of Biomedical Materials Research Part B: Applied Biomaterials* 2008. 491-500
14. Li, D., and Y. Xia. Electrospinning of Nanofibers: Reinventing the Wheel? *Advanced Materials* 2004, 16.14, 1151-170
15. Katsarava, R., Beridze, V., Kharadze, D., Chu, C. C., Won, Y., Arabuli, N. Amino Acid-based Bioanalogous Polymers. Synthesis, and Study of Regular Poly(ester amide)s Based on Bis(α-amino acid) α, ω-Alkylene Diesters, and Aliphatic Dicarboxylic Acids. *Journal of Biomaterials Science* 1988, *37*, 391-408
16. G. Jokhadze , M. Machaidze , H. Panosyan , C. C. Chu & R. Katsarava. *Journal of Biomaterials Science, Polymer Edition*, 18:4, 411(2007)
17. C. C. Chu and R. Katsarava, US Patent 6,503,538 (2003).
18. Tsitlanadze, G., M. Machaidze, T. Kviria, N. Djavakhishvili, C.C. Chu, and R. Katsarava. Biodegradation of amino-acid based poly(ester amide)s: *in vitro* weight loss and preliminary *in vivo* studies. *J.Biomaterials Science, Polymer Edition* 2004,15.1, 1-25
19. Li, Lei, and Chih-Chang Chu. Nitroxyl Radical Incorporated Electrospun Biodegradable Poly(ester amide) Nanofiber Membranes. *J.Biomaterials Science, Polymer Edition* 2009, 20.3, 341-361

20. Wu, Dequn, Jun Wu, and C.C. Chu. A novel family of biodegradable hybrid hydrogels from arginine-based poly(ester amide) and hyaluronic acid precursors.*Soft Matter* 2013, 9, 3965-3975
21. Wu, Jun, Martha Mutschler, and Chih-Chang Chu. Synthesis and Characterization of Ionic Charged Water Soluble Arginine-based Poly(ester Amide). *Journal of Materials Science: Materials in Medicine* 2011, 22.3, 469-79
22. He, Mingyu, Alicia Potuck, Yi Zhang, and C.C. Chu. Arginine-based Polyester Amide/polysaccharide Hydrogels and Their Biological Response. *Acta Biomaterilia* 10.6 (2014): 2482-492
23. Tobhmita, Yusuke, Akiko Rikimaru-Kaneko, Koji Hashiguchi, and Shoichi Shirotake. Effect of Anionic and Cationic-butylcyanoacrylate Nanoparticles on NO and Cytokine Production in Raw264.7 Cells."*Immunopharmacology and Immunotoxicology* 2011, 33.4, 730-37
24. Xia, Zhidao, and James T. Triffitt. A Review on Macrophage Responses to Biomaterials. *Biomedical Materials* 1.1 (2006): R1-R9.
25. Anderson, James M., and Amy K. Mcnally. Biocompatibility of Implants: Lymphocyte/macrophage Interactions. *Seminars in Immunopathology* 33.3 (2011): 221-33.
26. Rodriguez, Analiz, Howard Meyerson, and James Anderson. Quantitative in Vivo Cytokine Analysis at Synthetic Biomaterial Implant Sites. *J Biomed Mater Res A.* 89.1 (2009): 152-59.
27. Jones, Jacqueline A., David T. Chang, Howard Meyerson, Erica Colton, Il Keun Kwon, Takehisa Matsuda, and James M. Anderson. Proteomic Analysis and Quantification of Cytokines and Chemokines from Biomaterial Surface-adherent Macrophages and Foreign Body Giant Cells. *Journal of Biomedical Materials Research Part A* 83A.3 (2007): 585-96.
28. Brodbeck, W., Y. Nakayama, T. Matsuda, E. Colton, N. Ziats, and J. Anderson. Biomaterial Surface Chemistry Dictates Adherent Monocyte/macrophage Cytokine Expression In Vitro. *Cytokine* 18.6 (2002): 311-19.
29. Brodbeck, W. G. Biomaterial Adherent Macrophage Apoptosis Is Increased by Hydrophilic and Anionic Substrates In vivo. *Proceedings of the National Academy of Sciences* 99.16 (2002): 10287-0292.

Chapter 7. Development of Thermochromic Pigment Based Sportswear for Detection of Physcial Exhaustion

(In Preparation- Proposed March 2015) Potuck, Alicia, Sarah Meyers, Ariana Levitt, Eric Beaudette, Hong Xiao, C. C. Chu, and Huiju Park. Development of Thermochromic Pigment Based Sportswear for Detection of Physical Exhaustion. Fashion Practice

Abstract

Endurance athletes face a complex array of physiological changes as their core and skin temperature rises in vigorous exercise. To aid in facile determination of physical exhaustion, thermochromic pigments were applied to Nylon/Spandex fabric, using pigment activation temperature as an indication for exhaustion. Thermochromic pigments contain leuco dyes capable of changing chemical structure to alter the dye molecule absorbance, leading to a visual tool for skin temperature indication. This technology was coupled with conventional textiles to create smart apparel with satisfactory abrasion and color fastness capabilities. Using targeted placement of thermochromic panels in garment construction, a garment capable of serving as a "warning light" for physical exhaustion in athletes was created.

7.1 Introduction

Since the 1990s, various research and development efforts have been made in an attempt to integrate technology into fashion, which has expanded the meaning of clothing from the icon of aesthetics or daily necessity to a wearable form of human performance enhancement. One category of popular and functional garments is performance athletic wear, specifically geared toward athletic applications and sports enthusiasts. The biggest challenge in sportswear design is providing thermal comfort while the human body experiences elevated body temperatures and perspiration during athletic activity. Paralleling functionality, marketing analysis of the athletic apparel industry found comfort, fit, and style are the most desirable traits for athletic apparel, with a higher percentage of users preferring garments that can translate through both sports and casual wear (Fowler 1999).

Athletic wear is designed to parallel the needs and demands of its wearer including flexibility, durability, and breathability. The combination of technology and apparel design can further optimize wearer experience and meet the rigorous demands of athletes. For example, rise of heart rate and body temperature in marathon athletes is of great concern during arduous energetic output. To monitor real time physiological parameters, researchers such as Park *et al* described novel ways to merge "smart apparel" with medical functionalities, including the "Smart Shirt" which contains a motherboard within the apparel garment capable of monitoring and recording patient heart rate, respiration rate, and pulse oximetry for applications ranging from military, civilian, space, and safety (Park 2003). Although comprehensive physiological data can be collected, these systems suffer from pitfalls of ungainly electronic connections, cost, maintenance, and durability, making these systems not widely accessible.

Monitoring physical exhaustion of the wearer is pivotal in aiding healthy non-destructive exercise. Previous studies show fatigued athletes exhibited reduced cardiac output, central blood volume, and stroke volume, characteristic of the detrimental influence attributed to physical exhaustion (Gonzalez-Alonso 1999; Gonzalez-Alonso 1997). Similarly, heart rate at the apex of fatigue is approximately 98-99% of maximal heart rate. Mean temperatures taken of skin during fatigue (avg. of measurements taken of upper arm, forearm, chest, back, thigh, and calf) correlate well increased skin temperature (37.2 ± 0.01) and physical exhaustion (Gonzalez-Alonso 1999). Research indicates resting abdominal skin temperatures of normal weight subjects to be 32.8 ± 0.03℃ (Savastano 2009).

Looking more closely at this colorimetric technology, thermochromic pigments are leuco dyes that have become popular due to their color changing abilities (Zhu 2005; Kulcar 2010). When the temperature surrounding the pigments rises, the solvent present within the pigment microcapsules undergoes transition to liquid phase, followed by salt dissociation, pH shift, and protonation of the leuco dye resulting in a significant shift in the absorption of the molecule, leading to a colorless appearance. Depending on the temperature of the transition, the pigments can appear colored or colorless on the textile material. In order to apply this technology to apparel design and fabrication, thermochromic pigments can be applied onto the surface of the textile material (Mather 2001; White 1999; Tang 2006), then used to create an overall athletic apparel piece. Unlike smart clothing that has already been developed, thermochromic pigments offer a new design solution for functional sportswear that does not require external electronic components and color change is based solely on the indications (skin temperature) given by the wearer.

Therefore, innovations such as thermochromic pigments can enhance activewear by preventing exhaustion during athletic exercise while providing key desirable elements such as comfort and functionality. By employing thermochromic pigments that undergo a color change in the temperature range of elevated skin temperature during brisk exercise, the wearer of the garment can assess whether or not he is exercising too vigorously based on the garment panel colors. The purpose of the project was to create both a functional and fashionable design with thermal sensing technology to create a performance athletic garment capable of signaling physical exhaustion to the wearer. In this paper we describe a method for thermochromic pigment application to textiles, assessment of pigment performance, and design of novel apparel.

7.2 Execution of design: material preparation and prototype production

Thermochromic pigments of various activation temperatures (black 35°C, blue 33°C, 38°C, and magenta 38°C), scouring reagents (Invatex AC-US (poly maleic acid), Invadine DA (alcohol C13-C15 poly(1,6) ethoxylate)), binding agent (Lyoprint PBA (poly butyl acrylate)) and thickening agent (Lutexal, First Source Worldwide) were used. Sodium hydroxide (NaOH) pellets were purchased from Mallinckrodt Chemicals (Phillipsburg, NJ, USA). White (for thermochromic coating) and black (remainder of garment) 87% Nylon/13% Spandexfabric was purchased from Spandex World Inc. (New York, NY, USA).

Scouring the Fabric

Tap water was placed in 1000ml beaker (30x total weight of fabric) with 50g/L NaOH, 3g/L Invadine DA, and 8 g/L Invadex AC-US. Once the solution reached a rolling boil, Nylon/Spandex fabric was added with the temperature lowered to a simmer for 30 minutes. The

hot scouring solution was carefully decanted and the fabric rinsed well (10x) in tap water. The scoured fabric was then dried at ambient temperature until dry.

Pigment Solutions and Application to Fabric

Pigment solutions were created using the following composition; 4-10% pigment, 18-20% binding agent, 10% thickener, and 70% water. For example, 7g of water was added to a small beaker, followed by 2g binder. Next, 0.4g pigment was added. Lastly, 1g thickener was placed in the beaker. Upon vigorous stirring, the solution became noticeably viscous. In order to balance wearer comfort with the most striking color change effect, the weight percent of pigment in solution was varied, starting with the least amount to give good effect (~4 total solution wt%). At this pigment feed ratio, color change was well recognizable and reversible, yet overall appearance of color on the fabric was medium/light. For example, at a total solution concentration of 4 wt%, blue 33℃ thermochromic pigments were reasonably colored at this weight percent, but lacked a striking depth of color on the surface. To increase the color saturation of thermochromic pigments on the fabric, the weight percent of pigment in solution was raised to ~10%, and the overall effect was an increase in color saturation with acceptable textile surface texture. The result of increasing the weight percent of thermochromic pigments in the solution slurry increased the color depth (in the case of blue 33℃) from medium blue with hints of white base textile to rich royal blue with no visibility of spandex fabric.

Nylon/Spandex was cut to the appropriate size and ironed to remove wrinkles. Once the fabric was secured well to a flat surface, a brush was used to apply the viscous pigment solution to the surface of the fabric using even brush strokes. Once applying pigment to surface of textile, it was imperative to place a thin but consistent layer. Too thick a layer caused bulk pigment on the

surface, leaving an uneven patchy appearance that over time excess started to peel away [Fig. 41(a)] (i.e. crocking). Furthermore, experiments showed that using an extremely thick coating layer caused ineffective crosslinking of the binder. The resultant effect was removed of the pigment coating upon immersion in an aqueous environment [Fig. 41(b)]. To mitigate the difficulty with ineffective binder, experimentsal results indicated that applying a consistent thin coat with subtle stretching of the fabric facilitated good pigment adherence. Coated fabric pieces were dried in an isotemp oven at 100℃ for 10 minutes or until completely dry. The fabric was then removed to heat the oven to 160℃. Once at temperature, the fabric was placed back in the oven and crosslinked for approximately 5-7 minutes.Care was taken in the pigment application process to minimize exposure of pigment treated fabric to high temperatures.

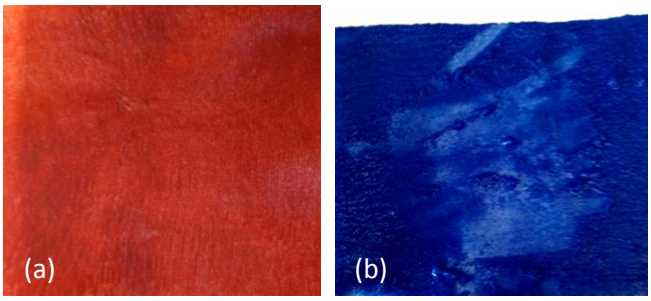

Figure 41. Thermochromic pigment applied to Nylon/Spandex material exhibiting, (a) crocking of pigment coating on surface, (b) insufficient binding of pigment to textile surface (prominent in aqueous environments)

Abrasion Characterization

In order to better understand how durable thermochromic apparel would be for repeated wear, abrasion testing was used.The testing done was based on ASTM D4966-12-Standard Test Method for Abrasion Resistance of Textile Fabrics (Martindale Abrasion Tester Method) with

minor modifications (Blau 1999). A 5.5 inch circular sample of fabric (coated with blue 38°C thermochromic pigment) was cut on a piece of felt with a circular cutter. The samples were placed on the abrasion tester and were rubbed against the standard test fabric (jersey knit). The samples were first observed for every 100 cycles to observe how the appearance of the fabric changed (noting any color differences or formation of broken yarns, holes, or pilling). This was done until the fabric was subject to 2000 cycles. The samples were then checked every 500 cycles until the fabric was subject to 10,000 rubs. Finally, the fabric was then checked every 1500 cycles until the fabric reached 13,000 rubs.

Colorfastness Characterization

As athletes set constant and vigorous workout schedules, activewear must be able to withstand laundering while maintaining colorfastness. To quantify colorfastness of thermochromic textiles, mechanical colorimeter was used. The ability of the thermochromic pigment to adhere to the fabric was assessed. In addition to the thermochromic fabric retaining its functional capabilities, it also must retain its color for aesthetic purposes. One factor that can influence the colorfastness of the garment is the molecular structure of the pigment (or dye); this in turn can affect the interaction of the pigment with the fabric. Material characteristics can impact the colorfastness including the size (diameter) of the thermochromic microsphere are the size of the particle (Leelajariyakul, 2008).

External factors such as UV and chlorine bleach can also shape the colorfastness of thermochromic apparel. Therefore, the durability of the thermochromic pigment against non-chlorine bleach was assessed (The fabric was not subjected to chlorine bleach due to potential permanent damage to the thermochromic pigments). The results from this exam could further

dictate the instructions on a car label (Fan 2009). To assess the performance against nonchlorine bleach, the fabric was subjected a modified version of the AATCC 188 Test: Colorfastness to Sodium Hypochlorite Bleach in Home Laundering. The fabric changes in color were quantified via L (lightness to darknesss), A (red to green), and B (blue to yellow) respectively.

The testing done was based on AATCC Test Method 172- Quick Method for Colorfastness to Non-Chlorine Bleach (Easter 2006). In brief, fabric coated with thermochromic pigment was cut into 3"x 3" squares. Non-chlorine bleach (peroxide-based laundry agent) was applied to the fabric pieces (denoted treated) and allowed to sit at room temperature for 5 minutes. Control and treated thermochromic fabric swatches were tested for colorfastness using Macbeth Color Eye Colorimeter (X-Rite Ltd., Grand Rapids, MI, USA). An average of four independent measurements were measured with L (lightness to dark scale), A (red to green), and B (blue to green) values recorded. ΔE values for colorfastness were calculated using Equation (1).

$$\Delta E^*_{ab} = \sqrt{(L^*_2 - L^*_1)^2 + (a^*_2 - a^*_1)^2 + (b^*_2 - b^*_1)^2}$$

(Equation 1)

Where a: represents the difference between green (a^*_2) and red (a^*_1), b: represents the difference between blue (b^*_2) and yellow (b^*_1) and L: represents the difference between black (L^*_2) and white (L^*1). This equation was used to assess the scale of color difference between two samples.

Garment Design and Construction

The design of the garment integrated both the aesthetic design of athletic apparel and the function of the thermochromic pigments. Fabric was bought from a spandex retailer, chosen for fiber content, optimal thickness, and a matte finish. The fabrics chosen were black and white 87% nylon/13% spandex knits. Hydrogen bonding of polyamide chains within the nylon contributes to the mechanical properties of high modulus, stiffness, abrasion resistance, and low friction coefficient. These properties reduce wear-and-tear of the fabric, while also increasing tactile comfort. Spandex was needed to allow the stretch for a compressive garment, while also having dimensional stability after deformation. The high percentage of Spandex brings much more elongation to the fabric properties than a high modulus. The thick material followed the functionality of the clothing for outdoor running, while the matte finish offered both enhanced aesthetics and feasibility of construction. The white was chosen to apply the pigment to while the black was for the remainder of the garment. A two-piece tight fitting compression ensemble, long sleeved hooded top and running pants was sketched to have maximum contact to the skin and pigments.

The design lines on the hooded top emphasize an ideal muscular structure for a male. Pattern pieces on both sides of the torso highlight abdominal muscles. Additionally, the center back pattern piece of the top resembles the extension of the spine, leading up to the hood while design lines on the back follow shoulder blade curvature. Both garments relied on the stretch of the fiber in the hooded top or the waistband in the pants for easy dressing and undressing.

The design considerations for the pants followed those of the hooded top. The segmented pieces on the outer leg of the pants were constructed to highlight thigh and calve muscular

structure. Lines from the geometric pattern pieces are horizontally continuous around side seams, and vertically continuous from top to bottom creating interesting views from all angles.

Pigments were assigned to pattern pieces of the garment by looking at skin temperatures relating to extreme core body temperatures. The black and coated white pieces were sewn together. Thermochromically-coated apparel pieces were integrated into the design to highlight physiological areas that generate heat through the skin during rigorous exercise. For example, in the upper body piece, the sleeve inserts are coated with black 35°C pigments, while the core inserts are coated with blue 33°C and magenta 38°C (Fig. 42). To best show a range of temperature as core and skin temperature increases, the upper thigh is coated with blue 38°C, followed by magenta 38°C, ending with blue 33°C. Pigments having an activation temperature around 38°C are crucial as this is on the upper limit of skin temperature for physical exhaustion. Thus, when thermochromically coated inserts in the upper thigh change from colored to colorless, the athlete has a quick, effective, and visual method for determining when rest is needed to maintain healthy cardiac output.

Evaluation of Effects of Thermochromic Ink Using a Sweating Thermal Manikin

The garment was tested on Walter® (Hong Kong Polytech University, Hong Kong), a sweating thermal manikin. Following ISO11097 (Ergonomics of the thermal environment, BS EN ISO 11079; 2007 standard), the mean skin temperature of a sweating thermal manikin was controlled at 35C to simulate mean skin temperature of human body. Environmental chamber remained at 21°C ±2°/65% ±5% relative humidity. Qualitative observations were recorded for garment panel color change as a function of time from the program Walter® – Sweating Fabric Manikin System 2012. Qualitative observations included photographically documenting the

amount of time after placing the garment on the manikin for each colored pigment piece to activate based on the manikin surface temperature.

7.3 Results and Discussion

Pigment Application

Pigment solutions were created using the aforementioned composition. It was found that the order in which each component was added in succession affected the overall uniformity of the mixture; adding the water first, followed by binder, pigment, with thickener last afforded the best solution. Mixing the pigment with water before addition of binder caused the powder to become unmanageable; the pigment spheres would not integrate well into solution and the resulting slurry became uneven and patchy in distribution. Applying a thin consistent layer of thermochromics pigment slurry to the fabric surface afforded an even coating, good color saturation, and reversible color change. A general schematic of the overall garment in given in Figure 42.

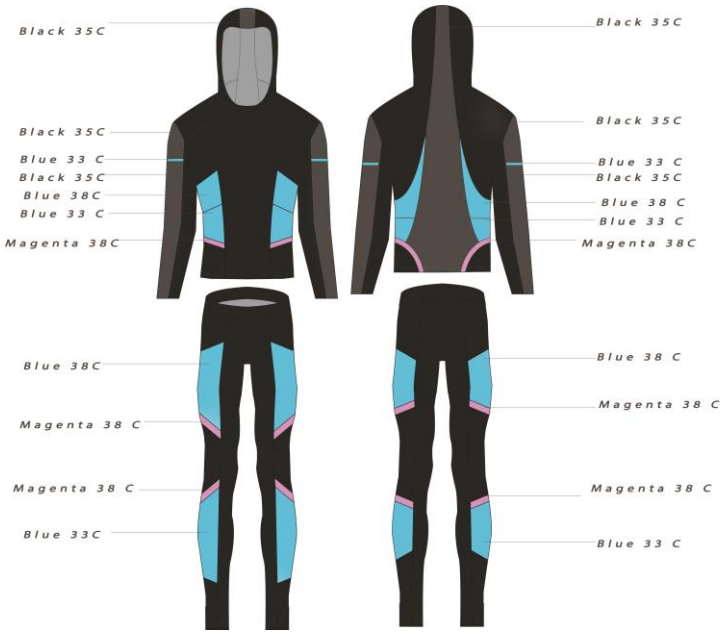

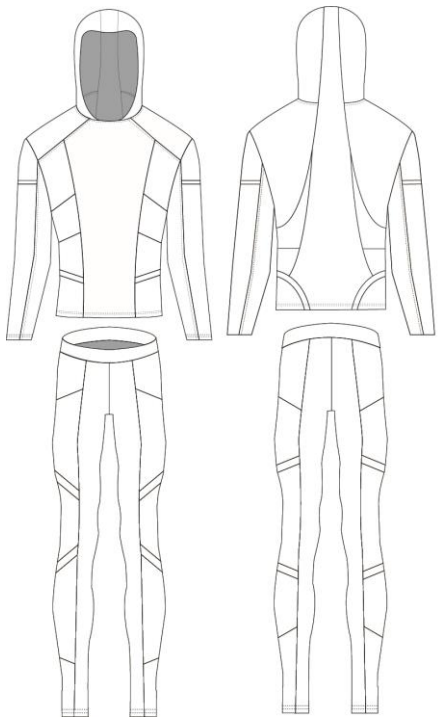

Figure 42. Artistic rendering of apparel design for detection of physical exhaustion with varying thermochromic pigment colors and activation temperatures

Garment Performance

Due to the stringent and high impact wear of athletic apparel, it was necessary to characterize garment performance using standard textile assessment protocols. In order to ensure acceptable durability and quality of the bodysuit made with thermochromics pigments, it was necessary to assess abrasion resistance, color fastness, and pigment activation sensitivity.

Because dynamic body movements are likely to cause abrasion leading to degradation of the surface thermochromics pigment coating, it was paramount to determine how robust the coating was to surface agitation. Furthermore, since athletic apparel must be stable when subject to repeated washing, color fastness was an imperative parameter to examine to determine durability and stability to common detergent. Lastly, testing on a thermal manikin was used to confirm that pigment color change in a physiologically relevant system (i.e. mimicking normal and elevated skin temperature) was observed for each thermochromic activation temperature, indicating appropriate color change would occur while the user was wearing the garment to ensure proper function.

Abrasion Analysis

Abrasion testing was used to assess the overall durability of thermochromic coating on the surface of the fabric. It was noted that some pilling and broken yarns began to form (minimally) at around 1400 cycles. Nonetheless, the pigment remained in tact on the fabric. Thermochromic activity of the fabric at the activation temperature was still observed after 10,000 cycles [Fig 43(b)]. Once the fabric reached 13,000 cycles, it was difficult to detect the thermochromic capabilities of the fabric unless one applied forced heat on the fabric [Fig 43(c)]. The fabric utilized for the garments were purchased from Spandex World Inc., a company specializing in spandex blends for all functions. The fiber content of fabric used for thermochromic apparel was 87% nylon and 13% percent spandex, relatively low modulus and highly elastic fibers. In reference to ASTM D4970-Standard Test Method for Pilling Resistance and Other Related Surface Changes, this fabric received a rating of 4 after of 13,000 cycles, indicating slight surface fuzzing.

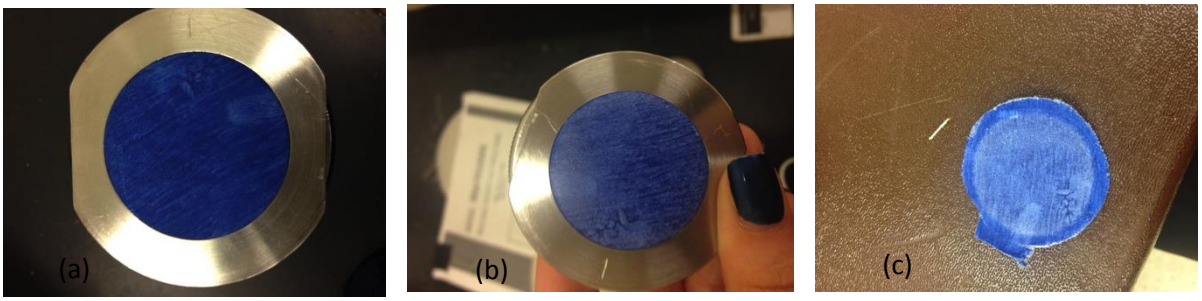

Figure 43. Abrasion resistance of thermochromic coated Nylon/Spandex after (a) 0 cycles, (b) 10,000 cycles, and (c) 13,000 cycles

Colorfastness Analysis

From theL,A,B values, the ΔE was calculated for three colors of thermochromic pigment on the fabric (Euclidian color space of the L,A,B values). The ranking in terms of greatest to least color change (as quantified by ΔE) were blue 33℃, magenta 38℃, and black 35℃; the ΔE values were 1.966, 1.427, 0.467 respectively (calculated using Eq. 1). Due to limited sample, each thermochromic was tested singularly. According to the AATCC standards, if the ΔE value is less than 2.0, there is no considerable difference in color change between the sample types. All thermochromic coated apparel types met this benchmark, demonstrating the durability of the fabric against non-chlorine bleaches, indicating sufficient wash resistance. In addition to assessing the impact of the bleach on the fabric, it was observed that the greater abrasion of the surface lead to increased crocking of the pigment of the surface. The increased crocking was expected to reveal a greater change in color and ΔE value.

Thermoregulating Manikin

To assess color change in an environment that mimics physiologically relevant conditions, the thermochromic garment was placed on a thermoregulating manikin with a skin temperature similar to that of elevated skin temperature during vigorous exercise. After 5 minutes on the manikin, color change was visually observed using qualitative photographs for the 33℃ blue only with minimal color change for pieces coated with 35℃ black (Fig. 44(a)). The locations of prominent color change were observed primarily in the lower calf region and arm inserts where the largest panel of blue 33℃ was integrated into the garment.

After 15 minutes on the heated manikin, black 35℃ panels located on the sleeves arms activated (Fig. 44(b)), along with stark color change in the blue 33℃ panels along the calf and arm side inserts. The 38℃ magenta and 38℃ coated panels did not change color throughout the heating process. The higher activation temperature magenta and blue 38℃ thermochromic panels were not expected to change color as the activation temperature was higher than the threshold of the manikin. Use of Walter® demonstrated that each targeted panel changed color at elevated skin temperatures in an environment similar to human use, proving our methodology for assigning the pigments.

Figure 44. Thermoregulating Manikin after 5 minute exposure to 35C(a) and 15 minute exposure (b). [inset: zoom of arm coated with 35C black thermochromic pigment]

7.4 Conclusions

This study presents a facile method for preparing and constructing athletic apparel that specifically targets exhaustion during workouts and can serve a functional purpose of visually signalling physical exhaustion via changes in apparel color caused by increasing skin temperature. Application of thermochromic pigments through surface treatment caused unexpected construction problems. The pigments were found to crock around areas pierced with the needle when sewing, such as seams and hems, and was further agitated when the fabric was stretched while compressed over the model. The coated thermochromic pieces of fabric were

scoured, causing the fabric to naturally curl, and was harder to sew seams evenly with untreated fabric due to the thickness difference.

Looking toward future optimization, in order to alleviate difficulties in construction, innovative techniques could be used. Adhesives may be used to make seams in future garments with surface treatments of thermochromic materials to eliminate the need to use a sewing machine. Thermochromic pigments could also be applied as a thinner layer by stretching the fabric, which would help the issue of crocking, and also, maintain properties, such as thickness, between treated and untreated fabrics. The possibility of applying a finish after surface treatment of thermochromic pigment could also increase durability and decrease the curling of the fabric.

This study was the exploration of applying a functional pigment to parts of the surface of designed athletic apparel. Further studies would include the optimization of applying pigment to the varying fiber types, and how the specific piece of athletic apparel would undergo stress on the fabric, surface of fabric, and seams. Although future optimization is needed to improve garment construction and longevity, preliminary testing indicates our thermochromic apparel meets many of the key needs of smart apparel including maintainability, durability, usability in the field, and most importantly, functionality through abrasion resilience, color fastness, and color activation verification using skin temperature modeling.

ACKNOWLEDGEMENT

The authors would like to acknowledge the generous support of the Cornell University Human Ecology Alumni Association (HEAA) for which their grant made this work possible. We would also like to acknowledge Drs. Margaret Frey, and Jintu Fan, for their valuable support and guidance. We would like to thank Huntsman International for their generous gift of reagents.

REFERENCES

1. Blau, P.J., K. G. Budinski., Development and Use of ASTM Standards for Wear Testing, *Wear*. 225-229 (1999) 1159-170.
2. Branson, D., P. Kamenidis, S. Peksoz, H. Park, S. K. An, C. Starr, *Proc. of The 8th International Meeting Manikins and Modeling*, Victoria, BC (2010).
3. Easter, E.P., B. E. Ankenman, Evaluation of the care and performance of comfort-stretch knit fabrics, *AATCC Review*. 6.11 (2006) 28-32.
4. Ergonomics of the Thermal Environment. Determination and Interpretation of Cold Stress When Using Required Clothing Insulation (IREQ) and Local Cooling Effects. London: BSI, 2008.
5. Fan, J., and L. Hunter. *Engineering Apparel Fabrics and Garments*. Cambridge, U.K.: Woodhead, 2009
6. Fowler, D., The attributes sought in sports apparel: A ranking,*J. of Marketing Theory and Practice*. 7.4 (1999) 81-88.
7. Gonzalez-Alonso, J., R. Mora-Rodrı´guez, P. Below, E. Coyle., Dehydration markedly impairs cardiovascular functionin hyperthermic endurance athletes during exercise, *J. of Applied Physiology*. 82.4 (1997) 1229-36.
8. Gonzalez-Alonso, J., C. Teller, S. Anderson, F. Jenson, T. Hyldig, B. Nielson, Influence of body temperature on the development of fatigue during prolonged exercise in the heat, *J. Applied Physiology*. 86.3 (1999) 1032-39.
9. Kulčar, R., M. Friškovec, N. Hauptman, A. Vesel, M. Klanjšek Gunde, Colorimetric properties of reversible thermochromic printing inks, *Dyes and Pigments*. 86.3 (2010) 271-277.
10. Leelajariyakul S., H. Noguchi, S. Kiatkamjornwong, Surface modified and micro-encapsulated pigmented inks for inkjet printing on textile fabrics, *Progress in Organic Coatings*.62.2 (2008) 145–61.
11. Mather, R. R., Intelligent Textiles, *Coloration Technology*. 31.1 (2001) 36-41.
12. Park, S., S. Jayaraman, Enhancing the Quality of Life through Wearable Technology, *IEEE Engineering in Medicine and Biology Magazine*. 22.3 (2003) 41-48.
13. Park, H., S. K. An, S. Peksoz, H. Cao, and D. Branson. *Proc. of 2010 Annual Conference of the American Association of Textile Chemists and Colorists*, Atlanta, GA (2010).
14. Peksoz, S., H. Cao, H. Park, S. K. An, and D. Branson. *Proc. of The 8th International Meeting Manikins and Modeling*, Victoria, BC (2010).

15. Savastano, D. M., A. M. Gorbach, H. S. Eden, S. M. Brady, J. C. Reynolds, J. A. Yanovski, Adiposity and human regional body temperature., *Am. J. of Clinical Nutrition*. 90.5 (2009) 1124-31.

16. Tang, S., L. Po, G. K. Stylios, An overview of smart technologies for clothing design and engineering,*Int. J. of Clothing Science and Technology*, 18.2 (2006) 108-128.

17. White, M. A., M. Leblanc, Thermochromism in Commercial Products, *J. of Chemical Education*. 76.9 (1999) 1201.

18. Zhu, C., A. Wu, Studies on the synthesis and thermochromic properties of crystal violet lactone and its reversible thermochromic complexes, *Thermochimica Acta*. 425.1-2 (2005) 7-12

Chapter 8. Conclusions

The objective of this thesis work is to examine the chemical and morphological influences of amino acid-based poly(ester amide) polymers (AA-PEA)s on macrophage and mast cells in a wound healing capacity. Different parameters in polymer synthesis were varied such as amino acid used and methylene chain length in the backbone to impart varying mechanical and chemical properties. Use of phenylalanine resulted in a more hydrophobic polymer with longer *in vitro* degradation stability, while use of Arginine in polymer synthesis resulted in a more hydrophilic, water soluble polymer with cationic surface charge. In addition, the methylene chain length in the polymer backbone was varied (based on the length of diol used in monomer synthesis) which influenced polymer parameters such as glass transition temperature (Tg) and contact angle.

Additionally, aside from varying starting materials in polymer synthesis, polymer fabrication into varying morphologies also influenced performance in potential wound healing applications. Hydrophobic phenylalanine-based AA-PEA's such as 8-Phe-4 were fabricated into nanoscale fibers using high voltage random orientation electrospinning to create a biomimetic surface similar to the extracellular matrix. Results indicate HeLa epithelial cell viability and mouse macrophage TNF-α proinflammatory cytokine and nitric oxide production comparable to that of the commercial control, poly(lactic acid) (PLA). In addition to fabrication a biologically relevant morphology, mast cell stabilization agent ketotifen fumarate (KF) was also incorporated within 8-Phe-4 electrospun fibers to decrease wound inflammation via reduction in mast cell degranulation. KF was released over an extended time period (30 days) with detectable mast cell

stabilization measured by reduction in % degranulation using a rat basophil leukemia (RBL) mast cell model.

Similarly, using principles of hydrogel fabrication, unsaturated arginine AA-PEAs (UArg-PEA) was combined with commercially available Pluronic F127 polymers to create cationically-charged hybrid hydrogels. This morphology is biologically relevant as cells could migrate into the hydrogel pores to promote deposition of extracellular matrix in wound healing as the hydrogel degrades. In the same vein, cationic charge promoted cell adhesion via electrostatic interactions with negatively-charged cellular phosolipid membrane.

F127 polymers were chemically modified before use to include end-capped double bonds via reaction with acryloyl chloride. Hydrogels were successfully fabricated and analyzed for swelling, degradation, interior morphology, and drug release. Hybrid UArg-PEA/F127DA promoted higher macrophage viability ($p < .05$) and lower proinflammatory cytokine production ($p < 0.05$) compared to the pure F127DA control hydrogel. Hybrid UArg-PEA/F127DA hydrogels degraded faster due to the presence of enzymatically-labile AA-PEA polymers and released KF at a slower rate than pure hydrogels, indicating potential for longer sustained release compared to the control. Finally, KF was released successfully from both pure and hybrid hydrogels, reducing % degranulation of RBL cells and promoting mast cell stabilization.

Along with fibers and hydrogels, AA-PEA polymers were incorporated into self-assembled microparticles based on electrostatic charge interactions. Again, unsaturated arginine-based AA-PEA polymers were used in an aqueous self-assembly with anionic naturally-occurring polysaccharide hyaluronic acid (HA) to form microparticles. These hybrid micron-scale microparticles showed little 3T3 fibroblast cytotoxicity, while decreasing mouse

macrophage proinflammatory cytokine production compared to HA alone. Moreover, these hybrid UArg-PEA/HA microparticles promoted similar anti-inflammatory cytokine production equal to or better than HA, while promoting advantageous wound healing arginase production.

Beyond morphological effects, polymer chemical influences were also probed to better understand cell-biomaterial interactions. In this case, polymer characteristics such as glass transition temperature, contact angle (relating to hydrophobicity), and surface charge were varied. Macrophage viability was not significantly influenced by slight variances in glass transition, but was extremely sensitive to surface charge (lower viability on anionic AA-PEAs owning to electrostatic repulsion, $p < 0.01$). Macrophage proinflammatory cytokine production indicated macrophage cytokine stimulation similar to the commercial control (PLA) for hydrophobic phenylalanine-based AA-PEA, a reduction in TNF-α for cationic AA-PEA ($p < 0.01$), and an increase in TNF-α for anionic AA-PEAs ($p < 0.01$). Similarly, 8-Phe-4 promoted IL-10 anti-inflammatory cytokine production equivalent to that of PLA, and significantly increased compared to the untreated control ($p < 0.05$). Overall, results indicate macrophage cells preferred a cationic surface with moderate hydrophobicity.

Lastly, promoting a multidisciplinary approach to science and project innovation, a group project combining expertise from Chemistry, Fiber Science, and Apparel design was created to design, make, and present a “smart” textile using thermochromic pigments. Use of thermochromic pigments with sport apparel serves to act as a “warning light” when the athlete’s skin temperature has risen near physical exhaustion. The garment was tested for color fastness, wash fastness, abrasion, and was presented at the Cornell Fashion Collective Fashion show. Due to the innovative nature of the work, a provisional patent was successfully filed.

Future work in AA-PEA chemical and morpohology studies would include more in depth examination of the influence of cationic polymeric surface charge in macrophage stimulation and promotion of wound healing. In particular, elegant gene activation assays can be completed to quanitiatively determine if M2 wound healing is influenced by surface charge. Futhermore, since KF drug release has been established as a model using AA-PEA materials, this widens the spectrum of opportunities to include a multitude of therapeutic agents to offer drug release for increased efficacy for prolonged drug delivery.